MADITRACE

Methodology for lab-based geoforensic supply chain due diligence audits

Deliverable D2.4

Version N°2.1

Authors: Róbert Arató (MUL), Yuan Shang (GTK), Guislain Hector Pierrot (CEA-LITEN), Delphine Losno (BRGM), Alban Moradell Casellas (BRGM), Gabriella Obbágy-Arató (MUL), Omar Amri (AHK Group), David Peralta (CEA-LITEN), Sébastien Perret (BRGM), Cyril Rado (CEA-LITEN), Laura Suarez Criado (UGent), Quentin Dehaine (GTK), Maria Dèzes (BRGM), Nathan Bordereau (BRGM), Théophile Lohier (BRGM), Anne-Marie Desaulty (BRGM)

Funded by
the European Union

Disclaimer

Document information

Grant Agreement	n°101091502
Project Title	Material and digital traceability for the certification of critical raw materials
Project Acronym	MaDiTraCe
Project Coordinator	Daniel Monfort, BRGM
Project Duration	1 January 2023 – 30 June 2026 (42 months)
Related Work Package	WP2
Related Task(s)	T2.2 Laboratory MFP techniques
Lead Organisation	MUL
Contributing Partner(s)	BRGM, GTK, UGent, AHK Group
Due Date	28 February 2026
Submission Date	27 March 2026
Dissemination level	Public report

History

Date	Version	Submitted by	Reviewed by	Comments
5-3-2026	1	Róbert Arató (MUL)	Daniel Monfort (BRGM), Wolfram Kloppmann (BRGM)	
20-03-2026	2	Róbert Arató (MUL)	Wolfram Kloppmann (BRGM)	
27-03-2026	2.1	Laurine Duivon (LGI)	Adeline Paul (LGI) Daniel Monfort (BRGM)	Formatting check and final submission

Funded by the European Union

Funded by the European Union

List of figures

Funded by the European Union

Funded by the European Union

Funded by the European Union

Funded by
the European Union

List of tables

Funded by
the European Union

Summary

This deliverable (D2.4) is part of WP2 of the MaDiTraCe project. WP2 focuses on developing material fingerprinting (MFP) methods to trace the origin of critical raw materials—cobalt, lithium, natural graphite, and neodymium—used in lithium-ion batteries (LIBs) and permanent magnets. One objective of the work package is to analyse the intrinsic signatures of these materials, such as their mineralogical composition, isotopic ratios, and trace element contents, and assess how well these properties are preserved throughout the entire production chain, from raw ore to final products. D2.4 is focussing on individual analytical techniques combined with data analysis, which can be used for traceability purposes and their applicability for production chain due diligence audits.

For **cobalt** (and nickel), our research demonstrates that the integrated use of trace elements and sulphur isotopic signatures provides a promising method to differentiate between Ni-Co bearing magmatic sulphide ores globally. However, the original trace element ratios and S isotopic signature of ores may change along the Ni-Co processing routes depending on the metallurgical processes applied and the introduction of external source of sulphur, e.g., sulphuric acid during hydrometallurgical processing. A traceability system based on a multi-isotopic dataset is needed to track the Co and Ni from ore to battery products.

For natural **graphite**, our research indicates that analytical methods used directly on graphite flakes, such as carbon stable isotopy and Raman-spectrometry have limited use in geoforensic applications, since most flake graphite deposits exhibit overlapping isotopic signatures and crystallinity parameters. On the other hand, it was discovered that graphite concentrates are ubiquitously intermixed with other mineral phases, which can be either separated from graphite flakes or co-analysed with them. The mineral paragenesis is characteristic for each deposit and the most resistant phases (e.g., zircon, rutile) can be traced down to the purity level of 99.99%. Datasets comprising multivariate data with many repeated measurements (SEM-based-mineralogy, LA-ICP-MS, LIBS) were found to be ideal for supervised machine learning-based multivariate classification (e.g., random forest classification) and the prediction of origin for unknown samples.

Lithium isotopes showed a large range of variability amongst lithium ore and ore concentrates from different geographical origins, in agreement with previous studies. However, overlaps in isotope ratios between classes of deposits (i.e. brines, geothermal fluids and hard rocks) make origin classification challenging. On the one hand, different machine learning (ML) algorithms were trained with Li isotopes and yielded good distinctions between the 4 groups of deposits. As foreseen, the issue related to signature overlaps could induce a few misclassifications in the predictions. On the other hand, major, minor and ultra-trace element analyses combined with advanced statistical models showed very promising results for the development of Li traceability systems on upstream Li value chain samples. For instance, the optimized LDA-based treatment model enabled three deposits from Canada, Australia and France to be distinguished from one another and could be further applied to other deposits.

For neodymium, ore samples and concentrates from Europe, South America, the US and China, show distinct Nd isotopic signatures that can be used for origin assessment. We also demonstrate the use of Nd isotope ratio as a conservative parameter over a large portion of the value chain (from the NdPr alloy to the final magnet) that can be a reliable tracer of the origin. Concerning REE patterns, the two analysed ore concentrates can be well distinguished. Magnet samples can also be identified and categorised by their relative proportions of light and heavy REE. Metallic samples from the same magnet production line

Funded by the European Union

show very small variation in their REE patterns throughout the value chain, highlighting their potential for provenance studies.

Funded by
the European Union

Keywords

Battery, magnet, production chain, MFP, lithium, cobalt, natural graphite, neodymium.

Abbreviations and acronyms

Acronym	Description
AAM	Anode active material
ALS	ALS Laboratories (commercial)
BHVO-2	Basalt reference material (USGS)
BGS	British Geological Survey
BRGM	Bureau de Recherches Géologiques et Minières
CAM	Cathode active material
CEA-LITEN	CEA platform for permanent magnets (alloys to sintered magnets)
Ccp	Chalcopyrite
CHUR	Chondritic Uniform Reservoir
CI	C1 chondrite (normalisation)
CRM	Critical raw material
DGA	Diglycolamide resin (REE separation)
DLE	Direct lithium extraction
DRC	Democratic Republic of the Congo
EDS/EDX	Energy-dispersive X-ray spectroscopy
EPMA	Electron probe microanalysis
FeS-1/5/6	FeS reference standards (UQAC)
GMTI	Global MFP Technic Index
GTK	Geological Survey of Finland
HREE	Heavy rare earth elements
ICP-AES	Inductively coupled plasma atomic emission spectrometry
ICP-MS	Inductively coupled plasma mass spectrometry
INAA	Instrumental neutron activation analysis
IRMS	Isotope ratio mass spectrometry
JNdi-1	Neodymium isotopic reference material
KDE	Kernel density estimation
LA-ICP-MS	Laser ablation inductively coupled plasma mass spectrometry
LA-MC-ICP-MS	Laser ablation multicollector ICP-MS

Funded by the European Union

LDA	Linear discriminant analysis
LIBs	Lithium-ion batteries
LIBS	Laser-induced breakdown spectroscopy
LN-resin	REE extraction resin (LN; HDEHP/HEH(EHP))
LREE	Light rare earth elements
L-SVEC	Lithium isotopic standard (for δ7Li)
MC	Multicollector
MC-ICP-MS	Multicollector ICP-MS
MFP	Material fingerprinting
MP	Mountain Pass (REE deposit, USA)
MS	Mass spectrometry
MUL	Montanuniversität Leoben
Nd–Fe–B	Neodymium–iron–boron (magnets)
NdPr	Neodymium–praseodymium
NMC	Nickel–manganese–cobalt (cathode family)
PB	Procedural blank
PGE	Platinum-group elements
PGM	Platinum-group metals
PLS	Pregnant leach solution
Pn	Pentlandite
Po	Pyrrhotite
PPB	Parts per billion
PPM	Parts per million
Q	Quadrupole
Q-ICP-MS	Quadrupole ICP-MS
QQQ	Triple-quadrupole ICP-MS
REE	Rare earth elements
REY	Rare earth elements including Sc and Y
RSD	Relative standard deviation
S1/G/D	Raman bands (second-order/graphitic/disorder)
SC	Single collector
SEM	Scanning electron microscopy
SSB	Standard–sample bracketing
TIMS	Thermal ionisation mass spectrometry

Funded by the European Union

TRA	Time-resolved analysis
TRU-spec	Ion-exchange resin for actinides/REEs
UGent	Ghent University
UQAC	Université du Québec à Chicoutimi
VCDT	Vienna Canyon Diablo Troilite (S isotope standard)
VMS	Volcanogenic massive sulphide
VPDB	Vienna Pee Dee Belemnite (C isotope standard)
WP	Work package
XRD	X-ray diffraction
µXRF	(Micro) X-ray fluorescence

Funded by
the European Union

1 Introduction

Deliverable D2.4 is part of WP2 of the MaDiTraCe project. WP2 aims to develop MFP (material fingerprinting) for cobalt, lithium and natural graphite in the production chain of lithium-ion batteries (LIB) and neodymium in the production chain of permanent magnets. In WP2 we use the intrinsic signature of deposits (mineralogical composition, isotopic composition, trace element composition, etc.) to identify parameters to distinguish their origins and to develop the traceability of cobalt, natural graphite, lithium and neodymium starting at the deposits and tracking fingerprints along the production chains. In this aim, WP2 tests a range of in-situ (LIBS, LA-ICP-MS, etc.) and bulk (e.g., XRF, solution ICP-MS) analytical techniques to analyse samples from ore until the end-product. During processing/beneficiation of the commodities and the production of LIB, the original ores will undergo many physical and chemical transformations potentially modifying their original intrinsic signatures. The aim of this deliverable is to determine how well certain methods can differentiate between different deposits and to identify the relevant parts of the value chains where each method can be applied for traceability. In other words, we evaluate the differentiating power and the production chain coverage of each method. In addition, we also evaluate the operational efficiency, the cost of implementation and the mobility of each method. To this end, a two-tier approach is also considered. The first tier refers to a simple and cost-effective method for routine analyses and the second tier to the application of a more sophisticated method for dedicated cases when value-chain inconsistency/fraud is suspected.

Within the broad range of available analytical infrastructure and expertise within the consortium, we chose the most promising techniques for each commodity, identified gaps in current analytical protocols and developed new approaches specifically suited for the respective commodities. The nature of the individual methods and resulting data shows large differences. The results vary in terms of detection limit, accuracy, precision, number of repeated measurements and sampling volume in addition to the geological nature and inherent heterogeneity of the studied materials. Therefore, the suitable methods, the potential combination of results from different methods, the prediction probability and the representativity of predictions largely varies on the commodity and specific methods applied.

For cobalt (and nickel), we analysed samples along the upstream of battery production chain, from magmatic Ni-Cu sulphide ores to intermediate smelted product (Ni-Co matte), and to chemical product, i.e., nickel sulphates used as high-purity precursor in the production of cathodes of LIB. For natural graphite, we analysed a range of samples from raw ore to purified natural graphite, commonly used as anode active material (AAM) in LIB. For lithium, we covered the whole battery production chain from ore to the end-of-life battery. We analysed samples from raw materials produced within the upstream portion of the Li production chain: ore, concentrate, salt, and from the downstream portion of the production chain including samples of CAM, cathode, cell, cycled cell produced by CEA-LITEN. In the permanent magnet production chain, the complete production chain was covered through the analysis of REE concentrates, Nd-Pr alloys and downstream samples, which consisted of ribbon, magnet powder and final magnet produced by CEA-LITEN.

The results and conclusions drawn from these analyses are developed in the various parts of this report.

Funded by the European Union

2 Suitability of analytical methods for traceability

In this section, we summarize our results obtained by a large variety of analytical methods on the four commodities. We describe the rationale behind using each method and the analytical/instrumental details of each method as well as their discrimination potential between deposits and traceability potential along the value chain. Where applicable, the data analysis approach is also described.

2.1 Cobalt

Cobalt (Co) is globally mined as a by-product of nickel (Ni) and copper (Cu), as well as in small volumes as primary cobalt or as a by-product of platinum-group metals (PGM) production. Sediment-hosted Cu-Co, Ni-Co laterites and magmatic Ni-Cu (-Co) sulphide ores are the three primary deposit types from which Co is extracted (Dehaine et al., 2021). In 2024, more than 2/3 of global Co mine output was supplied by the Democratic Republic of the Congo (DRC) with the sediment hosted Cu-Co ores as the primary deposit type (IEA, 2025). While for nickel, Indonesia, Philippines and Russia supplied 77% of the total global Ni mining. Due to the challenges to obtain ore samples from DRC and Ni-Co laterite samples from the major operations in South Asian countries, in the MaDiTraCe project, we mainly focused on cobalt sourced specifically from magmatic Ni- Cu (-Co/-PGE) sulphide ores. This is the main type of cobalt-hosting deposit in Finland, the EU and the northern hemisphere, from which Co is extracted as a by-product of Ni. Hence the traceability system developed from laboratory MFP techniques in this project for Co is also relevant for Ni. Hereafter, we present these methods, which have been applied jointly for Co and Ni.

2.1.1 Sample corpus

Giant magmatic Ni-Cu sulphide deposits are distributed mainly in Australia, Canada, China, Russia, South Africa and USA (Lu et al., 2019) and moderate size deposits are found in Zimbabwe and Finland as well. Finland holds a strategic role in Europe's cobalt supply, hosting both the largest known cobalt resources in Europe and the EU's only active cobalt-producing mines. Finland hosts diverse types of Co deposits, including but not limited to: 1) magmatic sulphide deposits (or orthomagmatic deposits) formed from magmatic processes in mafic-ultramafic rocks, historically important sources of Finnish cobalt; 2) Outokumpu-type deposits, well known from the classic Outokumpu mining district containing Cu-Co-Zn sulphide assemblages within metamorphosed ophiolite complexes; 3) Talvivaara (black shale–hosted) type, in which cobalt occurs with nickel and zinc in organic-rich black shales (Konnunaho et al., 2023). Key producing operations for Co in Finland include Terrafame, which uses bioheap leaching to produce Co bearing solutions for battery chemicals, Boliden Kevitsa, which produces cobalt as a by-product in Ni-Co concentrates and Boliden Harjavalta, which processes Ni-Co concentrates and produces cobalt-containing intermediates from smelting (Ni-Co matte) (Konnunaho et al., 2023).

In the MaDiTraCe project, we aim to deliver a proof-of-concept traceability system for cobalt sources from magmatic Ni-sulphide deposits, developed from laboratory MFP techniques. To this end and by taking the advantages of the Finnish cobalt industry, we have collected three categories of samples for the project:

(1) Magmatic sulphide ore samples from worldwide operations to investigate the spatial variability of geochemical fingerprinting for different ores at global scale, including ore samples from the Kevitsa mine in Finland, Norilsk and Pechenga in Russia, Raglan and Sudbury in Canada, Jinchuan in China, Selebi-Phikwe in Botswana as well as Leinster, Mount Keith and Forrestania in Western Australia (Figure 1a Figure 1a).

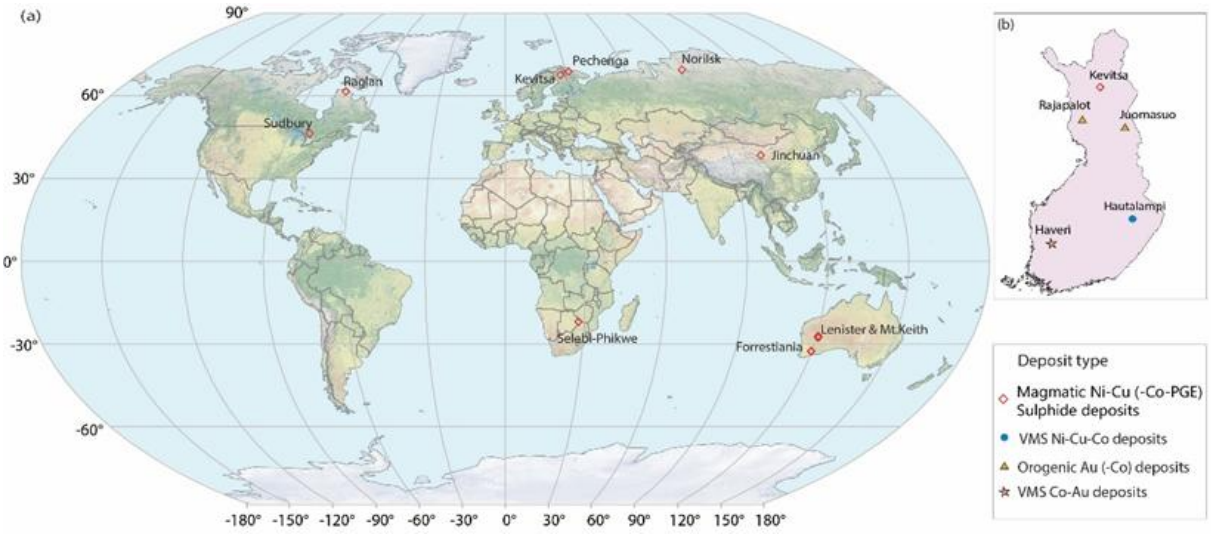

Figure 1 Samples collected for Co traceability. (a) magmatic sulphide ore samples collected globally; (b) samples of different types of cobalt-enriched deposits in Finland.

(2) Different types of cobalt ores from deposits in Finland to investigate the variability of geochemical characteristics for different deposits at regional scale, including magmatic Ni-Cu-Co (-PGE) sulphide samples from Kevitsa, volcanogenic massive sulphide (VMS) Ni-Cu-Co deposits from Hautalampi, orogenic gold (Au) and cobalt deposits from Rajapalot and Juomasuo, and VMS Co-Au deposits from Haveri (Figure 1b).

(3) Production chain samples, all sourced or produced using material from the a magmatic sulphide mine operation in Finland, to investigate and identify robust geochemical fingerprints that are possibly preserved along the value chain (mainly upstream), including samples of core, crushed ore, mineral concentrates, smelted intermediate product, i.e., Ni-Co matte, solutions, residues and products from refining stages (hydrometallurgy), such as nickel sulphates ($NiSO_4$) used as precursor for cathode active materials (Figure 2).

Funded by the European Union

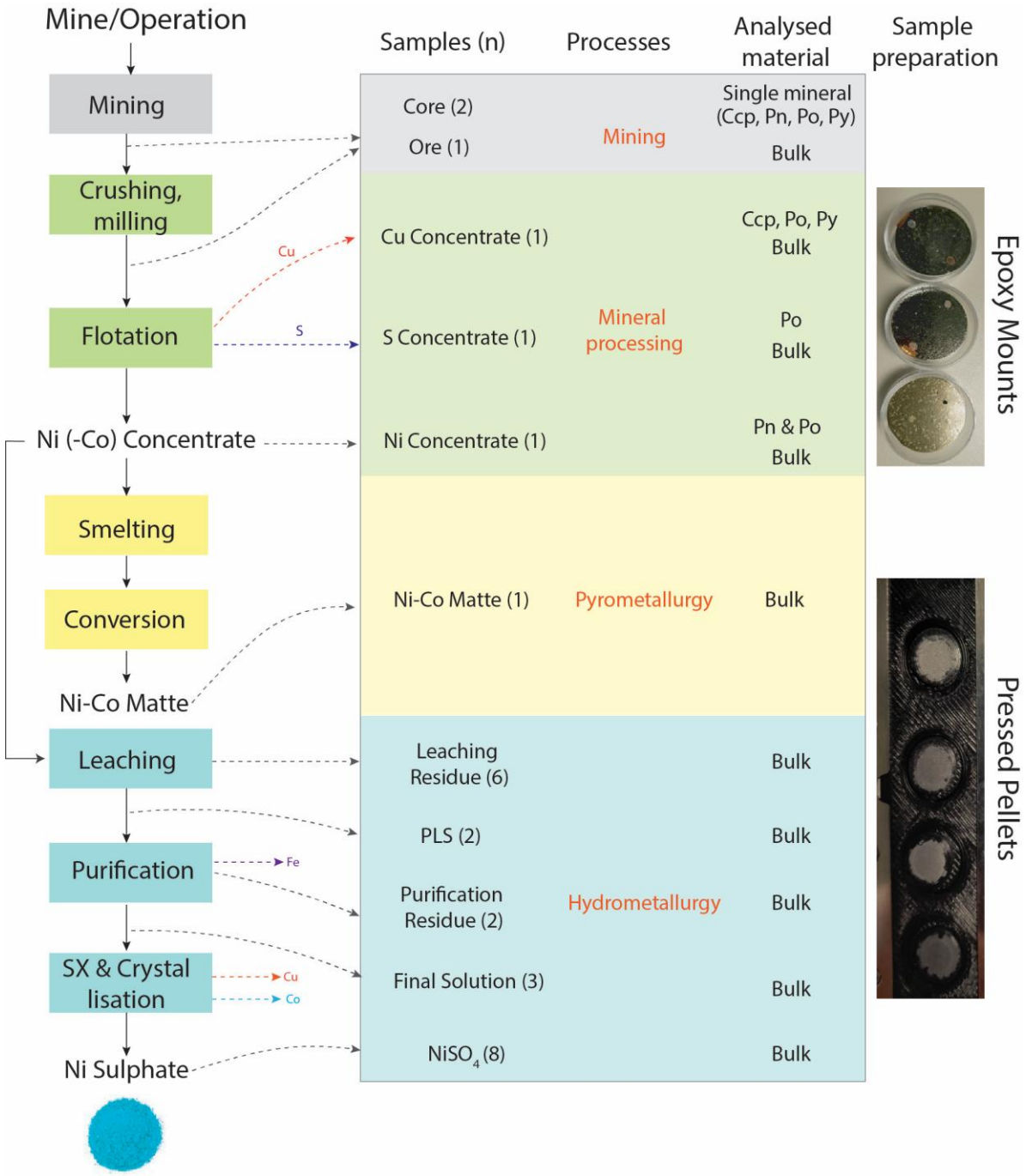

Figure 2 Samples collected along the Ni-Co processing route sourced from a known magmatic sulphide mine in Finland and their respective sample preparation for laboratory analysis.

2.1.2 **Laboratory MFP techniques applied**

Since we have several types of samples in terms of their physical and chemical properties, the preparation style and laboratory techniques used for different samples are also varied. For the drill core, ore and mineral concentrate samples in which the minerals are still preserved, we prepared the samples as epoxy mounts to go through in-situ single-mineral analysis. For the Ni-Co matte and chemical samples from the hydrometallurgical process, we ground the samples and prepared them as pressed pellets for in-situ bulk geochemical analyses (Figure 2). We also used wet chemical methods, which offer better precision, for bulk geochemistry and isotopic composition (e.g., $NiSO_4$ samples). For this approach, the samples need to be ground to powder and then digested, which is relatively laborious.

Funded by the European Union

Our analytical toolkit comprises diverse mineralogical and geochemical techniques, including XRD and SEM for mineral characterisation, μXRF and EPMA for in-situ analyses of major, minor and trace element composition, ICP-AES for wet chemical analysis of bulk major, minor and trace element composition, LA-ICP-MS for in-situ trace element analysis in sulphide minerals, LA-MC-ICP-MS for in-situ (S and Pb) isotopic analyses in sulphide minerals as well as liquid MC-ICP-MS and IRMS for bulk sulphur isotopic analyses. Except ICP-AES analysis, which was outsourced to a commercial laboratory (ALS) and IRMS for S isotopic analyses, which were conducted at BRGM in France, all measurements have been carried out at Espoo Research Laboratory of GTK, in Finland.

In practice, SEM (-EDS) is used to analyse the modal mineralogy of the ore samples and to map the sulphide minerals in the ore. Then, we measure the major (e.g., S, Fe and Ni) and minor (e.g., Co, Cu, As, Zn) elements in these sulphide minerals by EPMA. Based on the information obtained from SEM and EPMA analyses, we screen the suitable sulphide mineral grains for in-situ trace element and isotopic analyses. In the next section, we will describe these two methods in detail and present the key results we have obtained.

2.1.3 Trace element composition

2.1.3.1 LA-ICP-MS for measuring trace element composition

Trace elements in sulphide minerals and pressed pellets were analysed in-situ using a Nu AttoM single-collector ICP-MS (Figure 3) coupled to an Excite 193 nm ArF excimer laser. Laser parameters included a 5 Hz repetition rate, 2.17 J/cm² fluence, and spot diameters of 30–40 μm (minerals, depending on grain size) and 50 μm (pressed pellets). Each analysis consisted of 20 s background followed by 40 s ablation, acquired in time-resolved analysis (TRA) mode.

A standard–sample bracketing (SSB) approach was applied using UQAC FeS-1 as the primary standard and FeS-5 and FeS-6 as quality-control standards, with batches of 10 unknowns between standards. A total of 65 isotopes corresponding to 41 elements were measured in fast-scan, low-resolution mode. ^{57}Fe served as the internal standard for quantification.

Data reduction was implemented using the Iolite software package (Paton et al., 2011). The Fe composition obtained by EPMA for sulphide minerals was used as internal standard for matrix calibration. For pressed pellet samples, we used the bulk chemical composition (Fe, Ni, Cu and Co) obtained from ICP-AES analysis.

Figure 3 Nu AttoM single-collector ICP-MS used for trace element analyses at GTK.

Funded by the European Union

2.1.3.2 **Multivariate data analysis**

We used linear discriminant analysis to investigate the differences in trace element composition in different ore samples. The method attempts to classify observations described by values on continuous variables into groups. The group membership is defined by a categorical variable X, which is predicted by the continuous variables. These variables are called covariates and are denoted by Y. For the linear fitting, it assumes that the within-group covariance matrices are equal, and the covariate means for the groups defined by X are assumed to differ. The method estimates the distance from each observation to each group's multivariate mean using Mahalanobis distance. The observations are classified into the closest group (https://www.jmp.com/support/help/en/19.0/#page/jmp/overview-of-the-discriminant-platform.shtml#).

In our case, the input continuous variables are elemental compositions (e.g., Ni, Co, Zn, Se, Ag, Pd, Pb, Bi and element ratios such as Ni/Co, Ni/Cu, V/Cr, and Cu/Pb) from samples of different origins, i.e., the Y covariates, are used to classify the samples into categories. X is the origin of the samples, which defines the groups of the variables to be classified. The output is a 2-dimensional biplot called" Canonical Plot". The biplot axes are the first two canonical variables, which provide maximum separation among the groups (sample origin). The observations and the multivariate means of each group are represented as points in the biplot. A 95% confidence level ellipse is plotted for each mean. If the two groups differ significantly, the confidence ellipses tend not to intersect. An ellipse denoting a 50% contour is also plotted (Figure 4). The linear fitting discriminant analyses (LDA) were implemented by using the statistical software JMP 19 and detailed method description is provided in the platform webpage (https://www.jmp.com/en/software/new-release/new-in-jmp).

2.1.3.3 **Trace element composition in different Co-Ni deposits**

Figure 4 shows that different Co (-Ni) deposits can be well separated by their bulk trace element composition through LDA. In the discrimination map, the magmatic sulphide deposit type samples from Kevitsa and Western (W.) Australia plot closer; Rajapalot and Juomasuo are both orogenic Au-Co deposits and are mapped together. The Hautalampi ore sample, which is an Outokumpu-type (VMS) Ni-Cu-Co deposit, plots separately from the other two deposit types.

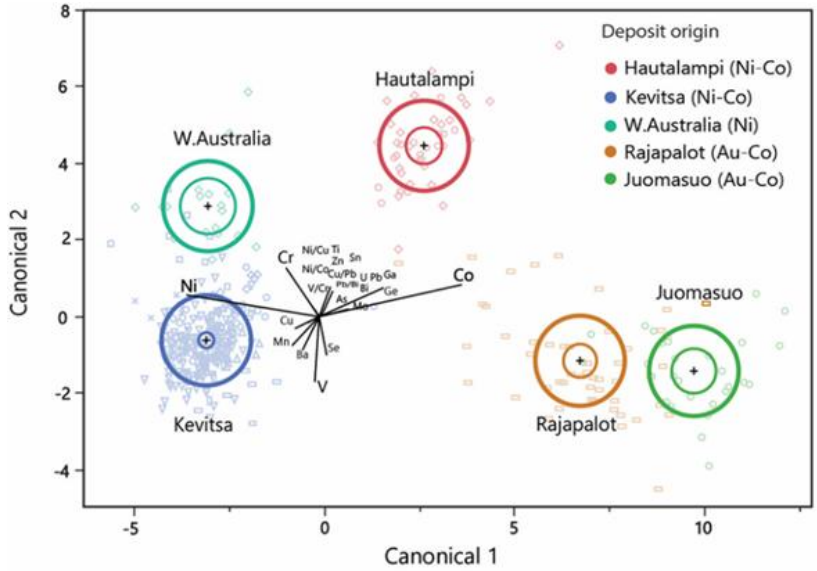

Figure 4 Discrimination map obtained from LDA on bulk trace element composition for different Co bearing ore deposits. (Crosses refer to means, small circles to 95% confidence intervals and bigger circles to 50% confidence intervals, respectively. Loadings related to each element/elemental ratio are also plotted, with the length of lines referring to their relative contribution to discrimination.)

2.1.3.4 Trace element composition in Magmatic Ni sulphide ores of different locations

Figure 5 presents the result of LDA based on trace element composition in pentlandite of magmatic sulphide ore samples from different locations. It shows that although these samples belong to the same type of ore deposits, they can still be separated based on the trace element signature in a single mineral type. For instance, samples from Leinster of the Western Australia, Jinchuan and Kevitsa can be well differentiated as they plot far away in the discrimination map, while ore samples of Raglan and Pechenga, Norilsk and Sudbury are located rather close in the map suggesting similar elemental composition in pentlandite of these locations.

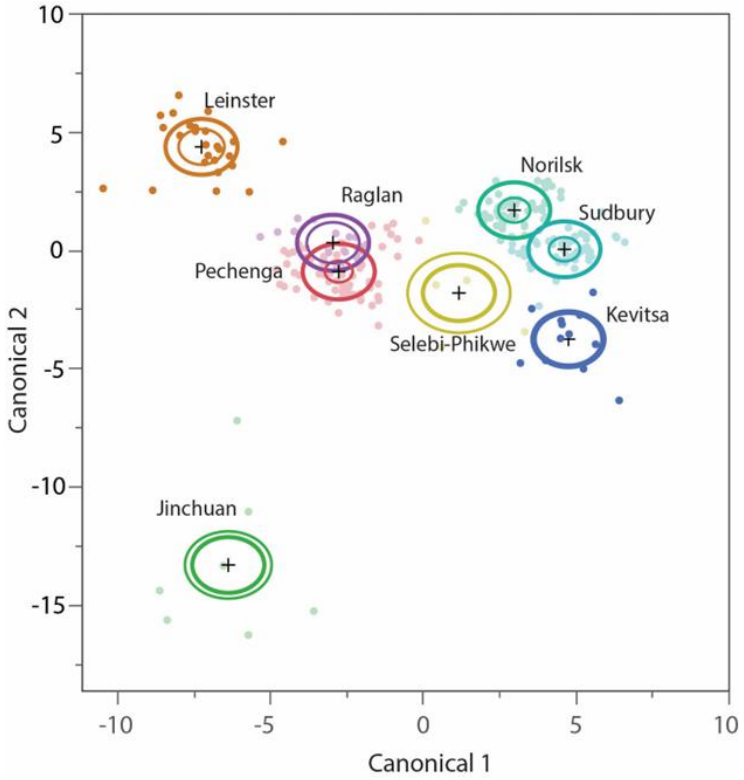

Figure 5 Discrimination map obtained from LDA on trace element composition in pentlandite from magmatic sulphide ores.

2.1.3.5 Preservation of elemental ratios in the samples along the production chain

We have analysed bulk (whole rock) trace elements in the samples along the production chain with a known source from a magmatic sulphide mine/operation in Finland. Here, we do not present all the elements for each sample since many elements become eliminated during processing. In principle, the refining processes to obtain Ni-Co matte and $NiSO_4$ are sequential procedures to enrich products in Ni and Co (Figure 2). We identified that some elemental ratios, such as Ni/Co and Ni/Cu stay consistent along the processing route until the late stages (Figure 6). The Ni/Co ratio remains unchanged, except for the higher values of the Ni-Co matte and the $NiSO_4$ samples (Figure 6a). For the Ni/Cu ratio, most samples show values in a range of 1-10. The Cu concentrate sample displays relatively lower ratio since the sample is dominated by chalcopyrite, which donates to higher Cu content (Figure 6b). $NiSO_4$ samples again show notably higher values as they are enriched in Ni and other elements have been removed after purification during the hydrometallurgical process.

Funded by the European Union

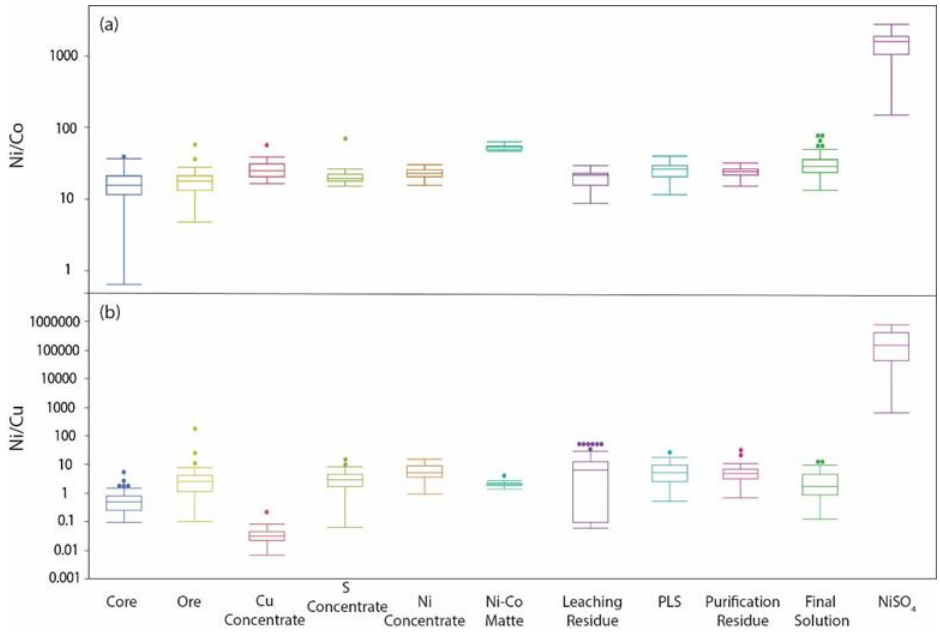

Figure 6 Bulk trace element ratios (a) Ni/Co and (b) Ni/Cu in different samples along the Ni-Co processing route. Note that the y-axis is on a logarithmic scale.

To better illustrate the Ni and Co elemental signature in the samples along the processing route, we plot the Ni composition against Co composition of the studied samples and apply a simple linear fitting to the data (Figure 7). It shows that Ni and Co contents can be well fitted into one line, except the data points from $NiSO_4$ samples, which are located distinctively in a peripheral region.

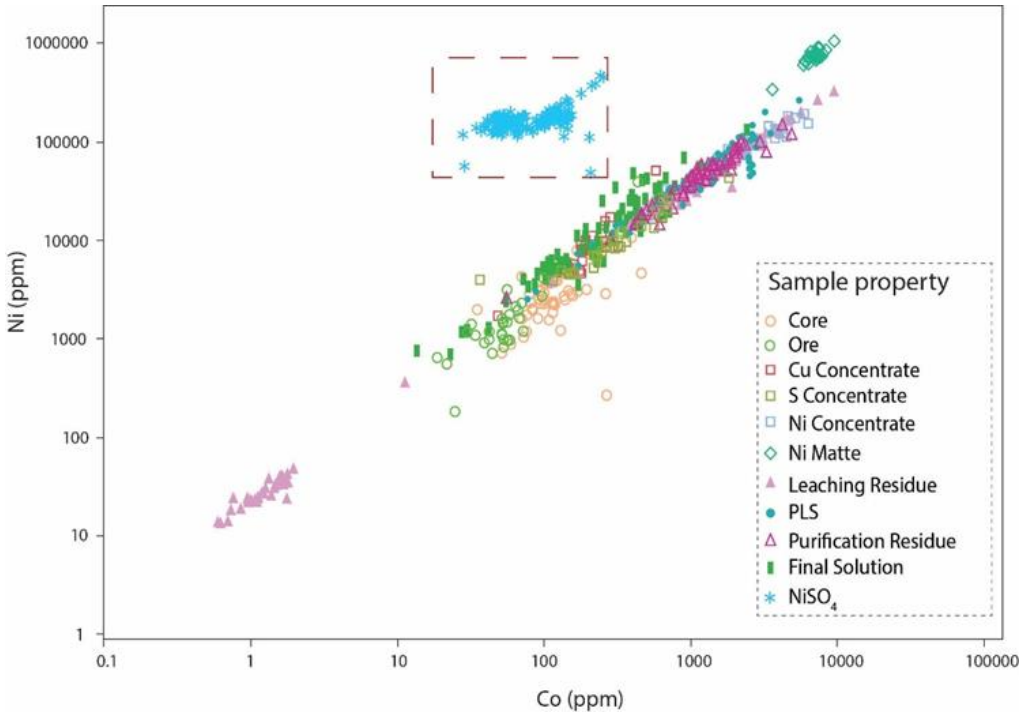

Figure 7 Ni vs Co (ppm) distribution in the samples along the Ni-Co processing route. The red dash-line rectangle marks the Ni-Co distribution in the NiSO4 samples.

Funded by
the European Union

2.1.4 Sulphur isotope composition

2.1.4.1 LA-MC-ICP-MS for in-situ S isotopic analysis

The major sulphide minerals in the magmatic Ni-Cu (-Co/-PGE) sulphide ores are pentlandite (Pn), pyrrhotite (Po), chalcopyrite (Ccp) and pyrite (Py). In-situ sulphur isotopic analyses for these sulphide minerals from Kevitsa ore samples were performed by a Nu Plasma High Resolution (HR) MC-ICP-MS, coupled to a Photon Machines Analyte G2 193 nm laser ablation (LA) system at GTK. Samples were ablated in a helium atmosphere (gas flows = 0.4 and 0.1 L/min) within a HelEx ablation cell. Sulphur isotopes were measured at medium resolution and the ^{32}S and ^{34}S data were collected in static mode during ablation. The sulphide minerals were ablated at a spatial resolution of 30-50 µm (depending on the mineral's grain size), using a laser beam fluence of 0.83 J/cm^2 and at 5 Hz. The total S signal obtained was between 0.5 and 3.0 V. A typical analysis includes a 20 s of baseline scan and 50-60 s of ablation to obtain an internal precision of $^{34}S/^{32}S \leq \pm 0.000005$ (1σ error). For each mineral, two matrix-matched in-house standards have been used as external standards bracketing and quality control. This method enables direct, spatially resolved S isotopic analysis at the micrometre scale, preserving mineral textures while providing high-precision isotopic data.

Figure 8 Neoma™ MS/MS MC-ICP-MS instrument for S isotopic analysis. (Image source: Thermo Scientific™ website)

During the implementation of the project, GTK has replaced the old MC-ICP-MS instrument with a new one: Neoma™ MS/MS MC-ICP-MS (Thermo Scientific™) (Figure 8). In-situ sulphur isotopic analyses for sulphide minerals in ore samples from other sources, i.e., Pechenga, Norilsk, Jinchuan, Leinster Selebi-Phikwe, Sudbury and Raglan were analysed with this new instrument, coupled with the G2 laser. Most of the grains were measured with a laser spot of 50 µm, using a laser beam fluence of 0.83 J/cm^2 at 10 Hz. Similar standards were used as for the previous measurements with the Nu Plasma instrument.

The S isotopic ratio is expressed as $\delta^{34}S$ (‰), which is the $^{34}S/^{32}S$ ratio calculated relative to the Vienna-Canyon-Diablo Troilite (VCDT) standard.

Funded by the European Union

2.1.4.2 S isotopic signature ($\delta^{34}S$) in the magmatic sulphide ores of different locations

The $\delta^{34}S$ values of sulphide minerals from the same ore fall within a similar range while there are large variations among different ores (Figure 9). Since we have less data points from pyrite in some ore samples, we excluded the S isotopic data for pyrite. Norilsk samples show significantly heavier $\delta^{34}S$ values in all investigated minerals, with a median $\delta^{34}S$ at 12.55 ‰ in Ccp, 11.55 ‰ in Pn and 12.05 ‰ in Po. On the contrary, ore samples from Leinster display more negative $\delta^{34}S$ values than other samples, with a median $\delta^{34}S$ value at -1.47 ‰ in Ccp, -2.17 ‰ in Pn, and -1.78 ‰ in Po. There are also significant overlaps in the S isotopic signature among Raglan, Pechenga, Kevitsa, Jinchuan and Sudbury in the investigated sulphide minerals. For instance, the median $\delta^{34}S$ value in Ccp is 1.82 ‰ for Kevitsa, 2.51 ‰ for Jinchuan and Sudbury. Both Raglan and Pechenga show heavier $\delta^{34}S$ in Ccp, with a median value at 6.13 ‰ and 6.26 ‰ respectively (Figure 9).

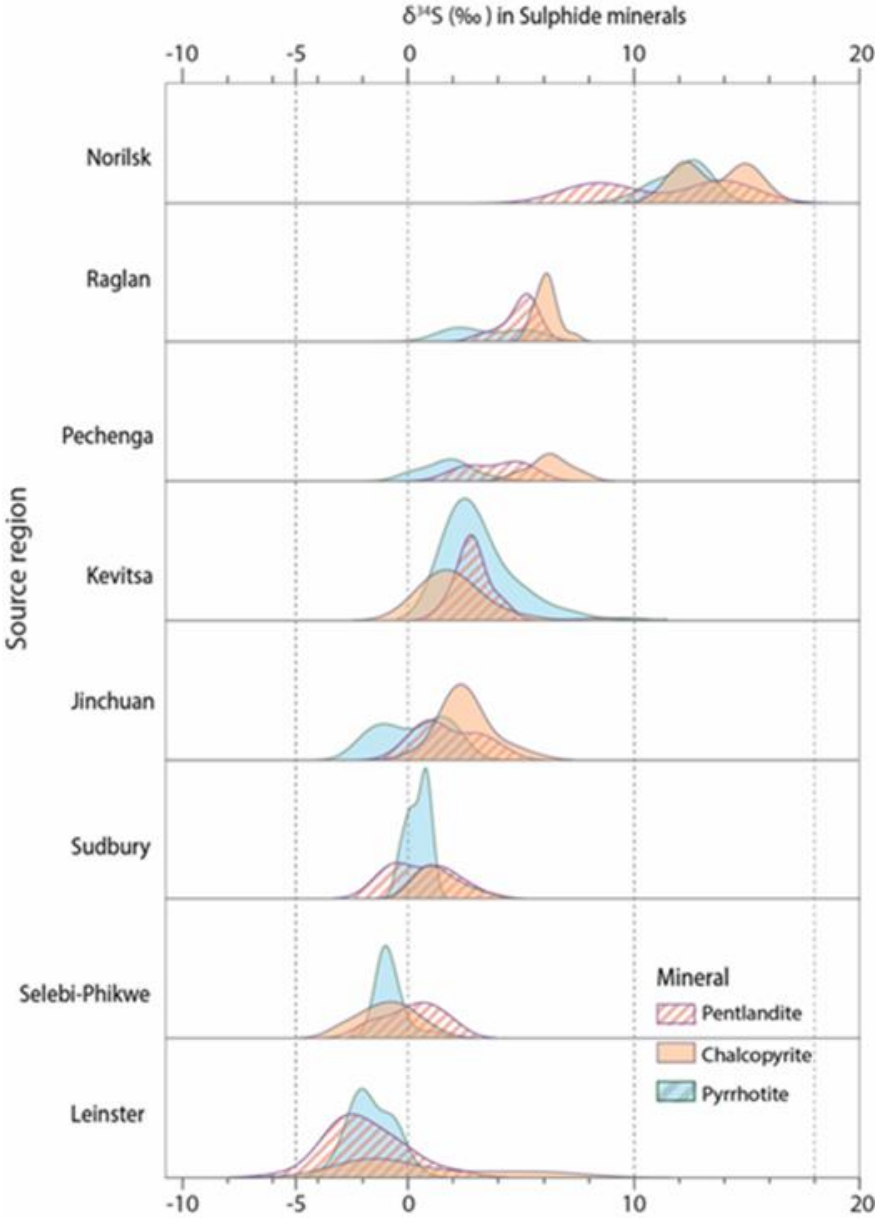

Figure 9 Kernel Density Estimation (KDE) for the distribution of $\delta^{34}S$ (‰) in sulphide minerals, i.e., pentlandite, chalcopyrite and pyrrhotite of magmatic Ni-Cu (-Co-PGE) deposits (Source: Shang et al., in prep.).

Funded by the European Union

Focussing on $\delta^{34}S$ values in pentlandite from magmatic Ni-Cu (-Co-PGE) ore samples of difference sources, it is apparent that the S isotopic signature can also vary from different mines in the same mining district (Figure 9). For example, the notable bimodal distribution in $\delta^{34}S$ of Pn from Norilsk ore samples is due the samples originating from two mines in the region. The median $\delta^{34}S$ of Pn of one mine is 8.35 ‰ while for another mine it is 13.92 ‰. The same pattern was observed in the Pechenga and Sudbury data where the samples were taken from two locations of the region.

2.1.4.3 Preservation of the S isotopic signature along the Ni-Co processing route

We investigated the bulk S isotopic signature ($\delta^{34}S$) along the Ni-Co processing route for samples with a known mine/ operation in northern Finland as a case study. We tracked the bulk $\delta^{34}S$ variation in the drill core and ore samples, mineral concentrates, to intermediate product Ni-Co matte, and to nickel sulphates used in the batteries (Figure 2). Bulk $\delta^{34}S$ is around 2-3 ‰ in the ore samples and falls in the range of 5-6 ‰ for Ni-Co concentrates and Ni-Co matte samples (Figure 10). Although the ore and Ni (-Co) concentrate samples show varied $\delta^{34}S$ value in the bulk composition, the $\delta^{34}S$ value stays rather consistent in the pentlandite of both samples, around 3 ‰.

Funded by the European Union

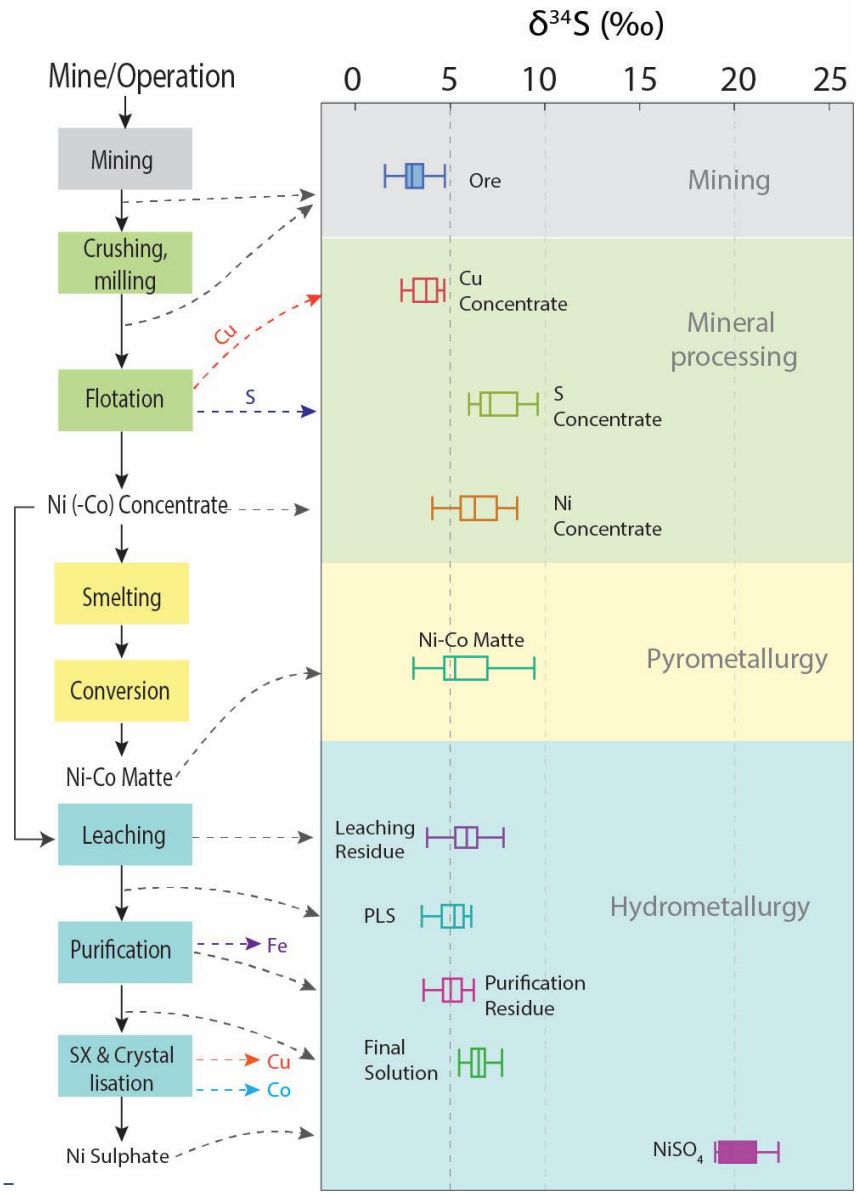

Figure 10 Bulk $\delta^{34}S$ (‰) distribution in different samples sourced from a known magmatic sulphide mine/operation in Finland along the Ni-Co processing route.

Note that S isotopic analyses for $NiSO_4$ was conducted through solution analysis while other samples were measured in-situ by laser ablation.

The S isotopic signature changed during the hydrometallurgical process. The leaching residue and final solution still show a closer $\delta^{34}S$ value (around 6 ‰) with that of the Ni-Co concentrate sample (median at 6.3 ‰) while the pregnant leach solution (PLS) after leaching and purification residue show slightly decreased $\delta^{34}S$ values around 5 ‰. The nickel sulphate samples show a notable high $\delta^{34}S$ value, up to 20 ‰ (Figure 10).

Taking Pb isotopic data into consideration (not shown here since the analyses are still in progress) from the samples of the same processing route, we deduce that the variation of $\delta^{34}S$ value in Ni-Co matte from the Ni-Co concentrate sample may be due to mixing (as this matte may have been produced from a blend of concentrate from this known mine and other feedstock from other sources) rather than S isotopic fractionation happened during the smelting process.

Funded by the European Union

The changes of $\delta^{34}S$ during the hydrometallurgical process are explained by the introduction of an external source of S via sulphuric acid used for leaching. The original S isotopic signature from the sulphide minerals remained in the leaching residue. The increased $\delta^{34}S$ values nickel sulphate ($NiSO_4$) samples are either the S isotopic signature of the sulphuric acid used during leaching or a mixture of both S signatures in the original Ni-Co concentrate and the externally added acid (Figure 10). In addition, different analytical methods may also have an influence on the bulk $\delta^{34}S$ values of the studied materials. Measurements of the bulk S isotopic ratio with IRMS are in progress to validate the results.

2.1.4.4 Discrimination analysis by combing the trace elements and S isotopic signatures together

Since pentlandite is the most valuable mineral in magmatic sulphide ore for Co and Ni, here we combined the trace element data and S isotopic signature in pentlandite to differentiate the studied magmatic sulphide ore samples globally (Figure 11). The same multivariate data analysis method (LDA) was applied, and a better discrimination result was obtained with the addition of sulphur isotope values to the dataset. While there are still overlaps between ore samples of Jinchuan, Sudbury and Selebi-Phikwe if only the first two linear discriminants are considered for practical reasons (plotting), Leinster, Norilsk, Raglan, Pechenga and Kevitsa can be well separated even in two dimensions.

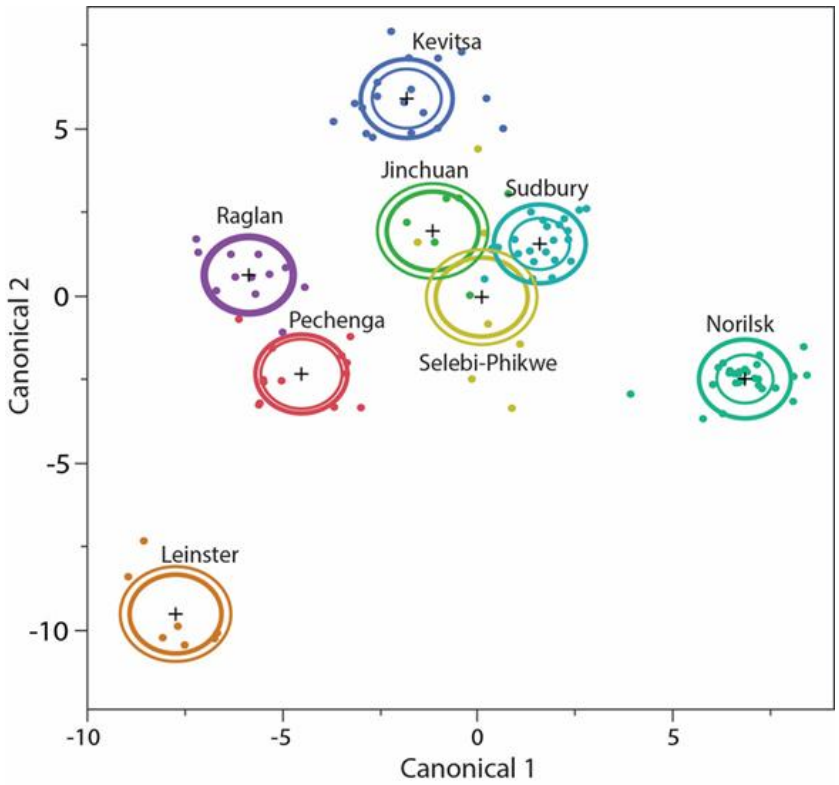

Figure 11 Discrimination map obtained from LDA on element composition and S isotopic signature (δ34S) of pentlandite from magmatic sulphide ores (Shang et al., in prep.).

2.1.5 Method evaluation

Figure 12 shows the overall evaluation of the laboratory techniques that have been applied. The techniques are evaluated from five aspects: the differentiating power, the production chain coverage, the mobility of the equipment, the cost of implementation and the operational efficiency. The Global MFP Technic Index (GMTI) is calculated accordingly based on the respective weights assigned to each criterion to evaluate the methods. For a detailed description of the GMTI, please refer to D2.3 of the MaDiTraCe project. The GMTI

Funded by the European Union

for SEM, (μ)XRF, EPMA is 4.1, 4.5 and 4.3 respectively. The ICP methods show higher GMTI, with 5.4 for liquid ICP-AES, 5.1 for MC-ICP-MS and 4.8 for LA-ICP-MS.

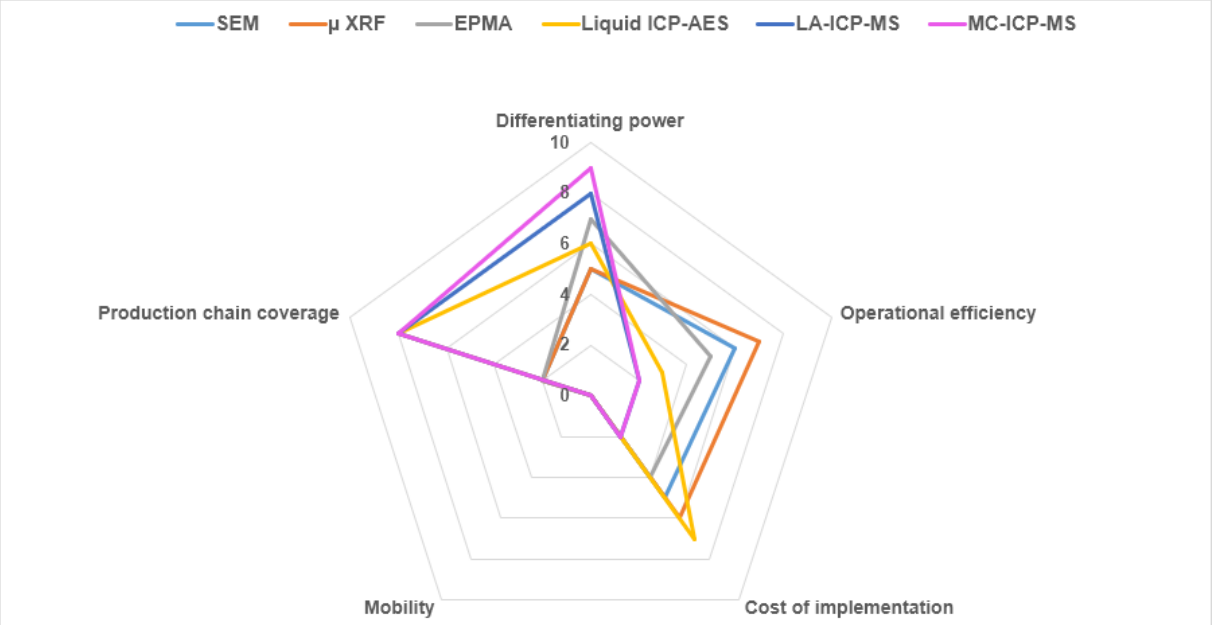

Figure 12 Radar diagram for the evaluation of laboratory techniques applied for Co-Ni samples. Note: we excluded XRD (X-ray Diffraction) and IRMS (Isotope Ratio Mass Spectrometry) from the technique evaluation since we only specifically applied the techniques to samples along the processing route.

In summary, LA-ICP-MS and in-situ (LA) /solution MC-ICP-MS show excellent differentiating power and value chain coverage accompanied with their relatively high analytical cost.

2.1.6 **Summary**

Based on the elemental compositions and sulphur isotopic signatures of the Co–Ni-bearing samples, we came to the following conclusions:

(1) Ni–Co magmatic sulphide ore deposits from different locations can be distinguished using combined signatures of major and trace elements together with S isotopic ratios in pentlandite.

(2) Some ores may exhibit overlapping geochemical fingerprints (e.g., trace elements and S isotopes), thus multivariate data analysis integrating elemental and isotopic datasets is essential.

(3) The sulphur isotopic signature remains largely conservative through mineral processing, and potentially pyrometallurgy, but changes significantly after acid leaching in the hydrometallurgy process.

(4) A combination of multiple isotope systems is promising in verifying materials that are derived from mixed or multiple sources.

2.2 Natural graphite

Battery-grade graphite can be sourced from natural graphite, mined from naturally occurring ore deposits, or synthetic graphite. Three larger groups of natural graphite can be distinguished: semi-graphite (micro-crystalline or "amorphous" graphite), hydrothermal graphite (vein or lump graphite) and flake graphite. Flake graphite is best suited for battery production and it is dominant on the natural graphite market. High-grade flake graphite ore usually contains up to 40% graphite, the rest of the ore being various kinds of other minerals, characteristic for each graphite deposit. During various stages of processing, the graphite content increases up to 99.99%, still retaining a certain amount of other minerals and/or industrial products, which appear in the material during processing through physical contamination or chemical reactions. This is an important aspect of graphite analysis as multiple studies in the literature refer to certain elements in natural graphite as elemental impurities (e.g., Natarajan et al., 2010; Ghosh et al., 2022). Yet there is no proof of the existence of impurities in natural graphite/graphite concentrates other than the two listed categories (i.e., natural minerals and industrial products). Given the mixed nature of the studied materials, the applied methods are categorized based on the phases from which they deliver information and their general approach (bulk or in-situ). Thereby we also acknowledge that these categories are not always mutually exclusive (e.g., during stable isotope measurements, bulk samples are analysed).

2.2.1 Sample corpus

In 2023, about 1.7 million tonnes of natural graphite were produced (World Mining Data 2025, (Schatz, 2025)), increasing from 0.9 million 41 tonnes in 2017. Production is concentrated in China (share of 73%), followed by India (7.8%), Mozambique (5.9%), Madagascar (3.7%) and Brazil (3.3%). Our sample collection includes most of the major producing countries with several countries represented by multiple deposits (e.g., China), except India (Figure 13). Our sample set comprises 150 samples, including 49 raw ore specimens, 62 flotation concentrates and 9 chemically purified samples, alongside further graphite-bearing specimens, crushed ore, anode materials and synthetic graphite.

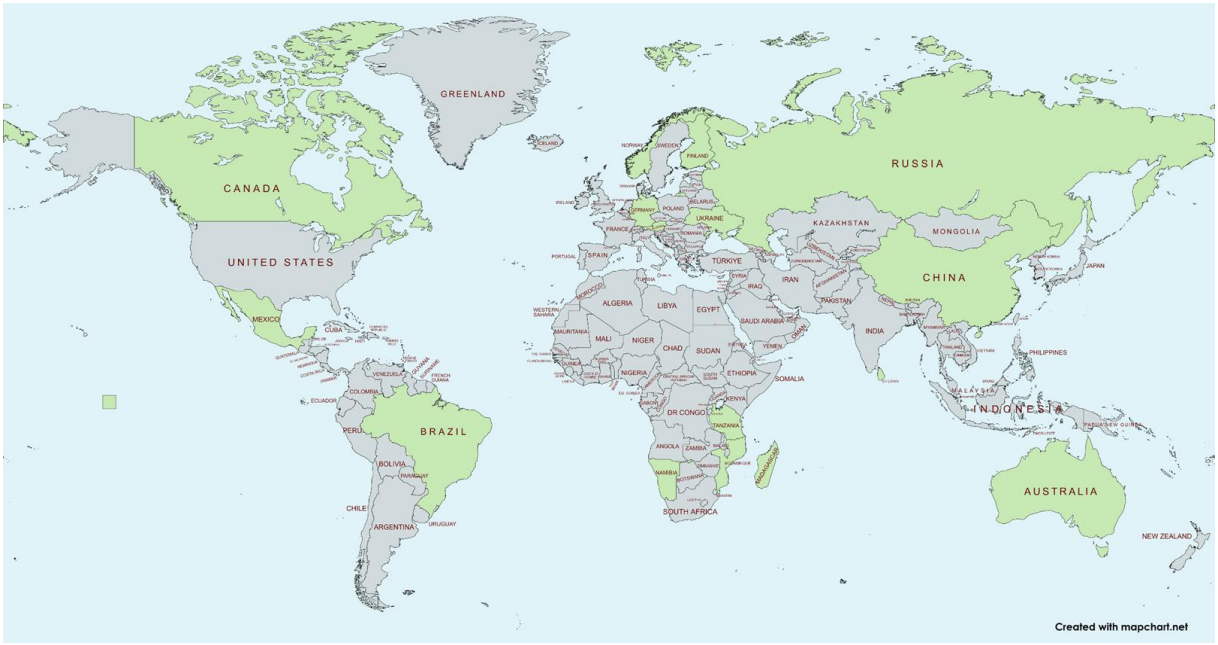

Figure 13 Map of countries where graphite samples were obtained from.

Our analyses mainly focus on flotation concentrates and chemically purified samples. Mineral concentrates for SEM-based automated mineralogy were prepared by conventional

Funded by the European Union

heavy mineral separation techniques. Carbon contents were determined via thermogravimetry, while bulk control measurements were done by instrumental neutron activation analysis (INAA; Technical University of Vienna). The instruments described in this section were utilized at the Technical University of Leoben (Figure 14), with the exception of LA-ICP-MS.

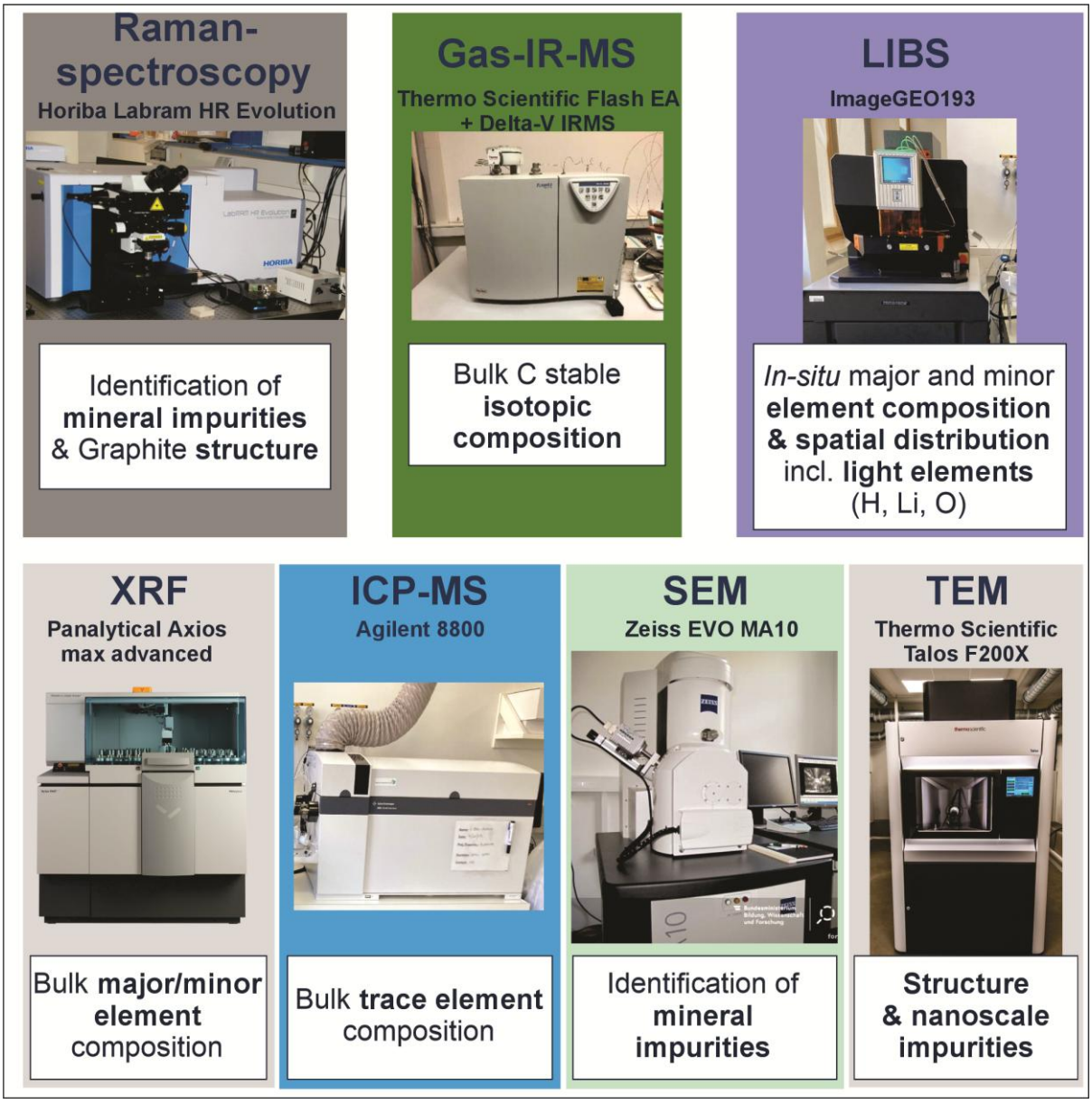

Figure 14 Instruments used for graphite fingerprinting purposes at the Technical University of Leoben.

2.2.2 **Direct measurement of graphite flakes**

2.2.2.1 **Carbon stable isotopy**

Carbon (C) has two stable isotopes and one long-lived radioactive isotope. The stable isotopes are carbon-12 (^{12}C), and carbon-13 (^{13}C). The ratio of these isotopes is reported in the $\delta\,^{13}C$ notation in per mil (‰) relative to the Vienna Pee Dee Belemnite (VPDB) standard according to the following formula:

$$\delta^{13}C_{Sample} = \left(\frac{\left(\frac{^{13}C}{^{12}C}\right)_{Sample}}{\left(\frac{^{13}C}{^{12}C}\right)_{VPDB}} - 1 \right) \times 1000$$

For the analyses, 0.5 mg of graphite concentrates were placed into tin foil containers and subjected to combustion using an elemental analyser (Flash EA 1112) at 1020 °C, while ensuring an excess of oxygen. The resulting CO_2, meticulously isolated through column chromatography, underwent real-time analysis employing a ThermoFisher DELTA-V IRMS isotope ratio mass spectrometer. The isotope ratios ($^{13}C/^{12}C$) of the CO_2 were subsequently cross-referenced with those of a monitoring gas, calibrated against the Vienna-Pee Dee Belemnite (VPDB) standard. The overall analytical procedure is reproducible within the range of 0.2–0.4 ‰.

Most flake graphite deposits show largely overlapping $\delta^{13}C$ values between -20 and -30 ‰ and are thereby indistinguishable via carbon stable isotopy (Figure 15). Exceptions include the Zavallia deposit in Ukraine and the Koivuinemi deposit in Finland (Figure 16) with median $\delta^{13}C$ values below -30 as well as the vein graphite deposit from Sri Lanka, with significantly more positive $\delta^{13}C$ values.

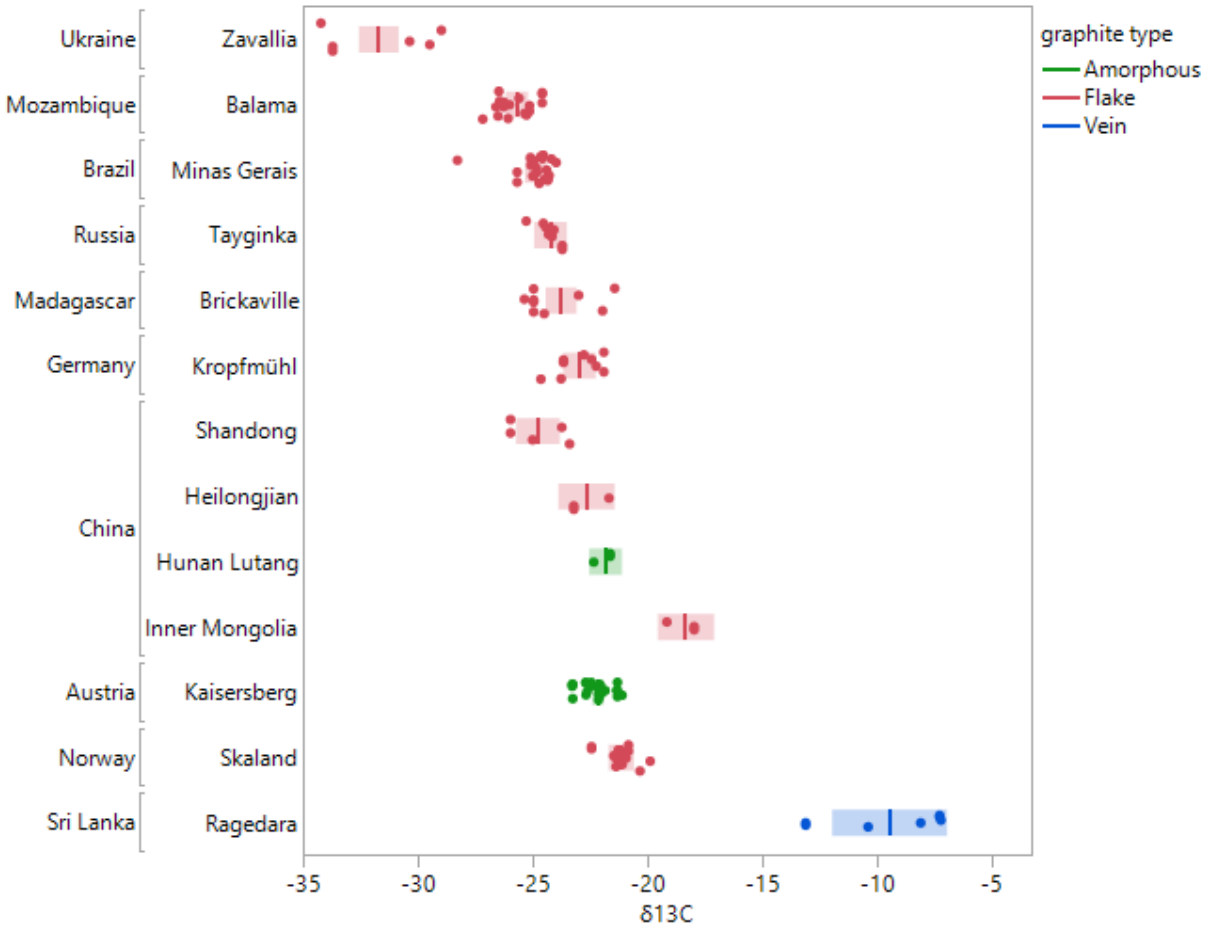

Figure 15 Boxplots showing carbon stable isotope ratios determined in worldwide natural graphite deposits of different formation environments. Amorphous=semi-graphite, Vein=Hydrothermal graphite, Flake=Flake graphite (Dietrich, 2024).

Funded by the European Union

Given these results, carbon stable isotopy is not suitable as a standalone method for distinguishing between flake graphite deposits. On the other hand, it offers opportunities for traceability along the value chain, as carbon isotope ratios remain consistent throughout all purification steps, between raw ore and product (). Further details can be found in Dietrich (2024).

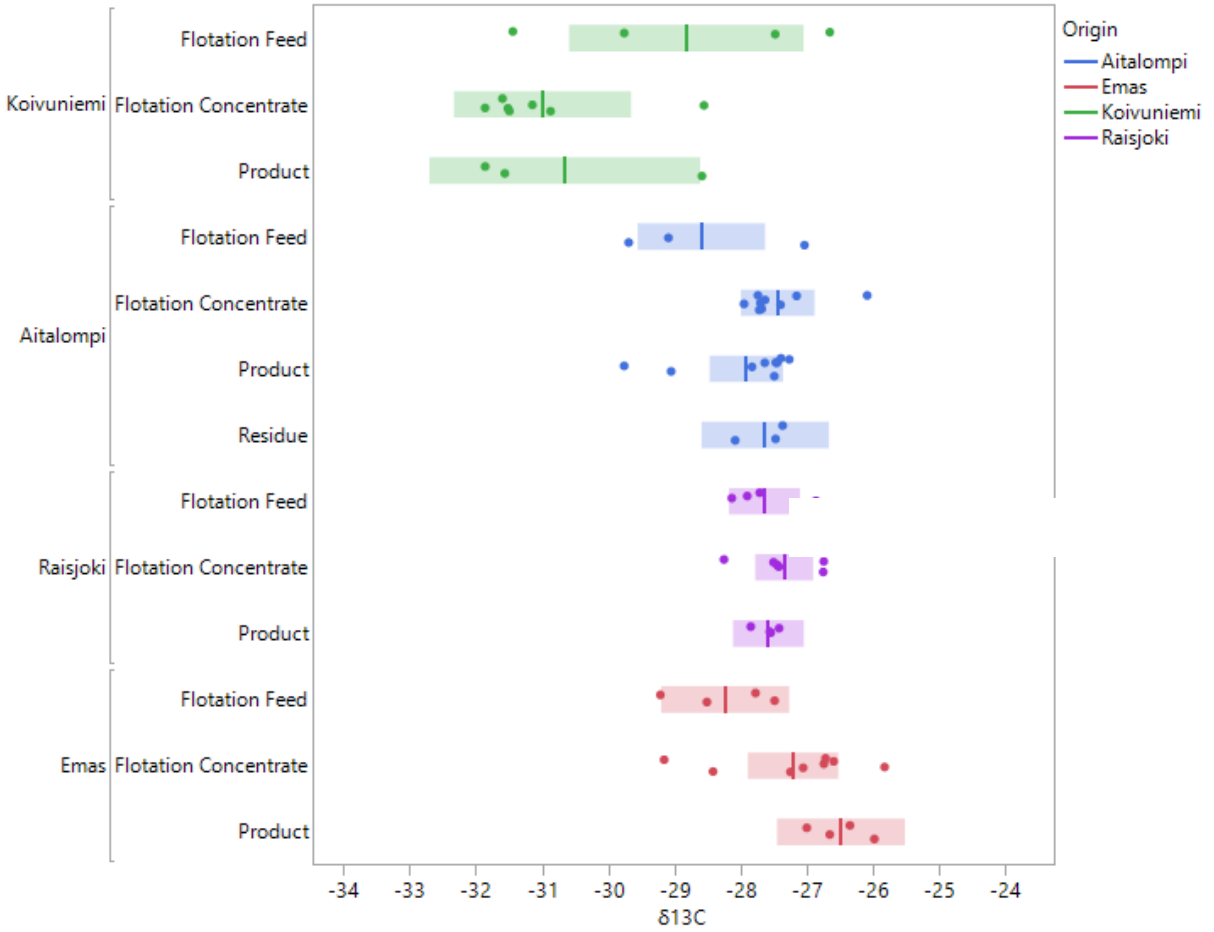

Figure 16 Carbon isotope values from different occurrences in Finland and different intermediate products along the value chain; vertical line in box represents mean value (Dietrich, 2024).

2.2.2.2 **Raman spectroscopy**

Graphitization is the conversion of structurally disordered carbonaceous material to a more ordered structural state. Semi-graphite serves as an intermediate phase bridging the gap between (meta-) anthracite and graphite (Kwiecińska and Petersen 2004). Graphite exhibits a Raman spectrum with several characteristic bands. The most significant Raman bands are the G-band (graphitic band) located around 1580 cm^{-1} and the D-bands (disorder-induced band D1 and D2), typically appearing around 1350 cm^{-1}. In highly crystalline graphite, the D-band is less pronounced compared to the G-band, reflecting the ordered nature of the material (Figure 17). The intensity ratio of the D-band to the G-band I_D/I_G is used as a parameter to assess the degree of disorder and defects in graphite. In addition, the second order band S1 around 2700 cm^{-1} can also be considered (Rantitsch, 2023).

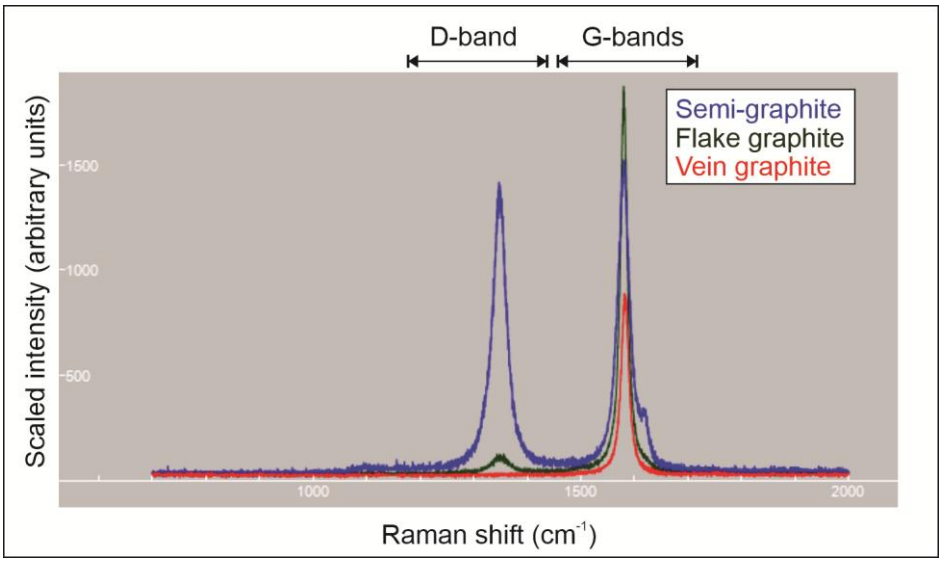

Figure 17 Typical Raman-spectra of different graphite types. Modified after Dietrich (2024).

Raman spectra were obtained using a Horiba Labram HR Evolution instrument equipped with a 100mW Nd:Yag (532nm) laser, a confocal microscope (hole aperture=100µm), a 1800 g/mm grating and a Peltier cooled CCD detector. Ca. 5-10 % of the full laser power of 100 mW was applied in order to avoid sample damage. For laser focusing and sample observation, an Olympus BX 40 microscope with a 100x objective lens was employed. In order to enhance signal-to-noise ratios, two scans were accumulated with an acquisition duration of 20 seconds within two distinct spectral regions: 700–2000 cm^{-1} (first-order) and 2200–3200 cm^{-1} (second-order). In total, 20 spectra were recorded for each sample and the calibration of band positions was achieved using a silicon wafer standard.

Important parameters describing the Raman-spectra of graphite, including D-band, G-band and S1-band positions, their maximum intensities and scaled total areas, were extracted using iFORS software (Lünsdorf et al. 2017). This numerical input was used for data analysis purposes. Linear discriminant analysis (LDA) reveals that, similarly to carbon stable isotopy, different types of graphite are distinguishable via Raman-spectroscopy (Figure 18a), however, as a standalone method it is not suitable for differentiating between the geographic origin of flake graphite deposits (Figure 18b). Here, continent-level results are presented, while deposit-level or country-level attempts for differentiation were similarly unsuccessful. This is the result of the fact that good crystallinity is a prerequisite for high-quality graphite (which is true for all of our flake graphite samples). Further details can be found in Dietrich (2024).

Funded by the European Union

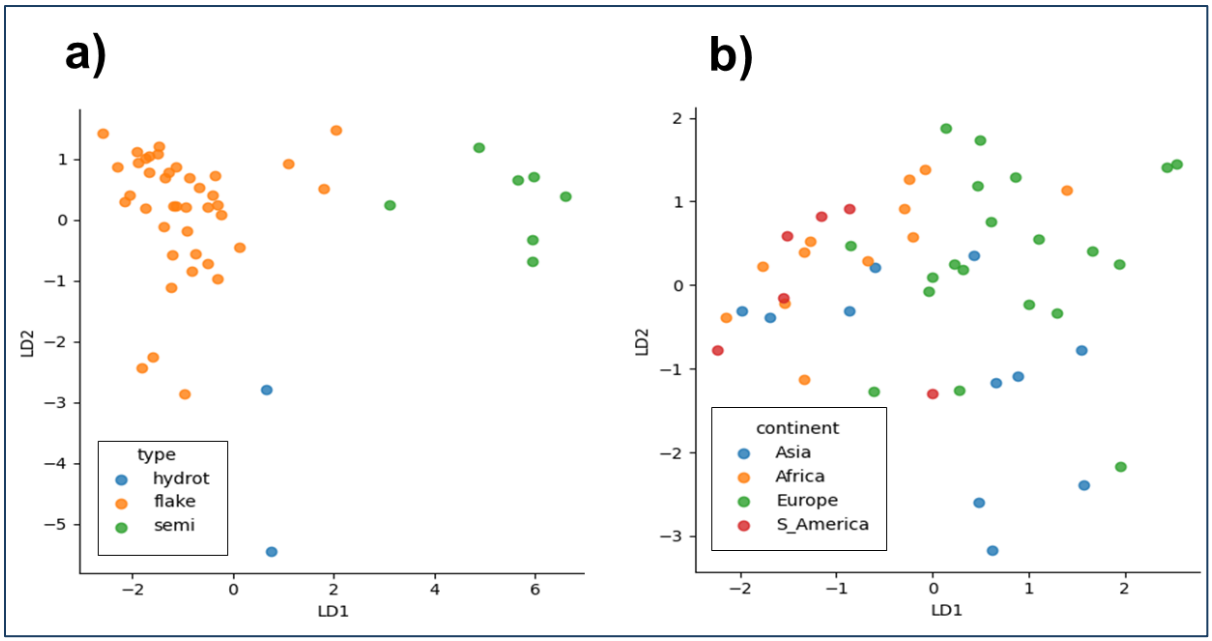

Figure 18 Linear discriminant analysis performed on numerical parameters extracted from the Raman-spectra of graphite concentrates. a) Differentiation between different types of graphite b) Flake graphite concentrates of different geographic origin.

2.2.3 **Bulk methods**

2.2.3.1 **X-Ray diffraction**

Most flake graphite ores contain less than 50% graphite, while graphite flake concentrates obtained after grinding and flotation reach typically 90–95% graphite content. Therefore, the largest amount of minerals is rejected during physical processing. We applied X-ray diffraction to raw ores and to several intermediate products obtained via physical purification to identify the dominant mineral phases and to see mineralogical differences between deposits, and if any significant mineralogical changes happen in the first steps of the value chain.

XRD was performed by a Bruker D8 Advance diffractometer, with Cu Kα radiation, a Soller slit, and a fixed divergence aperture (0.2 mm), equipped with LynxEye Super Speed strip detector, at a tube current 40 mA and a voltage of 40 kV. The measured angle range was between 5 and 70° with a step size of 0.01° per second. For graphite concentrations, a step size of 0.005° per second was used to improve the resolution of the diffractograms. The diffractograms were evaluated using ICCD PDF4+ database with the DIFFRACplus EVA subprogram. Rietveld refinement was performed using TOPAS 5 software to quantify the phases. To determine the graphite particle size, the Scherrer equation was used (Scherrer, 1912).

Figure 19 presents a comparison between raw ores from various world-class flake graphite deposits. While the number of available samples is largely limited, the quantitative mineralogical comparison of graphite ores from different graphite deposits shows significant differences between different deposits, therefore either the ratio of different mineral phases or their absolute concentration can be diagnostic of certain deposits.

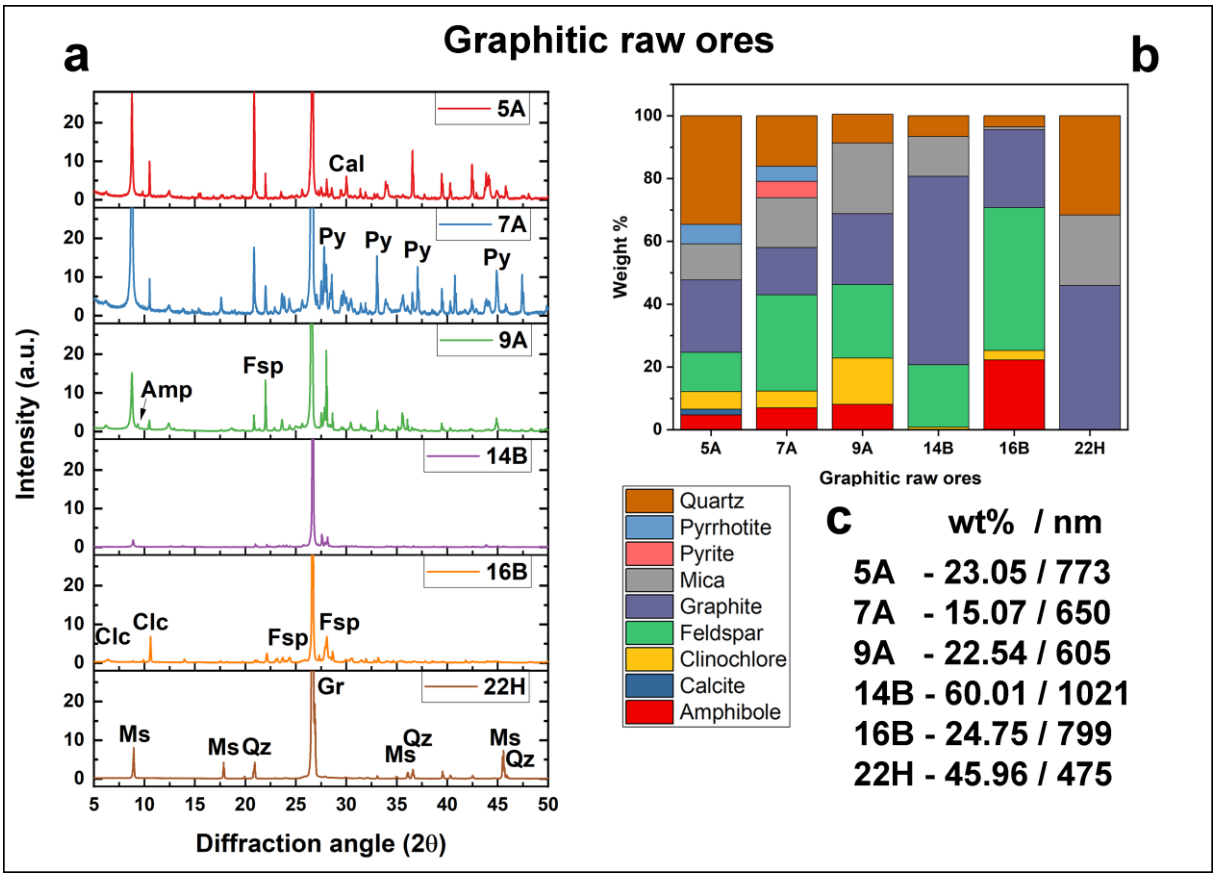

Figure 19 a) XRD patterns of graphitic raw ores; 5A to 22H refer to samples from different deposits: 5A: Finland, Emas; 7A: Finland, Raisjoki; 9A: Finland, Koivuniemi; 14B: Germany, Kropfmühl; 16B: Norway, Skaland; 22H: Mozambique, Syrah b) their quantitative mineral compositions and c) the calculated amount in wt% and average crystal size of graphite. Amp – Amphibole; Cal- calcite; Clc – clinochlore; Fsp – Feldspar; Gr- graphite; Ms – Mica; Py – pyrite; Qz – quartz (Dallos et al., under review).

From the first grinding step (P1) to the last flotation step (P4) the major peak positions do not change, meaning that the major mineral phases remain the same in the concentrates. However, their quantity gradually decreases until the last step (Figure 20a). It is also apparent at the physically purified concentrates, that the peaks of gangue minerals become rare and low in intensity (Figure 20b). Rietveld refinement is therefore not possible and X-ray diffraction cannot quantitatively resolve differences between deposits at this purity stage or further along the value chain. On the other hand, qualitative differences as well as potentially the appearance of the rhombohedral graphite phase and amorphous background can help tracing the origin of graphite or the processing facility. Further details can be found in Dallos et al. (under review).

Funded by the European Union

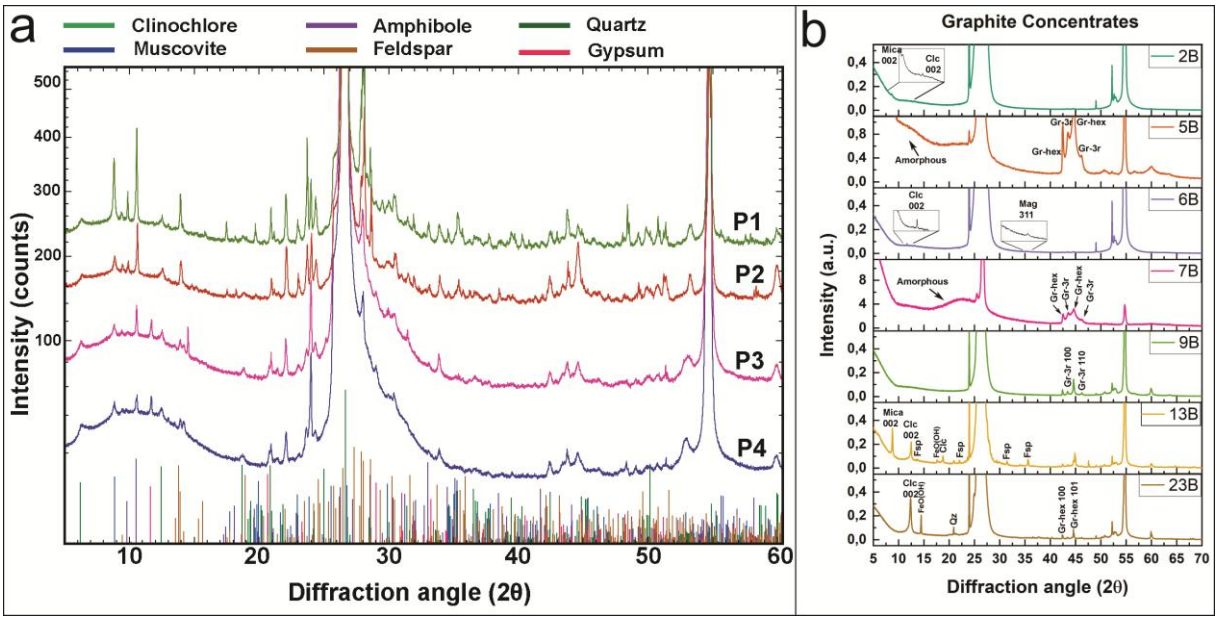

Figure 20 a) XRD pattern of flotation series P1-P4 b) XRD Patterns of graphite concentrates, Clc – clinochlore; Fsp – feldspar; Gr-hex – hexagonal graphite; Gr-3r – orthorhombic graphite; Mag – magnetite; Qz – quartz (Dallos et al., under review).

2.2.3.2 **X-Ray fluorescence**

X-Ray fluorescence (XRF) provides a simple and straightforward means for the bulk analysis of geological materials, making it a standard method for the bulk analysis of rock powders. LIBS analyses shed light on the actual nature of graphite concentrates (see Chapter 2.2.3.1), essentially being a mixture of graphite flakes and other mineral phases, rendering the application of XRF for the bulk chemical analysis of graphite products logical.

For this purpose, pressed graphite pellets were prepared by a conventional hydraulic press. 10^5 N force was applied to prepare pellets of 32 mm diameter and 2-3 mm thickness without additional binding matter.

XRF analyses were performed by a wavelength dispersive XRF Panalytical/Malvern Axios instrument with a semi-quantitative calibration. Carbon content was determined independently via thermogravimetry, which was used for matrix correction and to test if the total amount of element oxides and carbon made up 100 %. 2-3 pellets were analysed from each sample; each pellet was measured from both sides to check for potential heterogeneity and fractionation phenomena. Currently, the preparation of a standard series from high-purity graphite powder and certified rock powder standards is in progress. This will enable a fully quantitative workflow.

XRF was tested on our graphite concentrates and chemically purified products. Na, Mg, Al, Si, S, K, Ca, Fe and Cu were measured in all concentrates, usually in the 100s to 1000s ppm range. P, Cl, Ti, V, Cr, Mn, Co, Ni, Zn, Zr and Mo were detected in most samples, usually in the range of few tens of ppm. F, Ga, Se, Rb, Sr, Y, Ru and Pb were also detected, usually below 50 ppm. The exact detection limits are to be defined once the standard series are available as well as the peak positions and measurement times have been optimized. The obtained concentrations were also cross-checked with other bulk methods, with a very promising match for most elements, including some elements with a concentration below 100 ppm (Figure 21a). The first set of results already shows that the number of variables is significant, and major differences are observable between different deposits. Linear discriminant analysis (LDA) shows that the dataset is suitable for distinguishing between different deposits (Figure 21b). While this approach with LDA does not show if unknown

samples can be classified correctly, it rather serves as a proof of concept that the deposits are theoretically distinguishable. For multivariate classification and to determine the correct prediction probability, at least several hundreds of analyses per deposit would be preferable. This is not feasible in the current project, while it could be a potential approach in routine traceability applications, where comprehensive databases are available.

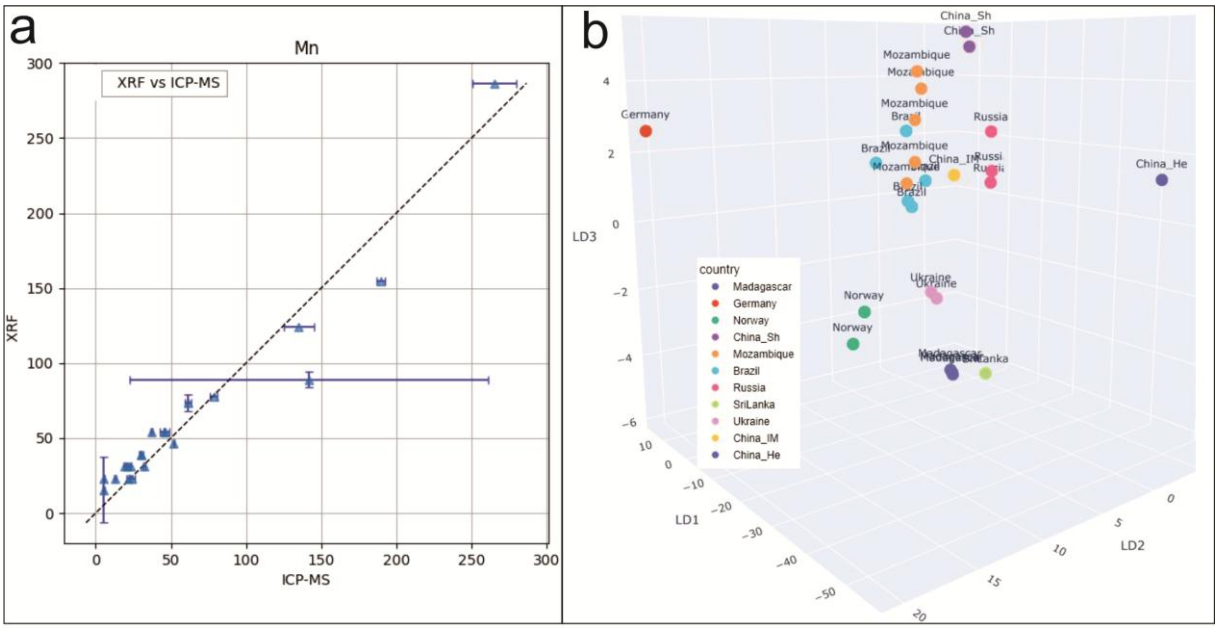

Figure 21 a) Comparison of Mn concentrations determined in natural graphite concentrates by XRF and solution ICP-MS b) Linear discriminant analysis based on XRF data. Here, the first three linear discriminants are plotted.

2.2.3.3 **Inductively-coupled-plasma-mass-spectrometry**

Solution-based inductively-coupled-plasma-mass-spectrometry (for details see Table 1Table 1 Solution ICP-MS analytical settings.

) was performed in the first year of the project without prior knowledge of the types of impurities in graphite concentrates. The primary goal of these analyses was to obtain a comprehensive list of elements that can be potentially found in graphite products and use the resulting dataset for multivariate classification if possible.

ICP-MS Agilent 7500cx		
Standard solutions	Merck VI, AHF-CAL-7	
Mode	No gas mode	Gas mode
Nuclides monitored (m/z)	24Mg, 27Al, 43Ca, 57Fe, 71Ga, 82Se, 85Rb, 88Sr, 97Mo, 107Ag, 111Cd, 137Ba, 89Y, 139La, 140Ce, 141Pr, 145Nd, 146Nd, 147Sm, 149Sm, 151Eu, 160Gd, 159Tb, 161Dy, 163Dy, 165Ho, 166Er, 167Er, 169Tm, 172Yb, 173Yb, 175Lu, 232Th, 205Tl, 207Pb, 238U	51V, 53Cr, 55Mn, 59Co, 62Ni, 65Cu, 66Zn, 75As

Table 1 Solution ICP-MS analytical settings.

For the ICP-MS analyses, conventional microwave digestion was applied by an Anton Paar Multiwave PRO closed-vessel digestion system, equipped with a 24HVT50 rotor and 30 mL PTFE vessels, was used for the microwave digestion of natural graphite concentrates. Approximately 0.2 g of graphite sample was weighed into PTFE digestion vessels directly

Funded by the European Union

and mixed with 5 mL of 4M HNO3 and 1 mL of H2O2 (w=30%). The microwave program was set to a maximum temperature of 200 °C, reached within a ramp time of 10 min, and held for 15 min. The ICP-MS analytical settings including the measured isotopes are summarized in Table 1. Notably, no Si, K and Zr were measured. 100µL portions of a 100 ng mL−1 In and Re internal standard solutions (CertiPur, Merch Darmstadt, Germany) were added to 5.0 mL of each sample solution and to the calibration solutions to correct for instrumental drift. Three independent digestion replicates were analysed from each sample. Additionally, total procedural blanks, containing the same amount of concentrated HNO3 and H2O2 used for sample decomposition, prepared in the same manner as the samples, were analysed. Two independent analysis runs were conducted, one for the analysis of non-Rare Earth Elements and one for REE. Further details can be found in Dietrich (2024).

Notably, all listed isotopes were reproducibly measurable in all analysed samples. The three independent replicates commonly showed variability below 5%, suggesting a high degree of homogeneity within the samples. To assess, whether solution ICP-MS data are reliable, the dataset was compared to data obtained by INAA (Figure 22). Overall, the comparison shows a good agreement between the datasets down to the level of 10s of ppb (Figure 22a). On the other hand, there is a systematic tendency towards false low concentrations determined by ICP-MS for higher concentrations (Figure 22b). Given our current knowledge about the existence of mineral impurities in graphite concentrates, it is reasonable to assume that certain resistant mineral phases were not dissolved by 4M HNO3 accounting for the systematic low concentrations of elements such as Ba, Ce, Fe, La, Lu, Sm and U. This is well-documented phenomenon in bulk chemical analysis of rock powders (e.g. Meisel et al., 2022). Further digestion approaches, such as alkaline fusion, remain to be tested on graphite concentrates.

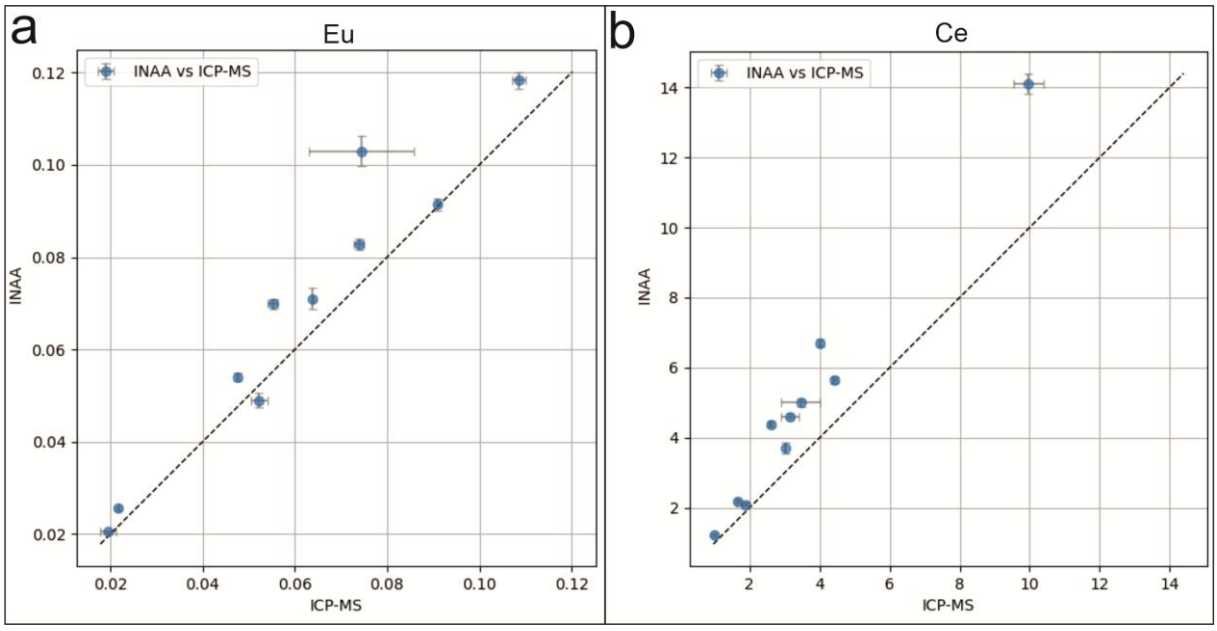

Figure 22 Comparison of concentrations (in ppm) measured in graphite concentrates via INAA and solution ICP-MS a) Good agreement between the two datasets at sub-ppm level b) Lower concentrations determined by solution ICP-MS compared to INAA.

The 38 isotopes measured resulted in a multivariate dataset with many variables and few repeated measurements with significant differences between individual deposits. Considering specific sets of elements, for example chondrite-normalized REE patterns,

systematic differences can be observed between different deposits, while patterns remain consistent in the same deposits throughout several years (Figure 23).

To test the hypothesis that mineral-related chemical signals can be measured also after chemical purification, trace element patterns of physically purified (grinding and flotation) concentrates were compared with a chemically purified (6B) sample (Figure 23). The chemically purified sample shows significantly lower but still measurable trace element contents, including all trace elements.

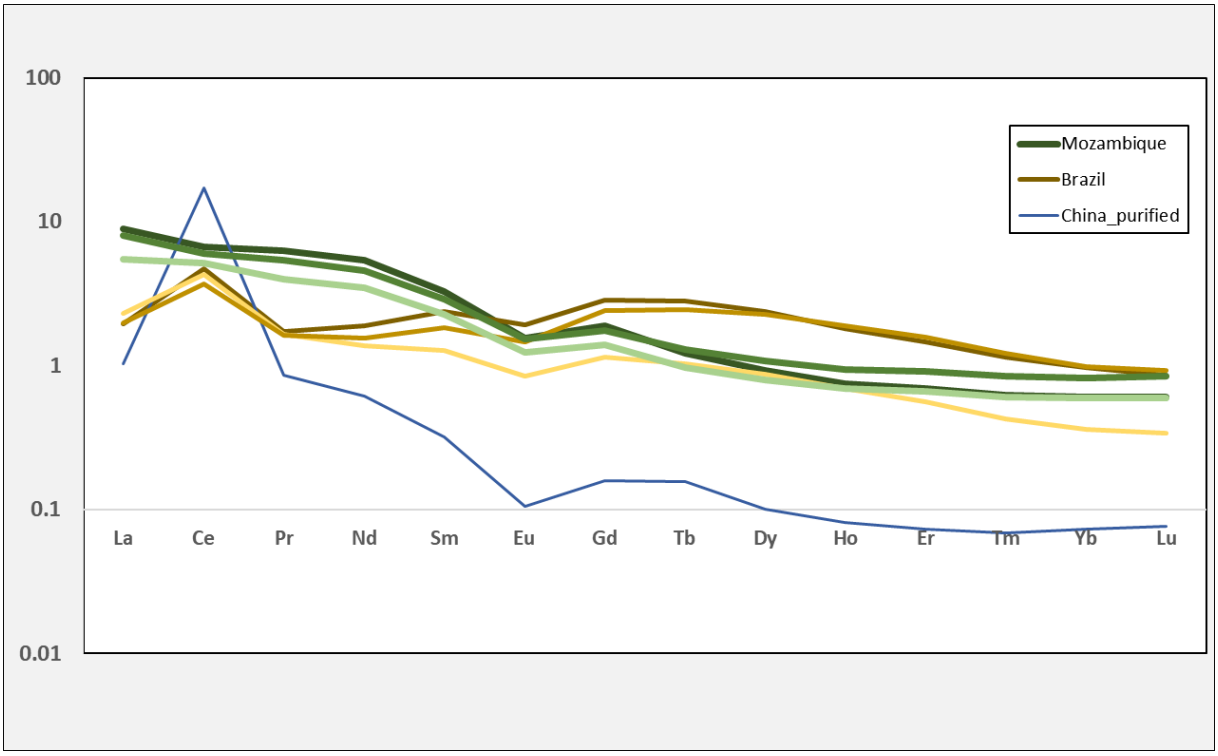

Figure 23: CI-normalized REE patterns of graphite concentrates based on solution ICP-MS analyses. Samples from three different years from Mozambique and Brazil, respectively. The sample from China is chemically purified.

LDA shows (Figure 24) that the multivariate datasets are highly specific and due to the number of variables, the separation of groups is even more clear and within-group variance is even smaller (i.e., different samples from the same deposit plot closer together) than in the case of XRF. Notably, the small number of repeated measurements does not allow for machine-learning-based multivariate classification. As such, the LDA plot has a limited practical meaning and solution ICP-MS can only be used for routine traceability tasks if a large database with many repeated measurements of the same deposit is available. On the other hand, solution ICP-MS could be a suitable method for generating robust multivariate

Funded by the European Union

datasets even from chemically purified graphite products in the future, if the correct digestion method is applied.

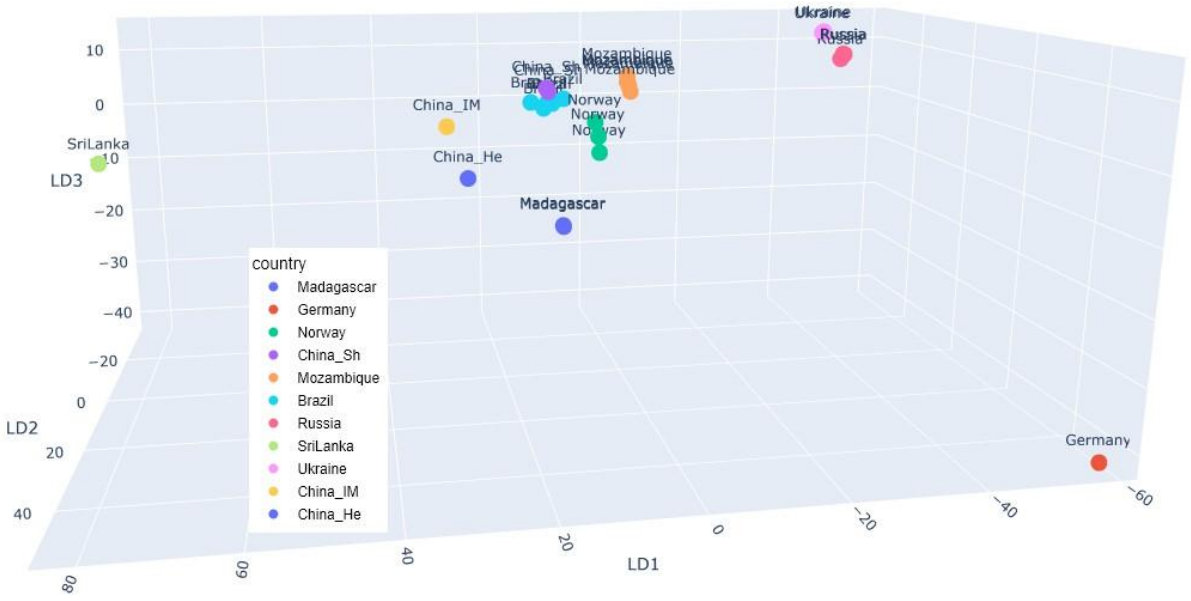

Figure 24 Linear discriminant analysis based on solution ICP-MS data. The first three linear discriminants are plotted.

2.2.4 **In-situ methods**

2.2.4.1 **Laser-induced-breakdown-spectroscopy**

Due to its chemical and thermal resistance, the in-situ chemical analysis of graphite is particularly challenging. Accordingly, the knowledge of the chemical composition of graphite products was hitherto largely limited to bulk methods. Key questions remained open with the lack of in-situ analyses regarding the nature and origin of impurities in natural graphite products and whether they can be used to fingerprint graphite deposits for traceability purposes. LIBS is a fast and efficient in-situ spectroscopic technique for detecting a series of elements simultaneously in various matrices (e.g., Harmon and Senesi, 2021) and it is therefore ideally suited for answering the above questions.

From each sample, 250 mg of flake graphite powder was extracted from different parts of the bags by a small spatula and loaded into a conventional hydraulic pellet press without a binding matter. The 13mm dies were loaded by 4 tons for two minutes for each pellet. The pellets were then mounted on glass slides, carefully levelled with the top of the sample drawer and placed in the laser-ablation chamber. Spectra were obtained by an ESLumen LIBS coupled to an ImageGEO193 laser-ablation system, comprising a 193 nm excimer laser and a two-volume (TwoVol3) ablation chamber (Figure 25). The laser is delivered to the sample through an XYR beam aperture and for LIBS analysis, the emitted light from the laser-induced plasma is collected by an optical fibre inserted directly into the laser-ablation chamber (see Manard et al., 2022) for details. The fibre optics consist of a 5-channel spectrometer with fixed-grating Czerny-Turner design, covering a spectral range from 188 nm to 1099 nm via a Complementary Metal-Oxide Semiconductor (CMOS) detector. The LIBS fibre was calibrated by using NIST SRM 612 glass for maximum intensity across the LIBS spectrum. Alignment consists of an X–Y adjustment of the LIBS fibre via adjustment screws (Figure 25C) and the Z-position of the sample is fixed to always keep the same depth into the analytical cup within the ablation chamber. The LIBS maps were acquired over an area of 1 mm × 1 mm on one to five samples from each deposit, by ablating with 100 mm × 100

mm rectangular spots and 90 mm overlap in X and Y directions, corresponding to a nominal 10 mm × 10 mm X–Y resolution. By this approach, high resolution 2D maps could be constructed, while maintaining high signal intensity due to larger spot size. 100 Hz laser frequency and ca. 13 J cm−2 laser fluence was applied in He atmosphere, flushed at a 1000 ml min−1 rate. The described settings resulted in a scan speed of 1000 mm s−1, which resulted in the acquisition of a 1 mm × 1 mm map within 100 seconds. All measurements were acquired within a single day (Arató et al., 2025).

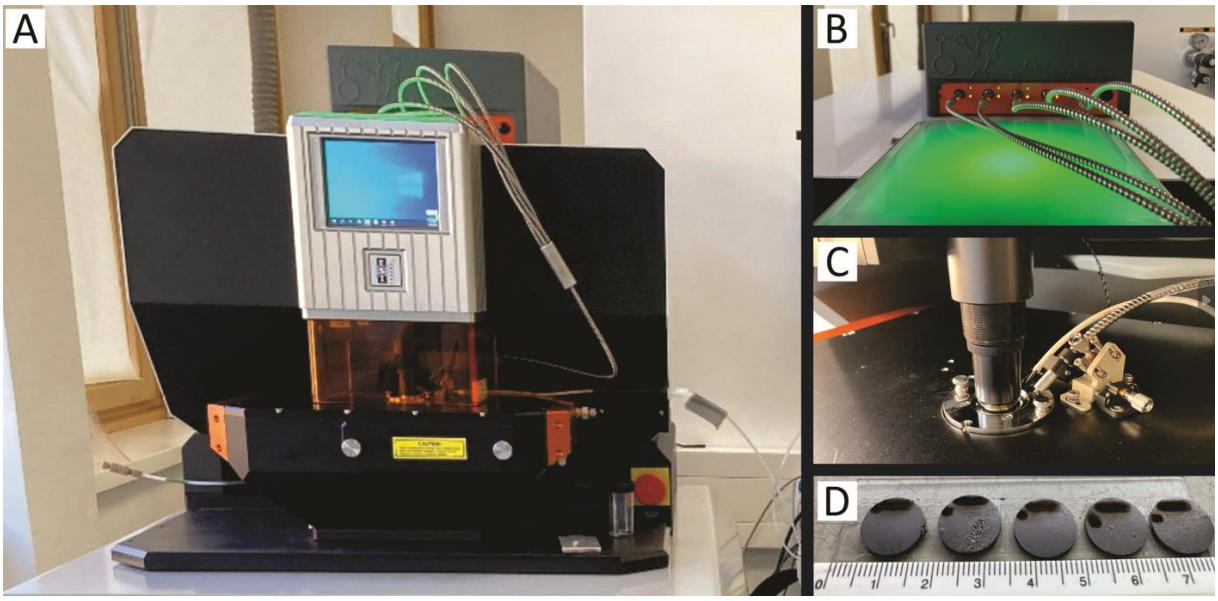

Figure 25 A) ImageGEO193 laser-ablation system. B) ESL Lumen LIBS unit. Each fibre is responsible for a wavelength range, adding up to a spectrum from 188 to 1099 nm. C) LIBS optical fibre entering the laser-ablation-chamber with a horizontal and a vertical adjustment screw for fibre alignment D) pressed pellets of graphite concentrates used for analysis.

LIBS spectra were processed in the 'iolite' v4 software (Elemental Scientific Lasers, Paton et al., 2011). Data processing within iolite included atomic emission line identification, intensity integration within selected spectral windows, normalization and the creation of 2D elemental images. Spectral windows for the characteristic optical emission lines of individual elements were manually set.

Funded by the European Union

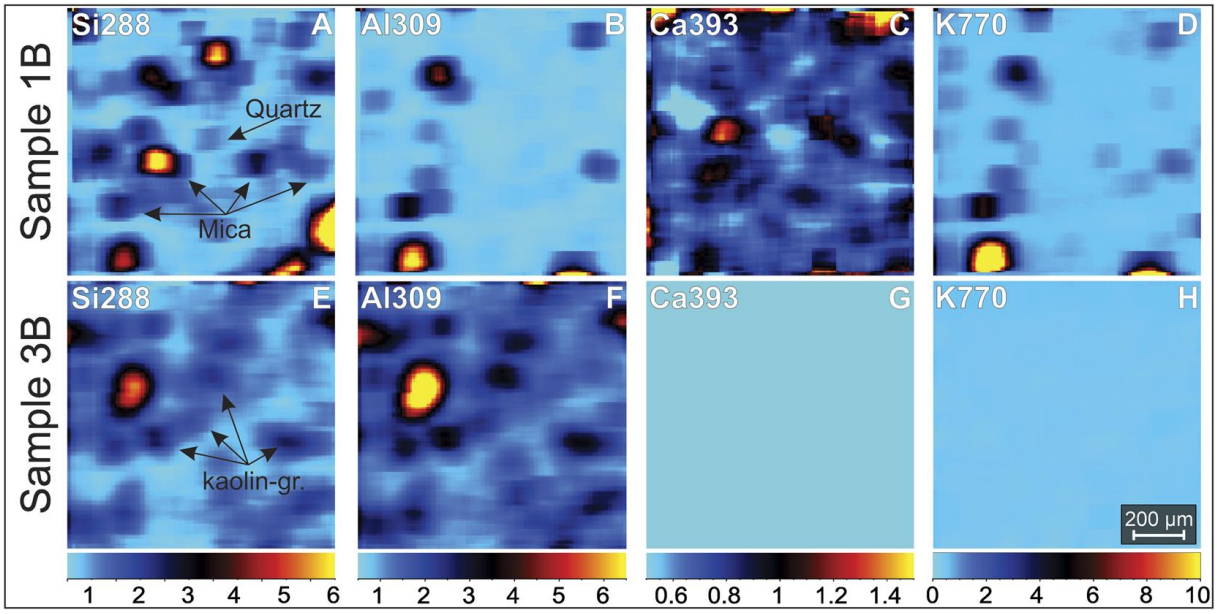

Figure 26 A–D) Representative elemental maps of a sample (1B) with abundant mica. E–H) Representative elemental maps of a sample (3B) with abundant kaolin-group minerals. Units are in 1000 counts. Note the different intensity ranges (Arató et al., 2025).

LIBS mapping shows that chemical inhomogeneities are omnipresent in all studied concentrates, an aspect to be considered for all analytical methods applied for graphite analysis. Based on the spatial relationship of the detected elements, it is also obvious that most chemical impurity elements stem from silicate minerals (Figure 26). Due to the processing of the concentrates via grinding and flotation, the suite of abundant minerals in the concentrates is restricted to a few mineral species with a similar hydraulic behaviour to graphite, most notably sheet silicates. Despite this, there are notable differences in the mineralogical composition of the deposits. As a result, the chemical fingerprint of graphite concentrates is a signature controlled by graphite and gangue minerals. This is in accordance with the mineralogical results (e.g., SEM-based automated mineralogy) and transmission electron microscopy observations and explains the chemical signatures obtained by bulk methods as well.

The real power of LIBS datasets lies in the multivariate nature of the collected data and the large number of repeated measurements. In this application, 100 complete spectra are obtained per second, resulting in a dataset comprising more than 300000 spectra for this set of samples (n=33). Even if there is no obvious chemical difference between deposits in terms of certain elements, the entirety of the acquired dataset is deposit-specific. The random forest classifier shows a robust overall deposit-level classification accuracy of ~93%, if 80% of all spectra are used for training and 20% for testing. While the model numerically does not overfit the data, given the extreme heterogeneity within and between samples, it is difficult to argue that a 1 mm × 1 mm map is sufficient to classify an entire deposit. To test the generalization potential of the model, entire samples should be left out from training and used for testing, rather than using 80% of the entire dataset for training and 20% for testing. If several samples are available from individual deposits covering a large range of variability, the correct classification of unknowns is possible, which is promising for potential routine applications in the future. If only deposits represented by four or more samples are included (Figure 27A), classification accuracy reaches ~65%. This is achieved by testing all combinations where one entire sample is left out for testing from each deposit and the other samples are used for training. This result shows the severe effect if we have no control over the geological heterogeneity of the deposits and the changes in processing practices,

Funded by
the European Union

which can both have a large impact on the chemical signature of the traded material. Low classification accuracy in the case of Madagascar is also diagnostic, as it can reflect different provenance (e.g., different mines from the same deposit), changing processing practices over years, on-site mixing or within-deposit heterogeneity. The results also showcase that, in this context, the amount and versatility of the available sample material is of greater importance than the choice of the classifier and its hyperparameters. Figure 27B demonstrates that if the underlying training data describes the test population well (i.e., the highly heterogeneous Madagascar deposit is not included), a correct prediction is made with a high probability. See Arató et al. (2025) for further details.

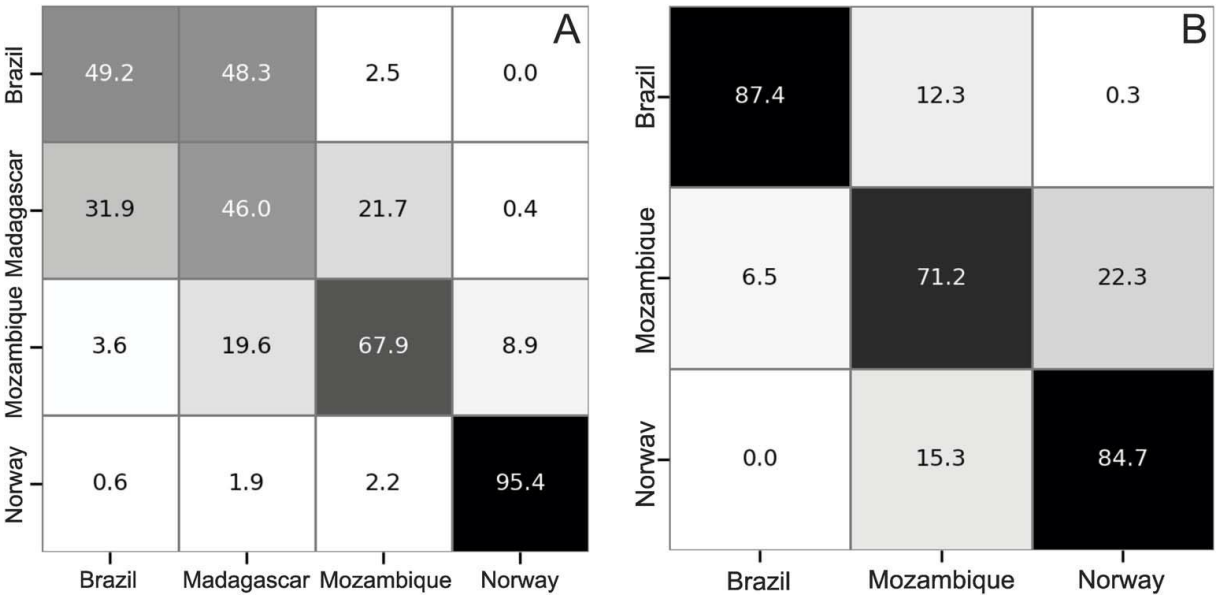

Figure 27 Confusion matrix of graphite concentrates with at least four samples, obtained by leaving out an entire sample when training the random forest classifier and using that sample for test. The number of correctly classified spectra is seen in the diagonal in percent. A) All combinations considered. B) Combinations considered excluding Madagascar samples (Arató et al., 2025).

These findings make LIBS a strong candidate for becoming a standard tool in graphite traceability and material fingerprinting tasks. The applicability of the same approach remains to be tested on chemically purified samples. This would require at least four purified samples from at least three deposits, meaning a series of leaching experiments by dangerous chemicals, such as hydrofluoric acid.

2.2.4.2 Scanning-electron-microscopy-based mineralogy

It became obvious from bulk analyses and LIBS results that the chemical signature of natural graphite concentrates is dominated by gangue minerals. To investigate the gangue mineral phases in detail, accessory minerals in physically purified natural graphite concentrates in the MUL collection (ca. 95% purity) were separated from graphite via conventional heavy liquid separation. Chemically purified, battery-grade, samples were subjected to the same procedure.

The separated mineral impurities were embedded in epoxy for further analysis. For morphological and chemical analysis, an SEM-EDS system (Carl Zeiss SmartPI™) was used. Each mineral phase was verified using Raman spectroscopy, and a database was created for automatic phase identification.

The most common mineral impurities in the graphite concentrates include quartz, mica, plagioclase, and iron oxides; at some localities, amphiboles, pyroxenes, talc, apatite, titanite, and sulphides are also found. The main phases detected align well with X-ray

Funded by the European Union

diffraction results from bulk graphite concentrates and enable to distinguish between graphite deposits via straightforward decision trees relying on the relative abundance of individual mineral phases (Figure 28).

Figure 28 a) A possible decision tree to distinguish between traded graphite concentrates based on their mineral impurities (δ>2.46 g/cm³). All values are in area%. b) Traceability of the mineralogical signature along the value chain.

While physically purified concentrates yielded hundreds or even thousands of mineral grains, the question arose whether these minerals can be found in chemically purified products at all. As a result of chemical purification, some mineral phases are completely removed, reducing the relative mineral impurity ratio. Conversely, the more resistant mineral phases (e.g., titanite, rutile, zircon) become enriched in the "heavy" fraction (Figure 28b), allowing traceability along the value chain even at the 99.99% purity level.

While mineral abundances are useful for creating straightforward decision trees, SEM also yields EDX data for all measured phases. This means that a multivariate chemical dataset is available for all analysed samples with many repeated measurements, ideally suited for machine-learning-based classification. Random forest classification shows promising results for concentrates and for chemically purified samples alike (Figure 29).

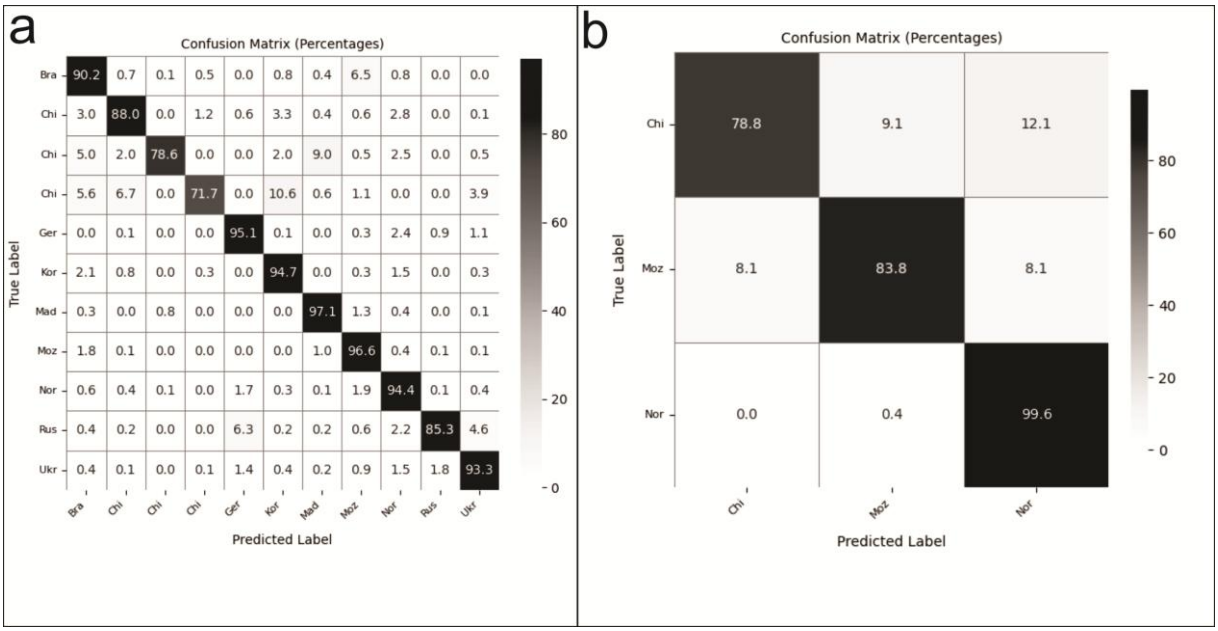

Figure 29 Results of random forest classification based on the SEM+EDX dataset obtained on mineral concentrates separated from graphite products. a) concentrates b) chemically purified samples.

2.2.4.3 **Transmission electron microscopy**

While LIBS revealed the ubiquitous nature of gangue minerals, several details remained unclear. What is the size distribution of gangue minerals? Are there also other sources of elemental impurities, such as processing-related impurities and eventually elemental impurities in the graphite structure? Therefore, we performed nano-scale elemental mapping on selected samples.

The measurements were carried out using a Talos F200X transmission electron microscope in scanning mode (STEM) equipped with an energy dispersive X-ray (EDS) system. The samples were gently mixed with ethanol in an agate mortar, and a drop of the suspension was deposited onto a lacey carbon-covered Cu grid (Ted Pella). Element mapping was done on a 512x512 pixel image with a dwell time of 40 µs. For data processing, the Velox software was used.

STEM-EDS maps show that mineral impurities can be found down to the nm size, attached to the surface of graphite (Figure 30). The presence of such small mineral impurities in the concentrates and the commonly observed graphite – sheet silicate intergrowths make it nearly impossible to completely remove mineral impurities by purification. This offers the theoretical opportunity to trace graphite concentrates along the value chain via mineral impurities. However, due to the significant costs related to individual STEM-EDS analyses, the technique is not suited for routine traceability tasks, but rather for second-tier applications, if inconsistencies/fraud is suspected in the production chain.

Funded by the European Union

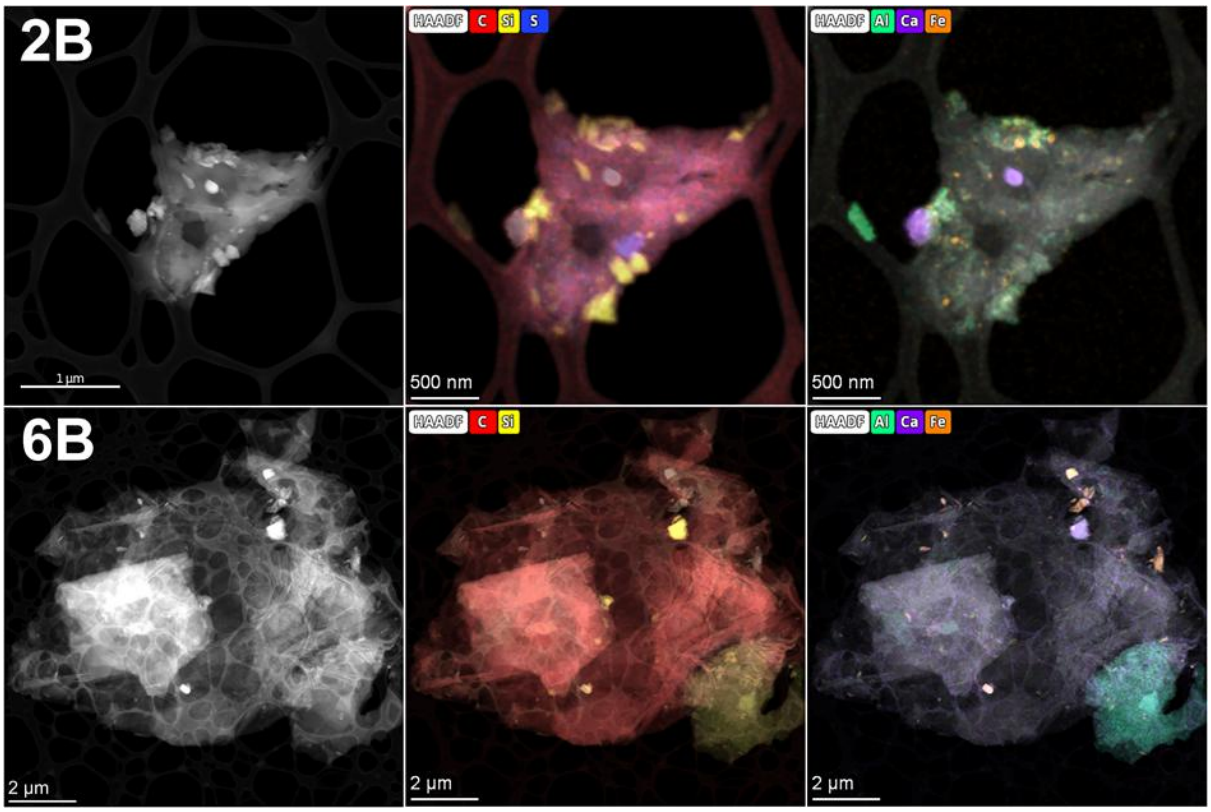

Figure 30 STEM-HAADF and EDS maps show the size and the chemical composition of nanometre-sized gangue minerals in flake graphite concentrates from two different deposits (Dallos et al., under review).

2.2.4.4 **Laser-ablation-inductively-coupled-plasma-mass-spectrometry**

LA-(SC or Q)-ICP-MS is a standard in-situ analytical tool, which excels at the quick multi-elemental analysis of various matrices, including geological materials. The method can detect elements down to the ppb level and generate quick and robust multi-elemental datasets, making LA-ICP-MS ideally suited for material fingerprinting (e.g., Gäbler et al., 2011). The evaluation of graphite LA-ICP-MS results is still in progress.

LA-ICP-MS analyses of graphite concentrates were performed at the Geological Survey of Finland (GTK), using a Nu AttoM SC-ICP-MS (Nu Instruments Ltd., Wrexham, UK) coupled with an Excite 193nm ArF laser-ablation system (Photon Machines, San Diego, USA). The mass spectrometry was tuned with NIST612 glass using a 40% output on 5mJ, a repetition rate of 10Hz, a circular spot of 50 µm. The laser was run at a pulse frequency of 10 Hz and a pulse energy of 5 mJ corresponding to an energy flux of about 10-15 J/cm2 on the sample surface in a line raster mode of 135µm circular spots. Prior to analysis, each line was pre-ablated with at 530 µm/s ablation speed. Each analysis was initiated with a 20-second baseline measurement followed by 60-90 seconds of signal acquisition. These analyses were made using time-resolved analysis (TRA) with continuous data acquisition for each set of lines (generally following the scheme of 2 primary standards and 15 unknowns).

An in-house spiked synthetic pressed nanopellet of graphite standard was used for external standardisation. The isotope 13C has been used as an internal standard, assuming a content of 98 wt.% carbon. The measurements were performed on 68 isotopes covering 61 elements at low resolution ($\Delta M/M = 300$) using the Fastscan mode. Data reduction including baseline subtraction, signal integration and quantification was done by the software GLITTERTM (Van Achterbergh et al., 2001). As there was no other matrix-matched material available for quality control, the analytical precision and accuracy were monitored by

treating Gh20220218 as an unknown. The results suggested a relative standard deviation (RSD) of 10-40% for all elements except Li, Ni, Ba, Bi, and an accuracy of ±5-10% for most elements except for Li, Fe, Ni, Ba, and Bi. See Dietrich (2024) for more details.

Similarly to solution ICP-MS, LA-ICP-MS also yields a multivariate dataset, including many trace elements, most importantly REE. REE seems to be highly deposit-specific, while there is less variability between samples from the same deposit.

The great advantage of LA-ICP-MS compared to solution ICP-MS is the number of repeated measurements. In the current dataset, 15 multielement measurements were considered for each sample, while for certain deposits samples from multiple years are available. This made it possible to apply machine-learning-based classification methods, such as random forests, for the underlying dataset (Figure 31). The classification was performed in a similar manner as in the case of LIBS data, where entire samples were left out from the training set to test for the generalization potential of the dataset. Figure 31shows that classification greatly improves compared to LIBS, owing to the larger number of variables (i.e., more elements are detectable by LA-ICP-MS).

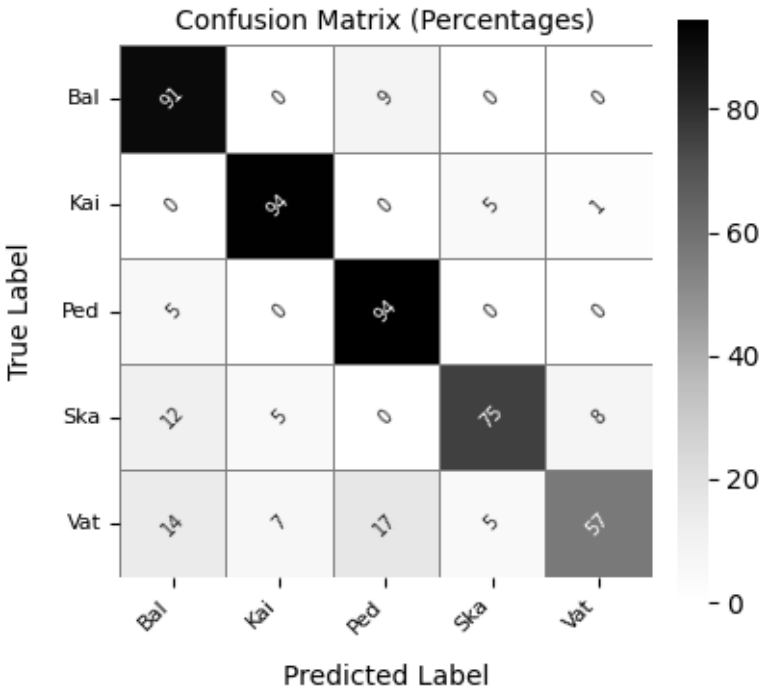

Figure 31 LA-ICP-MS-based confusion matrix of graphite concentrates with at least four samples, obtained by leaving out an entire sample when training the random forest classifier and using that sample for test. The number of correctly classified spectra is seen in the diagonal in percent.

The LA-ICP-MS technique is therefore a promising tool for routine graphite traceability tasks at the concentrate level. The interpretation of data obtained on purified samples is still ongoing.

2.2.5 Summary

Generally, all tested methods have a potential use in graphite fingerprinting (Figure 32-Figure 34). Methods targeting the direct measurement of graphite flakes, such as carbon stable isotopy and Raman spectroscopy have a very limited differentiating power due to the small number and overlapping nature of resulting parameters, while being applicable along the entire value chain (Figure 32). The applicability of XRD is limited to pre-concentrate

Funded by the European Union

stages, while TEM is generally not applicable for routine traceability tasks due to operational inefficiency, but rather for targeted questions in a possible second tier of analyses. XRF, solution ICP-MS, SEM-based-automated-mineralogy, LA-ICP-MS and LIBS yield multi-elemental datasets, which are better suited for data analysis and differentiation. The latter three methods can also be used for machine-learning methods owing to the large number of repeated measurements and excel at operational efficiency. SEM-based-automated-mineralogy and solution ICP-MS can be applied even at purity levels of 99.99%, covering the greater part of the value chain (Figure 33 and Figure 34). In summary, the best analytical options for graphite traceability are SEM-based-automated-mineralogy and solution ICP-MS, as these techniques excel at differentiating power and production chain coverage. It will be tested in the future, how far LA-ICP-MS and LIBS can be used along the production chain, as these two techniques would provide a significant benefit in terms of operational efficiency compared to SEM-based-automated-mineralogy and solution ICP-MS (see Figure 33 and Figure 34).

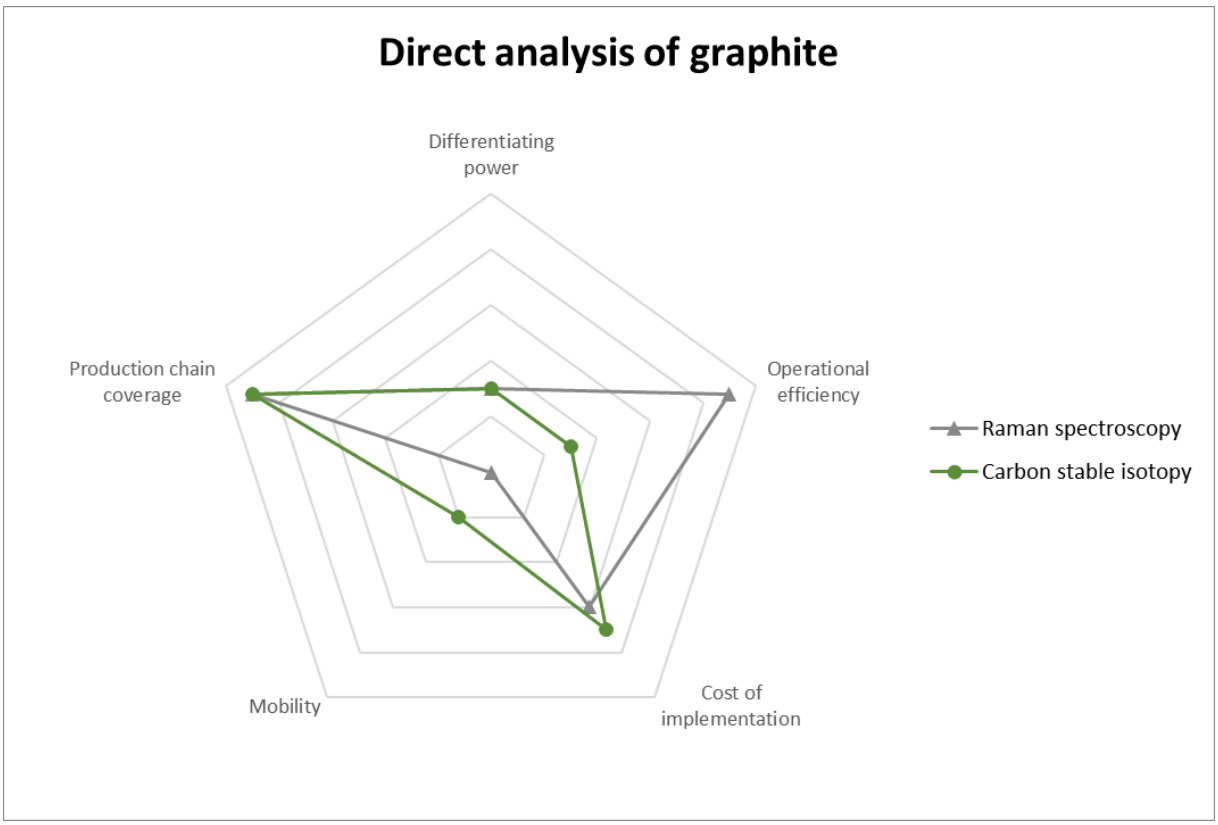

Figure 32 Method evaluation for techniques used for the direct analysis of graphite.

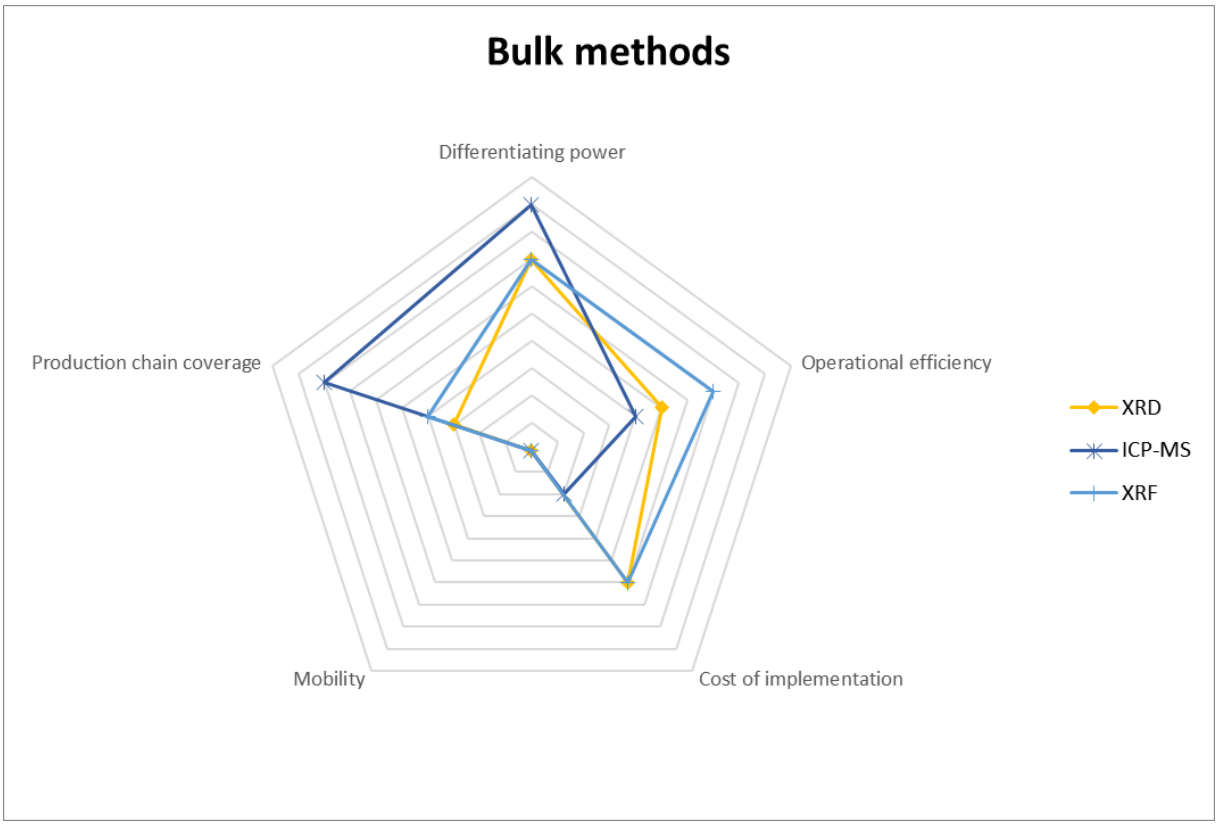

Figure 33 Method evaluation for techniques used for the bulk analysis of graphite samples/graphite products.

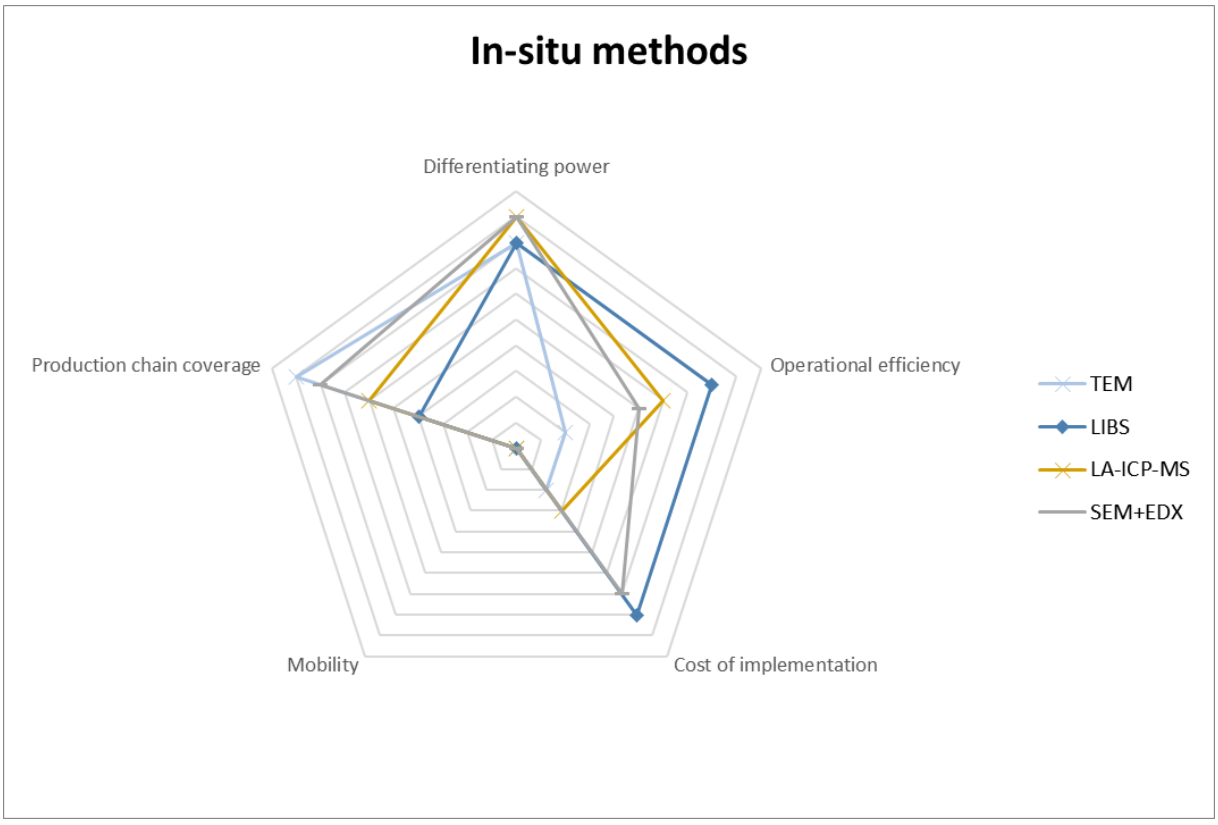

Figure 34 Method evaluation for techniques used for the in-situ analysis of graphite products/graphite-related materials. SEM+EDX refers to SEM-based-automated-mineralogy.

Funded by the European Union

The Global MFP Technic Index (GMTI) is calculated based on the respective weights assigned to each criterion to evaluate the methods. For a detailed description of the GMTI, please refer to D2.3 of the MaDiTraCe project. The GMTI is the following for individual techniques: direct graphite analysis: Raman-spectroscopy: 5.7, Carbon stable isotopy: 4.9; bulk: XRF: 5.5, solution ICP-MS: 5.5, XRD: 4.9; in-situ: SEM-based mineralogy: 6.7, LIBS: 6.4, LA-ICP-MS: 5.7, TEM: 5.0.

2.3 Lithium

2.3.1 Corpus of samples

According to the review of Kesler et al. (2012), mined lithium comes largely from pegmatite and related magmatic deposits, evaporative brines, and a growing group of unconventional deposits including both hard rock deposits and brines. While granitic pegmatites are widespread, rare metal pegmatites make up only about 0.1% of the total out of which Li-rich pegmatites represent an even smaller fraction (Laznicka, 2006). Usually, lithium-rich pegmatites also contain other rare metals (e.g. Sn, Be, Ta-Nb), and many pegmatites that are lithium-rich originally were of interest for other rare metals. Spodumene is the most important lithium mineral in pegmatites, amblygonite is widespread but rarely economic, while petalite, eucryptite and lepidolite are less common. The most important lithium pegmatite deposits are in the USA, Western Australia, Zimbabwe, in the DRC, in Namibia, China, Spain and Portugal, while there are also numerous smaller deposits on these six continents (Figure 35). Finland serves a pivotal role in the EU's lithium supply chain following the commissioning of the Keliber project in February 2026, which is the first dedicated lithium mine within the EU (YLE News, 2026).

Rare metal granites are defined by their significant enrichment in incompatible elements, specifically Li, Nb, Ta, Sn, and W (Linnen & Cuney, 2005). These deposits are geologically and economically distinct from rare metal pegmatites; while they typically exhibit lower metal grades (as low as several 1,000 ppm Li), they are characterised by substantially larger tonnages. Within these granitic systems, lithium is primarily hosted in Li-bearing micas (e.g. lepidolite, zinnwaldite and Li-rich muscovite) but it can also be found in amblygonite and montebrasite. Prominent European examples of rare metal granite deposits include Beauvoir in France and Cinovec/Zinnwald situated along the Czech Republic-Germany border (Gourcerol et al., 2019).

In contrast to lithium pegmatite and rare metal granite deposits, lithium brine deposits are usually associated with geologically recent basins with lacustrine evaporites, which formed as a result of high evaporation rate relative to precipitation. The most important lacustrine evaporite deposits are in the central Andes and China, and further smaller deposits are in the western United States and northern Africa (Kesler et al., 2012).

As part of the MADITRACE project, we analysed 141 samples (ores, concentrates, salt) from 25 different origins (Figure 35). These samples cover both conventional lithium resources (brines and hard rock deposits, i.e., lithium-rich pegmatites) and unconventional resources (geothermal fluid and Li-mica-rich hard rock deposits).

Funded by the European Union

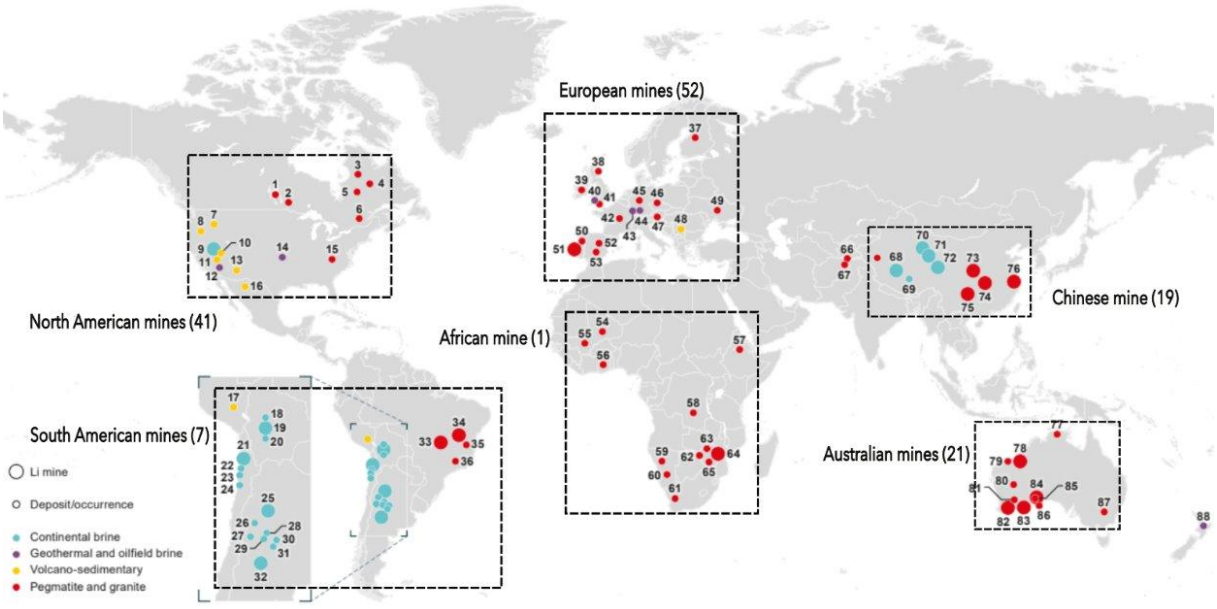

Figure 35 Map of lithium samples (ores, concentrates, salt) analysed as part of the MADITRACE project (modified after Shaw, R.A. (2021) Global (Li) mines, deposits and occurrences (November 2021, BGS).

2.3.2 **Trace element analysis**

Presently, there is no available method based on certain elements/elemental ratios to discriminate different pegmatites and rare metal granite types, or each deposit individually. Research often uses mineral chemistry or bulk rock (=ore) analysis (see Müller et al. 2022 for a review), which is not applicable for concentrates. Therefore, investigating the differences in major and trace element contents amongst various deposits is mandatory for the upstream traceability of lithium, as refining can potentially erase the primary geochemical fingerprint

Our goal is to determine geochemical parameters, which enable to differentiate between concentrates (and ores to a lesser extent) from different deposits around the world. We propose the analysis of a large array of minor, trace and ultra-trace elements with triple Quad (QQQ) ICP-MS coupled with multivariate data analysis for this purpose.

2.3.2.1 **Method description**

All samples were prepared in the BRGM laboratory. About 200 mg of ores and ore concentrates were dissolved in concentrated acid in a microwave oven. Analyses were carried out on samples digested in BRGM laboratories, using QQQ-ICP-MS (Agilent 8900) Figure 36). Measurement parameters were optimized to limit deposition and contamination in the introduction system and mass spectrometer, while achieving the highest possible sensitivities for trace element quantification. Depending on elements and possible interferences, different gas modes were used in the reaction/collision cell for accurate element quantification: without gas, with dihydrogen, helium or dioxygen (with or without mass transition). Each analyte was measured in multiple gas modes and/or multiple isotopes were selected. Quantification is based on an external calibration of each element, corrected by an internal standard added on-line (In, Re, or Ir). The calibrations were verified by cross-solution measurements. Regular quality controls were undertaken during the sequences to check the validity of the calibration and the drift of the signal over time. All the checks carried out were satisfactory during the acquisition of these samples. The elements Ag, Al, As, B,

Ba, Bi, Ca, Ce, Cd, Co, Cr, Cs, Cu, Dy, Er, Eu, Fe, Ga, Gd, Ge, Ho, Hf, Hg, La, Lu, Mg, Mn, Mo, Na, Nb, Nd, Ni, P, Pb, Pd, Pr, Rb, S, Sb, Sc, Se, Sm, Sn, Sr, Ta, Tb, Te, Th, Ti, Tl, Tm, U, V, W, Y, Yb, Zn and Zr were measured. For an accurate quantification of these elements in different samples, the detected signal of a given element on the ICP-MS should be above at least three times the limit of detection of the instrument (LoD). Elements below this limit were removed. Major elements were not selected because their measured values were far above the calibration range used for trace element quantification. According to the previous step, the filtered set of elements used for the data treatment includes: Mg, P, S, Sc, Ti, V, Cr, Mn, Ni, Co, Cu, Zn, Ga, Rb, Sr, Y, Zr, Nb, Mo, Pd, Ag, Cd, Sn, Sb, Cs, Ba, Hf, Ta, W, Pt, Au, Tl, Pb, Bi, Th, U, La, Ce, Pr, Nd, Sm, Eu, Gd, Tb, Dy, Ho, Er, Tm, Yb, Lu.

Figure 36 QQQ ICP-MS (Agilent 8900) used to analyse trace element compositions in Li-bearing samples in the MADITRACE project.

2.3.2.2 **Statistical treatment and results**

Figure 37 presents elemental concentrations of the above-described elements used in this work. We can observe that it is difficult to distinguish between the different deposits using this representation. Therefore, we utilize multivariate data analysis with the objective of an optimal exploitation of the ICP-MS data. Based on the number of samples available and elements analysed, we opted for a Linear Discriminant Analysis (LDA), which was optimized and modified for our specific needs and constraints. Further details on the methodology used are available and explained in the deliverable D2.5 and in a publication (Moradell Casellas et al., in prep).

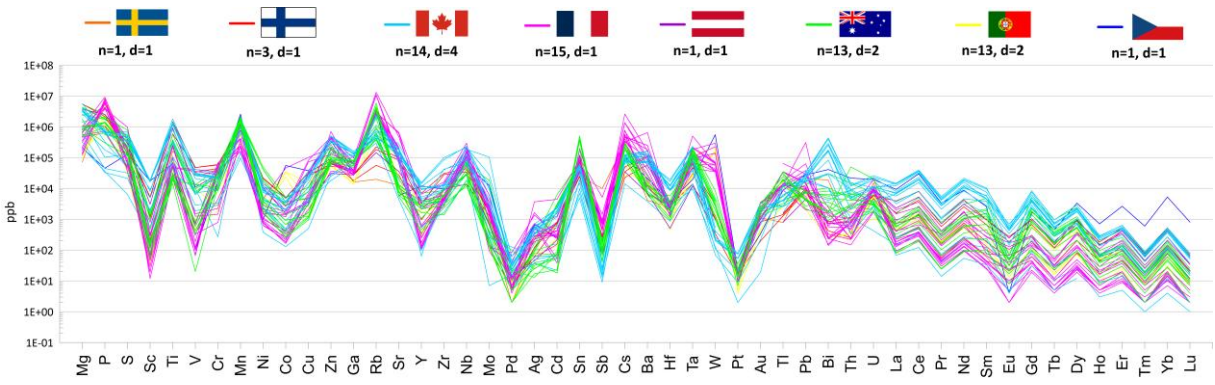

Figure 37 Minor and trace element concentrations in the ores and concentrates determined by solution ICP-MS, using acidic micro-wave digestion. (n= total number of samples; d=number of deposits)

Funded by the European Union

We trained the model on 3 main lithium deposits: an Australian spodumene pegmatite deposits (8 samples) a Canadian spodumene pegmatite deposit (11 samples) and a French lepidolite rare metal granite deposit (15 samples), later referred to as "referenced deposits" and samples. Other samples (referred to as "unreferenced deposits") were not used for the model training. The results of the LDA model are presented in Figure 38.

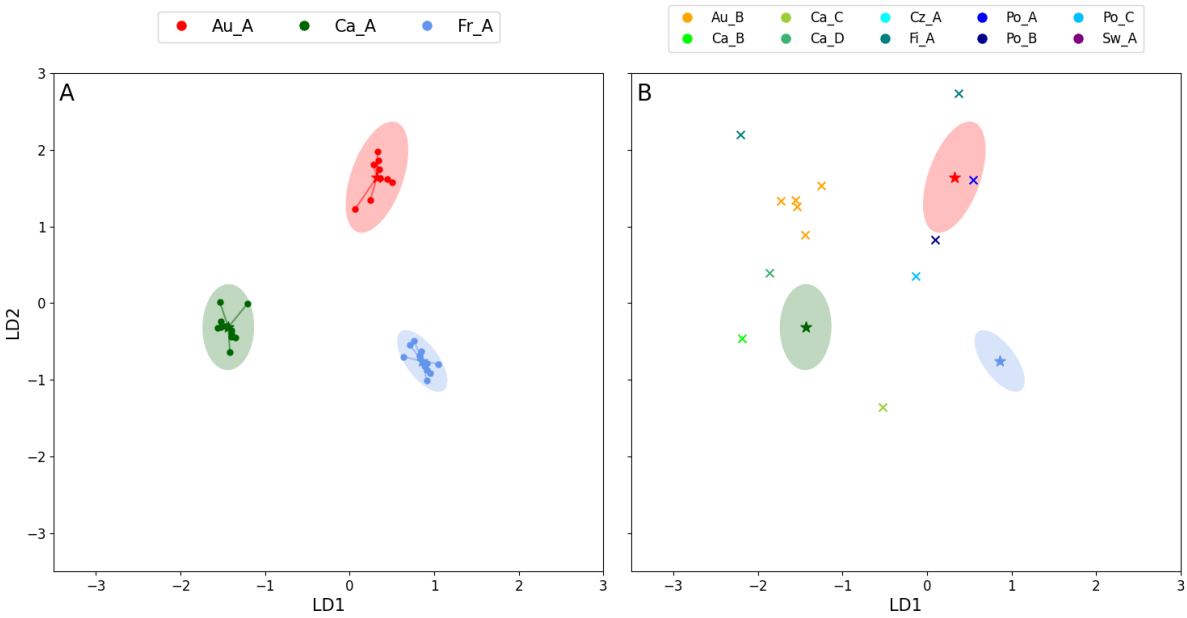

Figure 38 The two-dimensional space of the LDA procssed with ICP-MS minor, trace and ultra-trace element dataset of lithium ores and concentrates. A: Latent space of trained model, with the samples and confidence regions of the three deposits used for the training. In red, sample of the Australian deposit (Au_A); in green, the Canadian deposit (Ca_A) and in blue the French deposit (Fr_A). B: projection of the remaining unreferenced samples in the latent space, with confidence regions of previous deposits and stars representing corresponding deposit centroids. Au=Australia; Ca=Canada; Cz=Czech Republic; Po=Portugal; Fi=Finland; Sw=Sweden.

The trained model is able to separate the three referenced deposits completely, with relatively close within-deposit distance between samples (Figure 38). Unreferenced sample projection in the resulting latent space show high distances with the referenced samples except one Portuguese sample within the Australian confidence region (Figure 38B). The deposit B samples from Australia (in orange) are also regrouped, indicating that the model can separate deposits not included in the training. This suggests that the separation of groups relies on robust parameters that could differentiate deposits in a more generalized way, or at least not specifically to these three deposits. After this model, we ran prediction trials using leave-one-out cross-validation (LOO-CV), for the referenced deposits. These experiments demonstrate how sample provenance would be verified with ICP-MS analysis. The prediction matrix is presented in Figure 39.

Funded by
the European Union

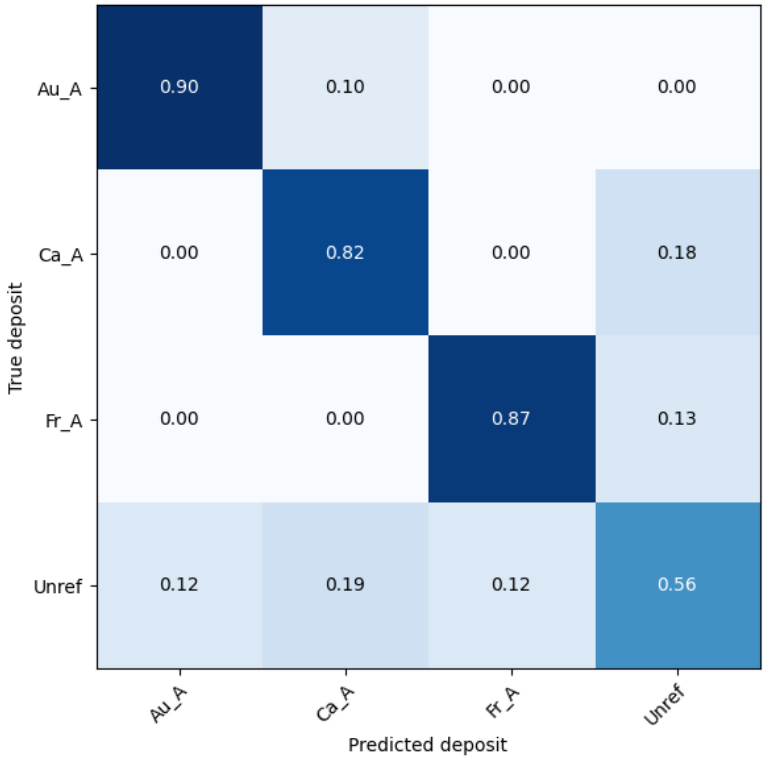

Figure 39 Prediction matrix of the LOO-CV prediction using the previous LDA model trained on the ICP-MS dataset of lithium samples. Anonymized samples from the Australian deposit (Au_A), the Canadian deposit (Ca_A) and the French deposit (Fr_A), and all unreferenced samples ("Unref") were used for model training and used for prediction. A prediction score of 1 between True and Predicted deposit would be a perfect compliance between true origin and predicted one, whereas 0 would be a total discrepancy between the two.

Prediction on the referenced deposits average a 0.86 score, with slightly better results on the Australian and French deposits. The Australian samples which were erroneously predicted, are attributed to the Canadian deposit, whilst those from France and Canada are attributed to the unreferenced deposits. Furthermore, the prediction score of 0.56 for unreferenced deposits is less conclusive. These deposits could be therefore confused with referenced deposits, meaning the model is more likely to produce false positives than false negatives.

2.3.2.3 **Method evaluation**

The trace element analysis by liquid ICP-MS was assessed according to the criteria presented in deliverable D2.3 (Figure 40).The ICP-MS is a fixed laboratory technique (i.e., Mobility=0), which is mandatory for the determination of trace elements up to part per billion levels. At present, there is no field technique capable of analysing trace elements with such a good detection limit. Although the work and results presented here only focus on the upstream of the production chain because of sample availability, this technique has been used successfully to determine elemental concentrations of salar brines, lithium salts (carbonate and hydroxides, battery grade) and cathode active material (standalone and on cathode sheets), and could be used for downstream samples. However, at present we have not been able to demonstrate that this technique can be used for traceability purposes downstream in the chain (i.e., Production Chain Coverage=5).Results presented above show that this method, combined with multivariate data analysis, can distinguish multiple deposits that are geochemically very similar. The prediction scores are promising, and the

Funded by the European Union

method seems to rely on robust geochemical tracers (Differentiating power=7). Liquid-mode ICP-MS analysis is moderately expensive because of the cost of the instrument (around 200k €), standards being used, gas and maintenance (Cost of Implementation=4).Despite needing a preparation time of about a week for the microwave digestion developed and used in this work, and instrument/analysis preparation, this technique can routinely analyse multiple samples in a short period of time (more than 50 within a week) on a quasi-routinely operating mode (Operational Efficiency= 4).

The Global MFP Technic Index (GMTI) for this technic is thus calculated to 4.7.

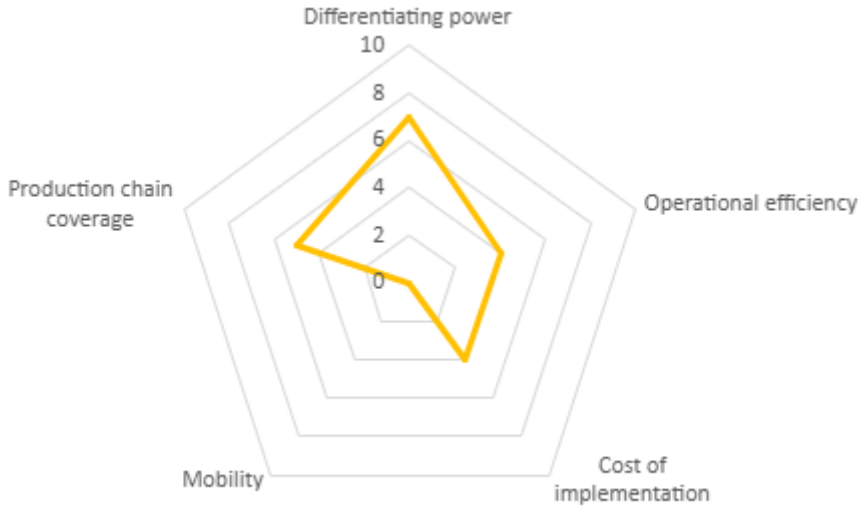

Figure 40 Method evaluation of the liquid mode ICP-MS analysis for lithium traceability along the battery production chain, based on criteria presented in deliverable D2.3.

2.3.3 Lithium isotope analysis by liquid-MC-ICP-MS

2.3.3.1 Method description

All samples were prepared in the BRGM laboratory. About 200 mg of lithium carbonate and -hydroxide were dissolved in 0.5 M HNO_3. About 200 mg of ore and ore concentrate were dissolved in concentrated acid in a microwave oven. The samples of lithium hydroxide and carbonate were dissolved in 0.5 M HNO_3 and analysed without a protocol of chemical purification. For the other samples, a volume containing ~100 ng Li was dried on a hot plate in the cleanroom. The residue was dissolved in a solution of 0.2 M HCl. Lithium was separated from matrix elements using an AG 50 W – X12 resin (200–400 mesh), before drying and re-dissolving in 0.5 M HNO_3. Total procedural blanks were measured to verify the cleaning procedure; Li concentrations in these blanks were generally less than 30 pg, representing >0.03% of the lithium mass analysed. Lithium isotope compositions were measured at a concentration of 50 µg/L with a Thermo Fisher Scientific Neptune MC-ICP-MS—upgraded to 'Neptune Plus'—in the BRGM laboratory, following the procedure developed by BRGM (Desaulty et al., 2022) (Figure 41). The Li isotope composition of each sample is expressed in δ-notation relative to the mean value of the bracketing Li standard (L-SVEC):

$$\delta^7Li = [(^7Li/^6Li)_{sample}/(^7Li/^6Li)_{standard} - 1] \times 1000$$

The quality of Li-isotope analyses was controlled by regular measurements of in-house standards, whose long-term reproducibility is 0.5‰ (2σ).

Figure 41 MC-ICP-MS Neptune Thermo Fisher Scientific used to analyse lithium isotopic compositions in the MADITRACE project.

2.3.3.2 **Results**

The isotopic compositions of the samples in the study are presented in Figure 42. There is a noticeable depletion of the heavy isotope in the hard rock samples (Canada, Australia, etc.) and an enrichment in the heavy isotope for samples from the Salar (Chili, Argentina) consistent with literature data (Desaulty 2022). Overlaps between various groups' isotopic signature can be observed.

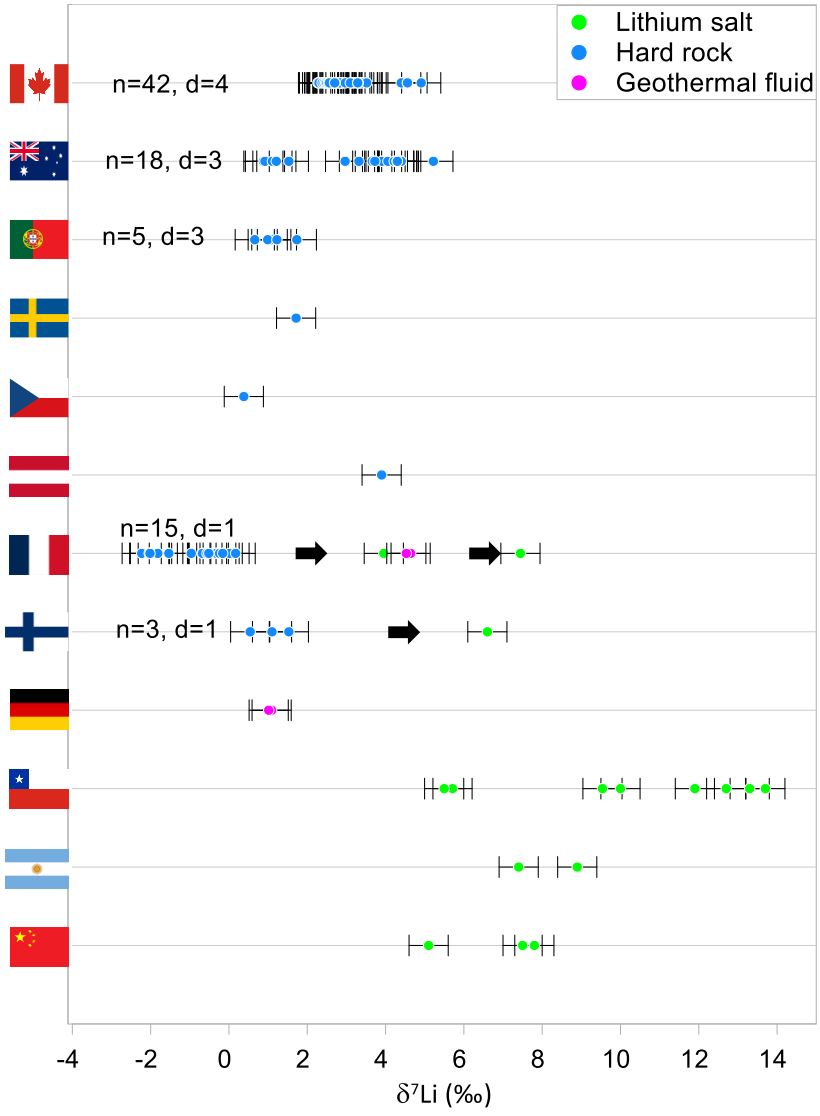

Funded by the European Union

Figure 42 Lithium isotopes composition of the MADITRACE samples: Ore and ore concentrate (n= 86), geothermal fluids (n= 4) and lithium salts (n= 16). The number of samples and deposits is indicated in brackets.

2.3.3.3 **Perspectives with machine learning as part of task 2.5.**

In the following step, a model using δ^7Li from lithium deposits was trained to predict the origin of lithium samples. A dataset of 446 samples was compiled from 55 scientific documents, and from MC-ICP-MS analyses performed in BRGM laboratories. These were categorized into four classes: South American brines (n = 108), Chinese brines (n = 77), Chinese hard rocks (n = 77) and hard rocks from other regions (n = 184). However, significant overlaps in δ^7Li values between classes make classification challenging with only one feature (Figure 43).

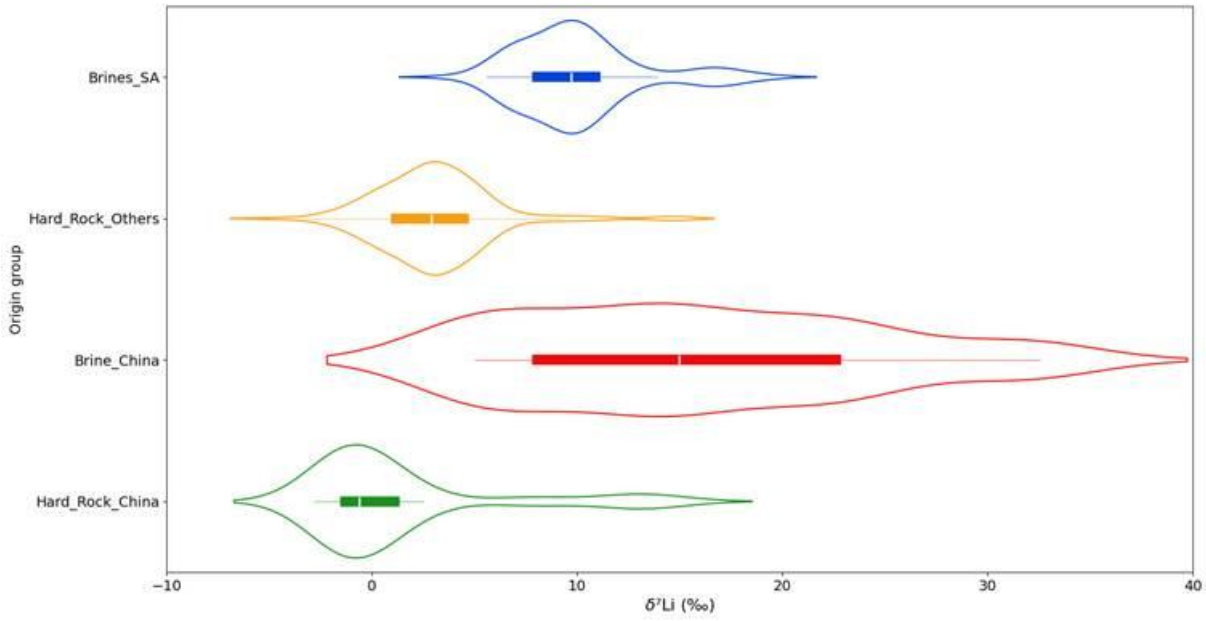

Figure 43 δ^7Li among four classes: brines from South America, brines from China, hard rocks from China, hard rocks from other locations.

Various supervised classification algorithms were tested and can be grouped into three categories (Figure 44): distribution-based models (Linear Discriminant Analysis [LDA], Naive Bayes [NB], Logistic Regression [LogReg]), projection-based models (K-Nearest Neighbours [KNN], Support Vector Machine [SVM]) and tree-based methods (Decision Trees [DT], Random Forest [Rm Forest], Gradient Boosted Trees [Grad. Bost.]).

Each approach relies on different assumptions: statistical relationships, distance metrics or data thresholding. The first category assumes that there is a statistical relationship between class labels and δ^7Li. The second relies on class separation by a distance metrics or hyperplane in a transformed feature space. The second considers that the feature space could be recursively separated into regions of increasing class purity, so the hierarchical decision rules could capture complex non-linear relationships between δ^7Li and class labels.

Model performance was evaluated using leave-one-out cross-validation. A comparison with class weighting considering annual global production between 2012 and 2021 has additionally been performed: 35.7% for South American brines, 4.0 % Chinese brines, 4.9% for Chinese hard-rocks and 52.5% for hard rock others.

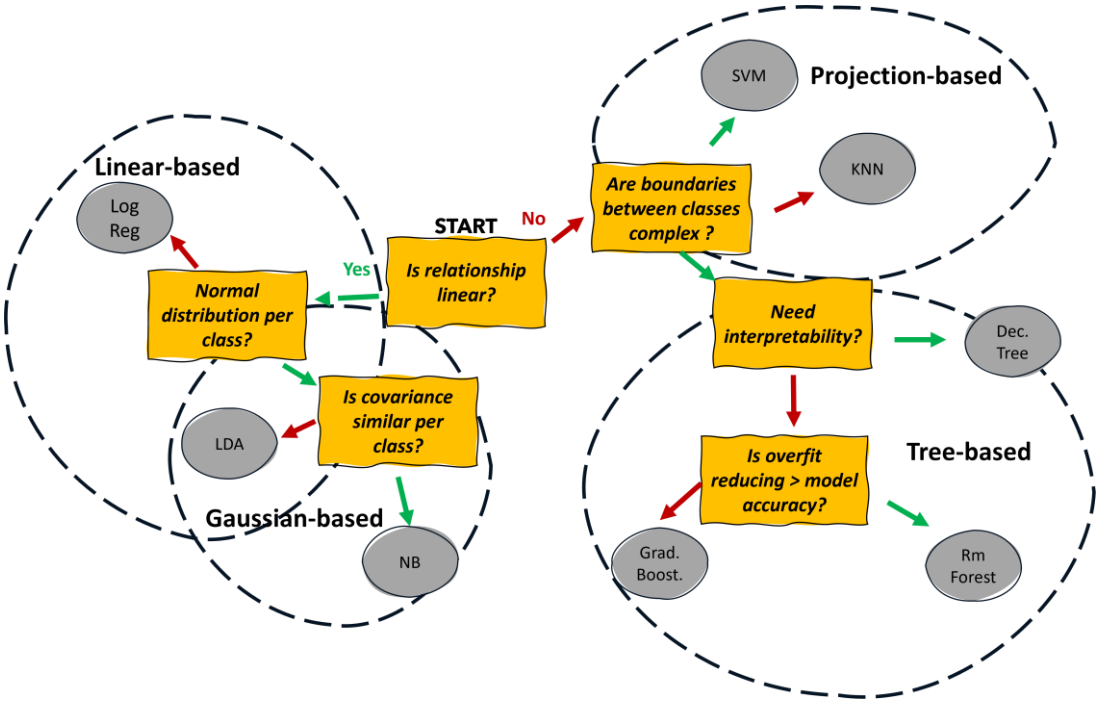

Figure 44 Choice of classifier according to certain dataset characteristics and assumptions.

Results show that distribution-based (Linear- and gaussian-based) models performed poorly due to their sensitivity to class overlap, while projection based and tree-based models highlighted higher accuracies reaching 0.75. These methods define explicit decision thresholds, effectively separating each class. Class weighting does not significantly increase the model performances considering that two classes (brines and hard rock China) represent negligible production proportions (Figure 45). Furthermore, some models do not consider class weighting in their parameters (i.e., Decision Tree, Gradient Boosting, KNN, LDA, NB, Random Forest).

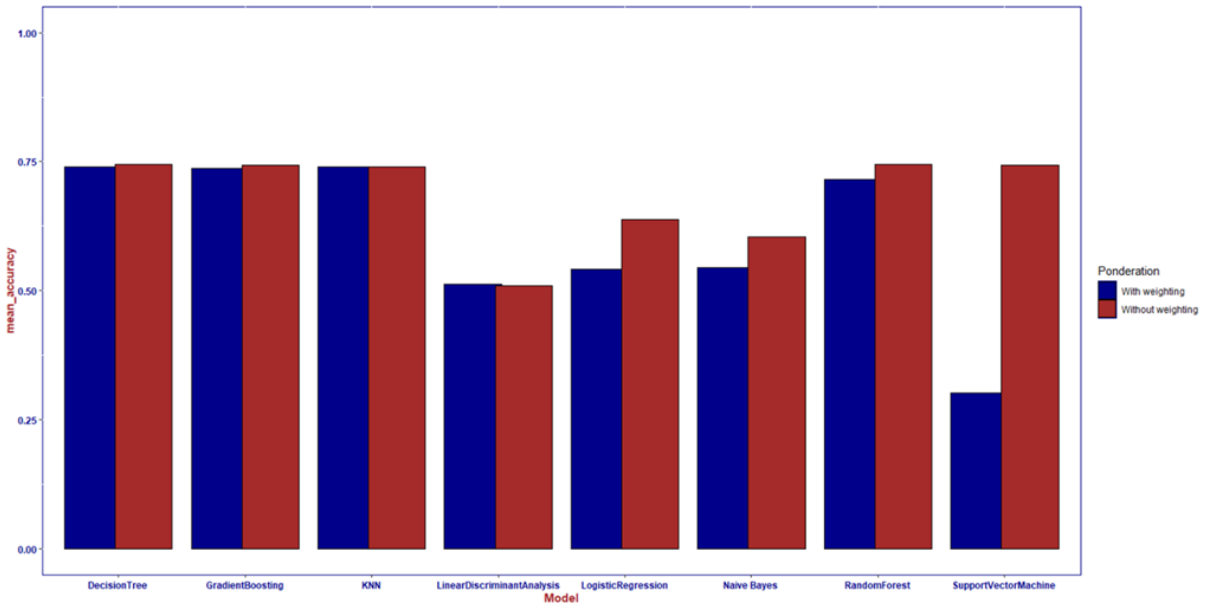

Figure 45 Prediction accuracies of model by leave-one-out with or without class weighting.

Funded by the European Union

For each model, confusion matrices confirmed that projection and tree-based approaches generally predicted classes well (e.g., KNN: Figure 46). The final step of this study aims to predict the origins of different samples with the trained models.

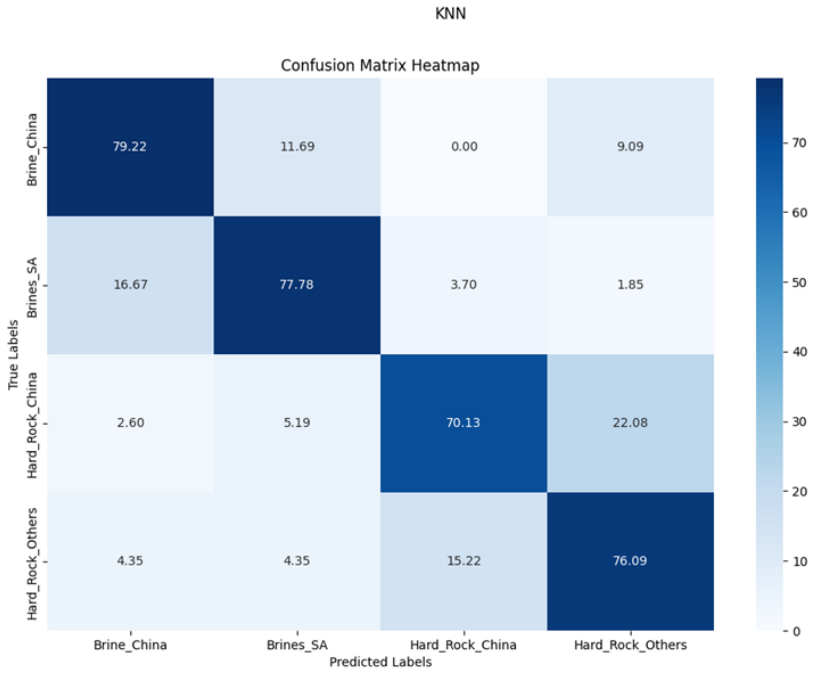

Figure 46 Confusion matrix between original and predicted classes obtained through K-Nearest Neighbours classification.

2.3.3.4 **Method evaluation**

The lithium isotopic composition analysis by liquid-MC-ICP-MS was assessed according to the criteria presented in deliverable D2.3 (Figure 47). The MC-ICP-MS is a fixed laboratory technique (i.e., Mobility=0). It is currently impossible to determine lithium isotopes compositions in the field or at production sites. This technique makes it possible to analyse the entire operational chain (i.e., Production Chain Coverage=10) from the ore to the battery (ore, ore concentrate, lithium salt, cathode active material, cathode sheet, battery, cycled battery). The confusion matrices indicate that the models generally predicted the different classes accurately Figure 46), showing good separation between deposits. This suggests a strong differentiating power, supporting the ability of the approach to assign samples to their correct origins, despite severe overlaps between groups (Differentiating power=6).The purchase price of an MC-ICP-MS is over 500 k € with an expensive and complex sample preparation (Cost of Implementation=0). The MC-ICP-MS analysis requires preparation in a clean room using ion exchange resins, expensive purified acids, PFA beakers etc. The preparation time for a sample is long and complex (several weeks). It requires the following steps: (1) dissolving of the sample, (2) determining its Li content, (3) separating and purifying the Li on ion exchange resin in a clean room, (4) analysing it on MC-ICP-MS with isotopic standard between samples. However, preparation and analysis do not require special authorisation due to safety constraints (Operational Efficiency=2).

The Global MFP Technic Index (GMTI) for this technique is 4.2.

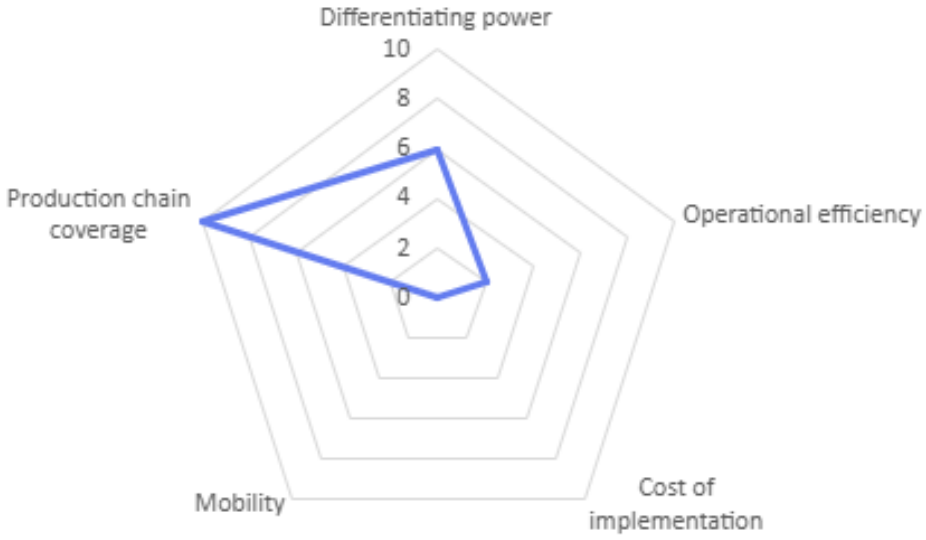

Figure 47 Method evaluation diagram for analysis of lithium isotopes by MC-ICP-MS.

Funded by the European Union

2.4 Nd, REE

2.4.1 Sample corpus

As part of the MaDiTraCe project, 63 samples were collected (ores, concentrates and metallic products from the permanent magnet value chain) with upstream value chain samples from 11 different origins (Figure 48). These samples cover a wide range of rare earth element (REE) sources, including conventional ores (i.e., carbonatites), and secondary ore deposits, which include unconventional REE-deposits such as phosphorites or black shales, or low-grade REE deposits (e.g., ionic clays). REE mining concentrates from major producing regions (Bayan Obo in China and Mountain Pass in the US) are also part of the sample set.

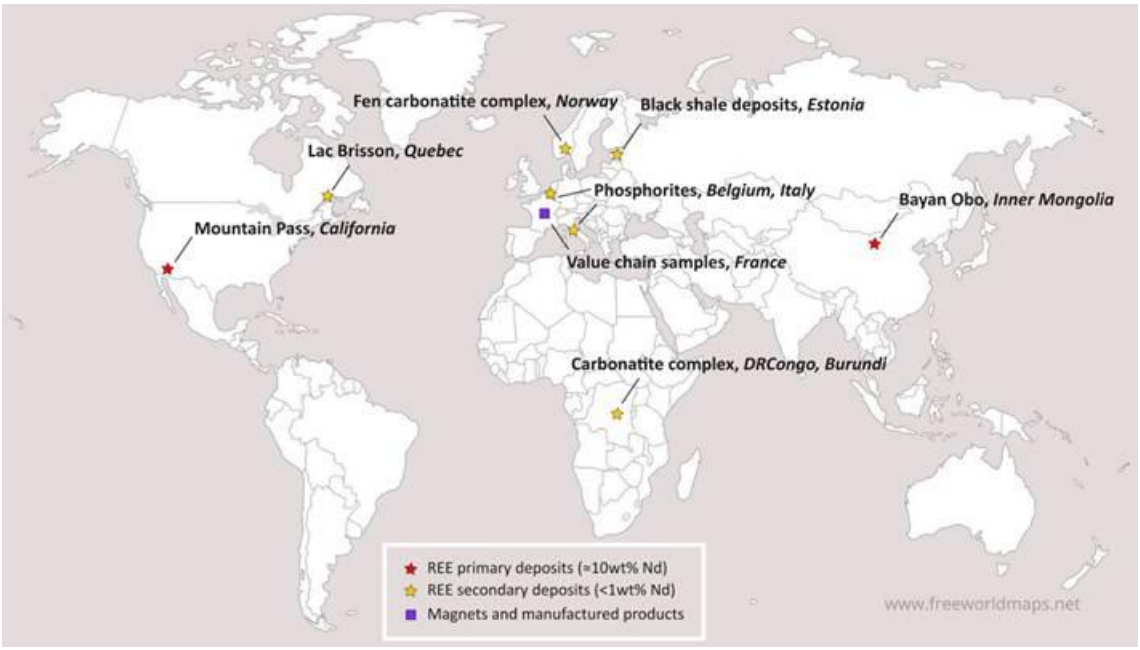

Figure 48 Map of Nd and REE samples analysed as part of the MaDiTraCe project.

In addition to the geologic samples (REE-rich deposits and ore concentrate), the corpus is composed of metallic samples from the different metallurgical processes (Nd-Pr alloy, FeB alloy, ribbon, magnet power, magnet; Figure 49) provided by the CEA-Liten. Two commercial ribbons (I1 and I2 respectively from Japan and Europe) and 8 magnets coming from the same wind turbine were added to the sample corpus.

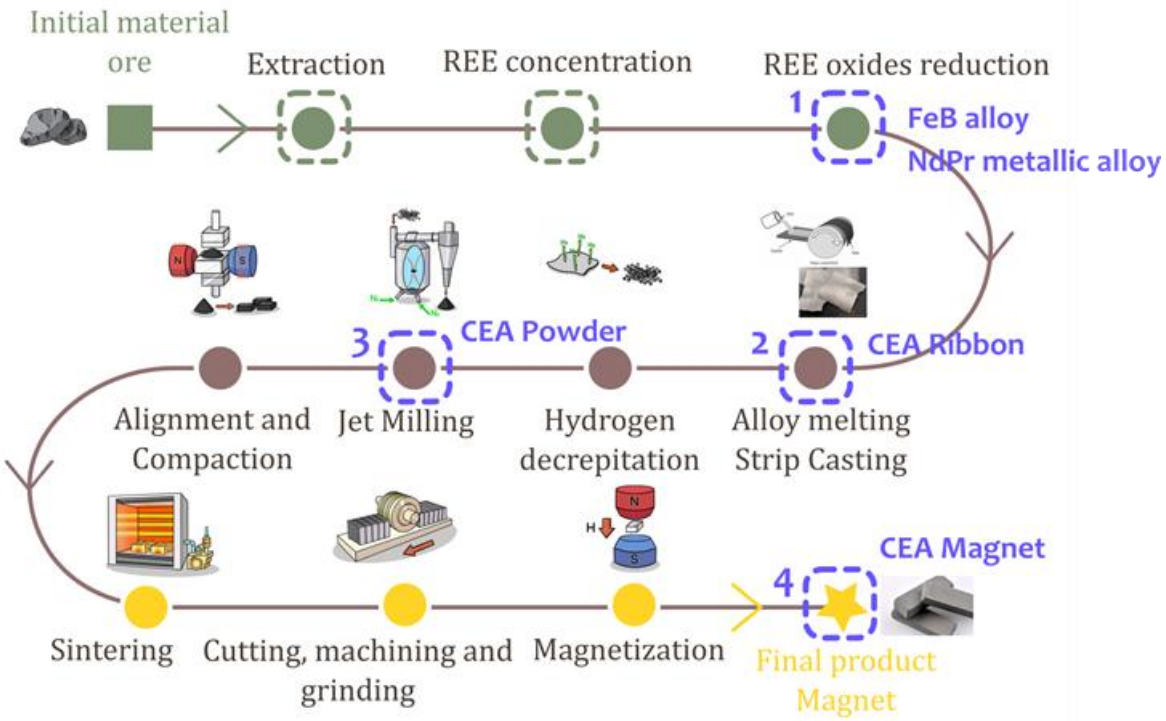

Figure 49 Summarized production chain of NdFeB permanent magnets. The different collected samples are indicated with dotted squares and metallic samples provided from the CEA-Liten are indicated in blue.

2.4.2 Neodymium isotope composition

The isotopic system of Neodymium consists of seven isotopes ^{142}Nd, ^{143}Nd, ^{144}Nd, ^{145}Nd, ^{146}Nd, ^{148}Nd and ^{150}Nd. Two of them are radiogenic (i.e. 142 and 143), meaning that they are produced by the radioactive decay of a radioactive nucleus. The isotope 143Nd is produced by the radioactive decay of ^{147}Sm, changing the abundance of ^{143}Nd relative to the other Nd isotopes. Natural rocks display various ^{143}Nd/^{144}Nd isotope ratios, reflecting their age of formation, the chemical composition of their parental magma and the chemical processes involved in mineral crystallisation. Thus REE-bearing minerals display specific Nd isotopic signatures attached to their geological history that could be used in origin certification systems. However, through the process of permanent magnet manufacturing, this primary geochemical signature could evolve. In this study, we measured samples from the permanent magnet value chain to evaluate if the Nd isotopic signature could be used as a geochemical fingerprint for certification systems and fraud detection, integrated into a geoforensic approach.

2.4.2.1 Description of samples

The Nd isotopic composition of 18 samples from the permanent magnet value chain was measured with the method described below. Samples comprise a primary material from the Fen Complex in Norway and an ionic clay sample from South America; mining concentrates from the giant mine of Bayan Obo in China and the historical REE mine of Mountain Pass in California; metallic samples from the CEA-Liten permanent magnet platform: NdPr alloy, ribbon, powder and magnet from the same production chain, and industrial ribbons I1 and I2 respectively from Japan and Europe as well as end-of-life magnets from a disassembled windmill generator. To ensure sample homogeneity, two sub-samples of the NdPr alloy were dissolved and measured for their Nd isotope signature. They were labelled respectively NdPr-1 and NdPr-4 in Fig. 51).

Funded by
the European Union

2.4.2.2 **Method description**

Sample preparation

A quantity of around 100 mg of previously powdered geological samples (REE-bearing material and mining concentrates) and metallic samples from the permanent magnet value chain were digested in 2 ml of aqua regia and 5 to 10 ml of 8 M HCl respectively. Geological samples were left on the hotplate at 110°C for a few weeks until complete dissolution. After evaporation, samples were taken up with 2 ml of HCl prior to both elemental and isotopic analysis. The ionic clay sample followed a different procedure described in the review of Moldovenu and Papanelaki (2016). For the leaching, around 8 ml of 0.15 mol/L ammonium sulphate ((NH4)2SO4) was added to 4 g of powdered clay at ambient temperature. The mixture was shaken by hand and put into an ultrasonic bath for 2 minutes to ensure total leaching of the REE. After filtration under vacuum, the leachate was cleaned with 2 x 100 ml of deionized water for optimizing REE recovery. The solution was stored in the laboratory, and an aliquot of 1 ml was sampled for further elemental and isotopic analysis.

Sample purification

For precise and accurate measurements, samples were purified prior to isotopic measurements. A significant part of the analytical development was dedicated to the optimization of previously published methods for Nd isotopic analysis, to adapt them to value chain samples and the specific REE-rich material studied in MaDiTraCe project (i.e. targeted ores, concentrates and metallic samples). The isolation of Nd required two steps because of the chemical similarities within the REE family. The first step allowed the separation of REEs as a group from major matrix elements using TRU-spec resin, while the second step focused on the separation of Nd from the other REEs with a DGA resin.

Nd isotopic analysis

Isotopic analyses were performed with a Neptune MC-ICP-MS (for multi collector inductively coupled plasma mass spectrometer) with a previously described setup (Ganio et al., 2012) and with TIMS at BRGM (Thiéblemont et al., 2014). The isotopic results are expressed normalized to the isotope ratio of the CHUR (for CHondritic Uniform Reservoir) in part per ten mill unit:

$$\varepsilon Nd = \left(\frac{\left({}^{143}Nd/_{144}Nd \right) meas}{\left({}^{143}Nd/_{144}Nd \right) CHUR} - 1 \right) * 10^4$$

2.4.2.3 **Results**

The isotopic composition of the samples is presented in Figure 50. Ores (Fen-Complex, Ionic Clay), concentrates (Bayan Obo, Mountain Pass) and the magnets are differentiated regarding their Nd isotopic signatures. Value chain samples provided by the CEA-Liten coming from the same production line do not show isotopic fractionation during the

different manufacturing processes. The two ribbons I1 from Japan and I2 from Europe display different isotopic signatures.

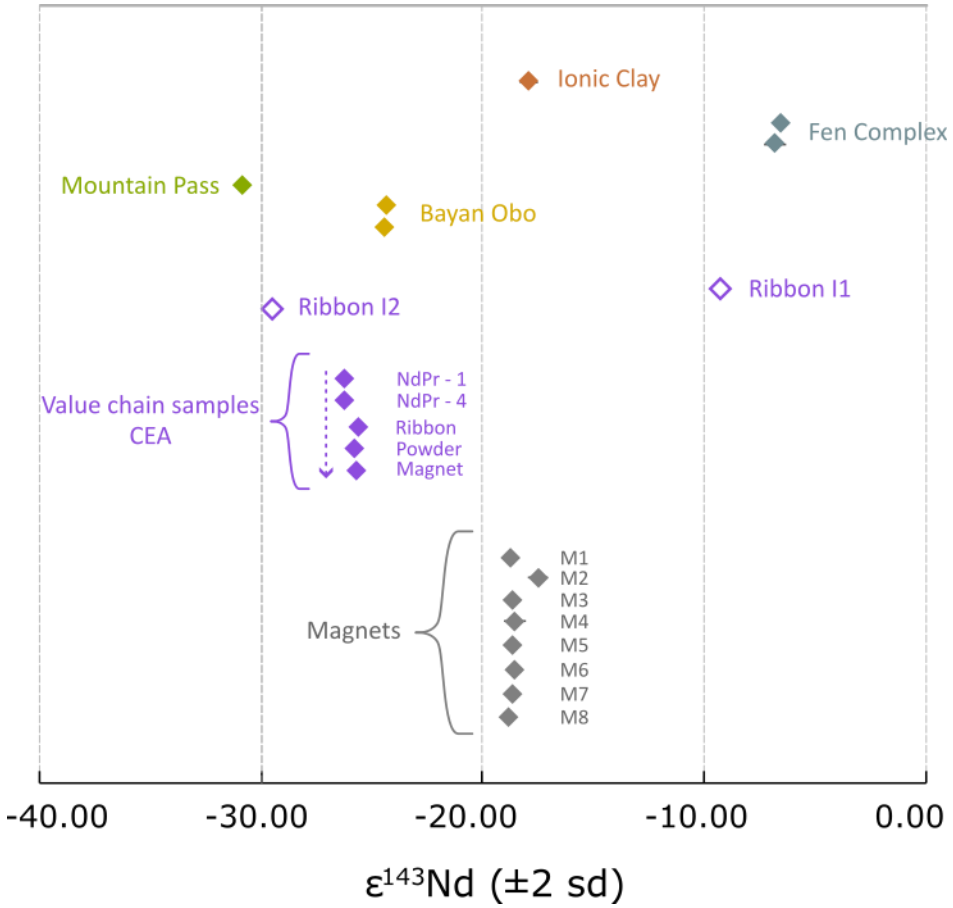

Figure 50 Isotopic composition of the samples analysed by MC-ICP-MS so far in the context of MFP, expressed in ε unit (part per ten mil).

2.4.2.4 **Applicability of the methodology in geoforensics**

The efficiency of the Nd isotopic method was evaluated with the same five criteria as for the other commodities: mobility, production chain coverage, differentiating power, cost of implementation, and operational efficiency. The scores are allocated on a scale of 0 to 10 and the scores for the present method are represented in Figure 51. The Nd isotope method covers the entire value chain along with a high differentiating power. However, complex multicollector instruments are required, combined with a relatively long analytical preparation of the samples compared to on-site techniques such as pXRF and LIBS. TIMS and MC-ICP-MS share the same values for the different criteria, except for the operational efficiency because of the relatively long time required for TIMS analyses compared with the Neptune.

The Global MFP Technic Index (GMTI) for the Nd isotopic technic with Neptune and TIMS is respectively 5.4 and 5.2.

Funded by the European Union

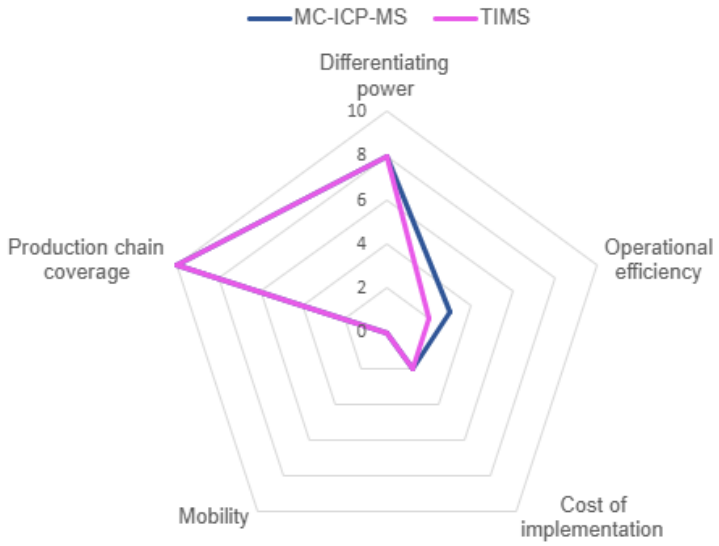

Figure 51 Method evaluation diagram for Nd isotopic analysis by MC-ICP-MS (Gent University, Belgium) and TIMS (BRGM, France).

The specific Nd isotope signature of the different samples is promising for the use of Nd isotopes as a traceability tool. More samples from the upstream value chain would be necessary to study possible overlaps in Nd isotope signatures. Likewise for magnets, as only a few samples of end-of-life (EoL) magnets were analysed. The samples from the value chain from the NdPr alloy to the final magnet product expressed the same Nd isotopic signature, strengthening the use of this technique for traceability studies for the downstream part of the value chain. However, the characterisation of one fundamental step of the value chain is missing: the reduction of REE oxides to metallic alloy. The measurement of samples representative of this reduction step would be mandatory for a complete understanding of Nd isotope signature evolution throughout the value chain.

Funded by the European Union

2.4.3 Rare Earth Element analysis

2.4.3.1 Method description

All samples were prepared in the A&MS unit at Ghent University. Approximately 100 mg of each sample—including REE concentrates, Nd-Pr alloys, industrial and lab-made ribbons, magnet powders, and sintered Nd-Fe-B magnets—was digested with either aqua regia followed by 8 M HCl (for concentrates) or 8 M HCl (for the other samples). High-Fe samples underwent Fe removal using AG® MP-1M anion exchange resin, followed by REE separation with LN-resin via stepwise HNO_3 elution (Arrigo *et al.*, 2021).

REE concentrations were measured using an Agilent 7900 quadrupole ICP-MS (Figure 52) equipped with a MicroMist nebulizer and Peltier-cooled Scott-type spray chamber. Light (L)REE and heavy (H)REE were monitored in no-gas and He-collision-gas modes, respectively, with Ru as internal standard and multi-element external calibration. The measurement conditions can be found in **Erreur ! Source du renvoi introuvable.**.

Figure 52 Q-ICP-MS (Agilent 7900) used to analyse REEs in the MADITRACE project.

ICP-MS Agilent 7900		
Nebulizer gas flow rate (L min^{-1})	1.05	
Integration time (s)	1	
Acquisition mode	Time resolved analysis	
Mode	No gas mode	Gas mode
He flow rate (mL min^{-1})	-	4.60
Nuclides monitored (m/z)	^{89}Y, ^{139}La, ^{140}Ce, ^{141}Pr, ^{146}Nd, ^{147}Sm, ^{153}Eu, ^{101}Ru	^{157}Gd, ^{159}Tb, ^{163}Dy, ^{165}Ho, ^{166}Er, ^{169}Tm, ^{173}Yb, ^{175}Lu, ^{101}Ru

Table 2 Instrument settings of the Agilent 7900 ICP-MS

2.4.3.2 Rationale behind using the method

The protocol was developed to accurately determine REE in Nd-Fe-B magnets and throughout their production chain, with the aim of improving traceability, transparency, and sustainability of critical materials production chains.

Although ICP-MS is the most powerful technique for REE, strong polyatomic interferences (oxides and hydroxides of LREE, especially Nd) occur in these types of samples, preventing reliable quantification of HREEs when concentrations are highly unequal.

Funded by the European Union

For this reason, the use of a prior chemical separation via ion exchange chromatography (AG® MP-1M + LN-resin) before ICP-MS is justified, as mathematical corrections are insufficient in matrices rich in Nd and Fe (Suárez-Criado *et al., 2026*). Eight chromatographic fractions were collected and quantified, summing across fractions when necessary. Procedural blanks and BHVO-2 reference material were analysed in parallel.

2.4.3.3 **Results**

The chemical separation effectively removes polyatomic interferences, enabling accurate quantification of HREE. Prior Fe removal is essential, as Fe significantly affects the elution behavior of LREE.

The values obtained for the entire set of samples analysed are presented in Figure 53 (A-D), after chondrite normalization and logarithmic scaling. Distinct REE patterns are observed between magnets of different origins, whereas materials along the same production chain show only minor variations. The REE composition is largely preserved from the alloy to the final magnet, with only slight process-related contamination.

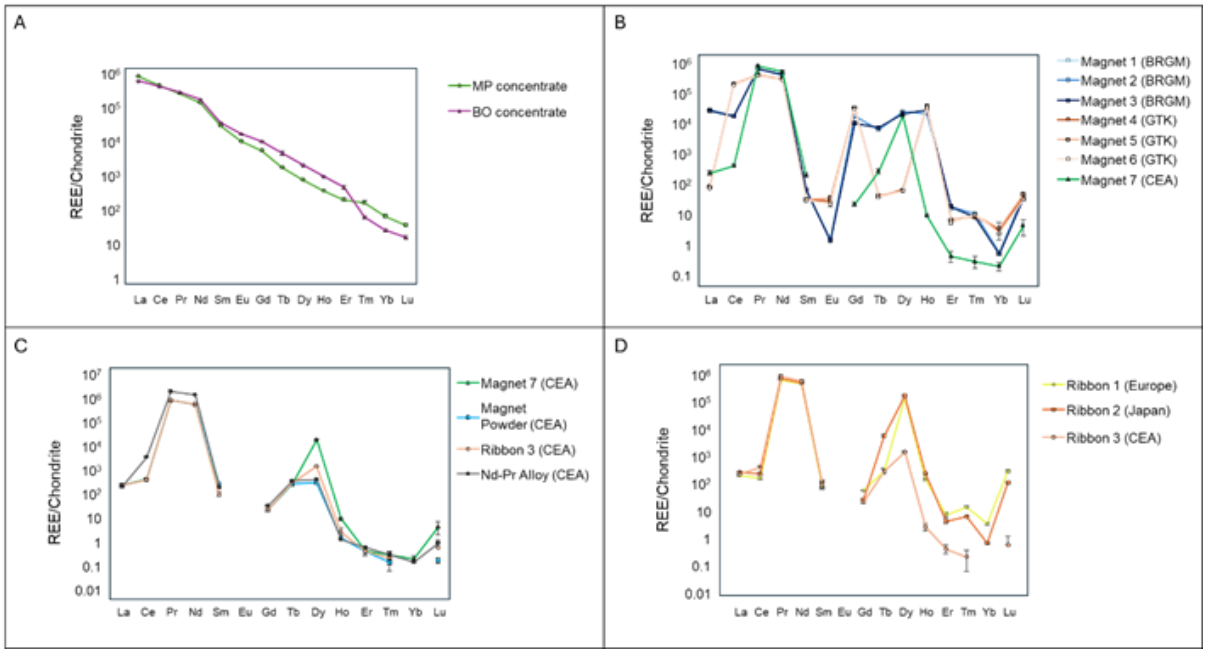

Figure 53 Chondrite-normalized REE patterns for: A) Mountain Pass (MP) and Bayan Obo (BO) concentrates, B) magnets received from BRGM, GTK, and CEA-Liten, C) samples from the value chain provided by CEA-Liten, and D) ribbons. Y-axis is on a logarithmic scale. Error bars represent the SD. The number of replicates per point ranged from n = 1 to 4. For samples with n = 1, a relative standard deviation (RSD) of 10% was used as SD estimate. In some cases, Eu and Yb concentrations are omitted because they remained below the procedural blank.

From a geoforensic perspective, the method allows differentiation of magnets based on their formulation and industrial origin and is useful for detecting cross-contamination –i.e., the unintentional transfer of REE from previously processed materials due to residues in shared production equipment–along with recycling or intentional additions of HREE.

While REE patterns alone do not unequivocally identify the mine of origin, they provide a key tool within a multi-technique approach, for example when combined with Nd isotopes.

The method can be applied across the value chain, from mineral concentrates to alloys, intermediate products, and final magnets. It is particularly valuable for quality control, industrial traceability, and provenance studies.

2.4.3.4 **Method evaluation**

The REE analysis by ICP-MS was assessed according to the criteria presented in deliverable D2.3 (Figure 54). The ICP-MS is a fixed laboratory technique (i.e., Mobility=0). It is currently impossible to determine REE in the field or at production sites. This technique makes it possible to analyse the entire operational chain from the ore to the Nd-Fe-B permanent magnet (i.e., Production Chain Coverage=10). The results show distinct REE patterns in permanent magnets from different origins, and the relative preservation of these patterns throughout the value chain suggests a strong discriminating power (Differentiating power=8). ICP-MS analysis is expensive because of the cost of the instrument (around 200k €), standards being used, gases required and maintenance (Cost of Implementation=3). The preparation time for each sample is lengthy and methodologically demanding, typically extending over several weeks; however, multiple samples can be processed in parallel, allowing several preparations to progress simultaneously within the same overall time frame (Operational Efficiency=2). The procedure involves the following steps: (1) complete dissolution of the sample, (2) separation of Fe from the REE using ion-exchange resin chromatography, (3) isolation of individual REE to eliminate oxide interferences during measurement, and (4) final quantification by ICP-MS. Despite the complexity of the procedure, neither the preparation nor the analytical stages require special authorization in terms of laboratory safety regulations.
The Global MFP Technic Index (GMTI) for this technic is thus calculated to 5.4.

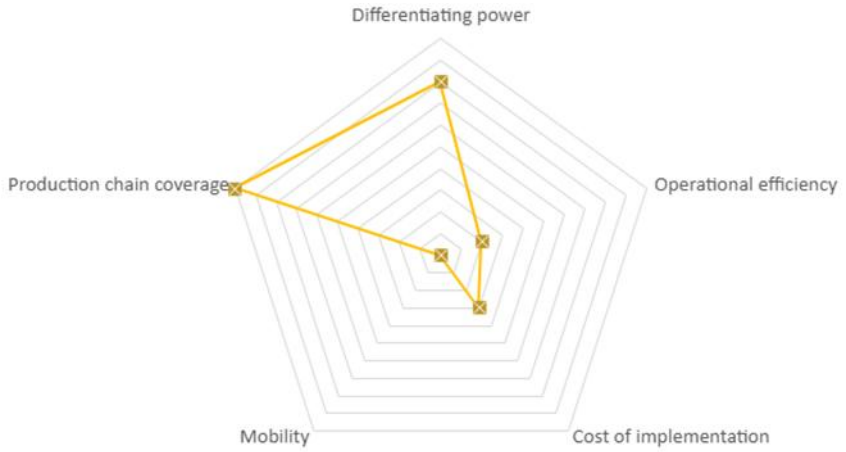

Figure 54 Method evaluation of the ICP-MS analysis for REE traceability along the permanent magnet production chain, based on criteria presented in deliverable D2.3.

Funded by the European Union

3 Conclusions

The results obtained in this project by various techniques lead to the following conclusions for the four commodities:

Cobalt and (nickel)

- Co-Ni bearing magmatic sulphide ore deposits of different locations can be differentiated by combined signatures of major, trace element and S isotopic compositions in pentlandite.
- Different ores may have overlapping fingerprints (e.g., trace elements and S isotopes), thus multivariate data analysis through comprehensive elemental and isotopic datasets is essential.
- Sulphur isotopic signature is conservative through mineral processing and potentially pyrometallurgy, but changes after acid leaching during the hydrometallurgy process.
- A combination of multiple isotope systems is promising in verifying materials that are sourced from multiple (mixing) origins.

Natural graphite

- Natural graphite at virtually any purity level contains gangue mineral phases, which dominate its chemical signature and define the characteristic fingerprint of each natural graphite deposit
- Certain resistant mineral phases, such as zircon or rutile remain in the concentrates even after chemical leaching. They enable the traceability along the value chain via SEM-based mineralogy of separated mineral phases or highly sensitive methods such as LA-ICP-MS or solution ICP-MS of bulk samples
- The data analysis approach depends on the number of acquired parameters and the number of repeated measurements. More parameters result in better differentiating power, while a large number of measurements from individual samples enables the application of machine-learning-based classification methods.

Lithium

- Fractionation of Li isotopes amongst the upstream value chain samples are related to the class of deposits (i.e. brines, geothermal fluids and hard rocks). The range of variability is large and thus leads to overlaps between the different localities.
- A first comparison of supervised models trained with Li isotopes highlighted promising results especially for the distinction Chinese brines and hard rocks with KNN, SVM and tree-based models. The moderate accuracy however indicated that overlaps signature between class could lead to misclassification.
- Major, minor and ultra-trace element analysis were performed on upstream samples that define the characteristic fingerprint of deposits and ore concentrates.
- Advanced probabilistic models for sample origin prediction were developed using a complete geochemical dataset. A LDA model was tested and optimized on clearly identified samples from three different localities (Canada, Australia and France) and allow a very good distinction between these three deposits.

Neodymium

- The Nd isotope composition is preserved for the downstream of magnet production chain from Nd-Pr Alloy until the final magnet.

Funded by the European Union

- Nd isotopes could be used as tracer of the origin as samples from various origins display distinct isotope signatures.
- However, the geochemical signature of the step from the mining concentrate to the NdPr alloy is still missing, limiting our knowledge about the evolution of the Nd isotopic signature or REE-ore throughout the entire value chain.

- The relative conservation of REE patterns along the value chain highlights the potential of the method for source tracking. Moreover, the REE patterns vary depending on the commercial origin of the material, further supporting the ability of this approach to discriminate between different sources.

In summary, we can conclude that the differentiation between different sources (e.g., deposits, producers) and the traceability along the production chain is possible for all four commodities. On the other hand, given the specific characteristics of each commodity, the optimal traceability approach is different. The most important aspect in method evaluation is the differentiating power of the discussed techniques, where at least one technique per commodity reaches an excellent score (8 to 10). The same statement holds for production chain coverage, while a high score in this aspect is usually paired with a high cost of implementation and/or low operational efficiency. As the focus of the document is on laboratory equipment, the mobility of all discussed instruments is minimal, while some instruments are also available in mobile version (see deliverable D2.3 for further details). Given these results, the best traceability approach needs to be selected on a case-to-case basis, while future work will be done to test if some of the above aspects can be improved.

Funded by
the European Union

Bibliography

Arrigo, L. M., Jiang, J., Finch, Z. S., Bowen, J. M., Beck, C. L., Friese, J. I., Greenwood, L. R., and Seiner, B. N. (2021). Separation and determination of rare earth elements in complex matrices. Journal of Radioanalytical and Nuclear Chemistry, 327, 457–463.

Arató, R., Quarles, D., Obbágy, G., Dallos, Z., Arató, M., Gopon, P., and Melcher, F. (2025). Towards a chemical fingerprint of graphite by laser-induced breakdown spectroscopy. Journal of Analytical Atomic Spectrometry, 40(9), 2526–2537.

Chen, Y., Liu, C., Chen, H., Zhang, Z., and Li, C. (2000). Carbon isotope geochemistry of graphite deposits and ore-bearing khondalite series in North China: Implications for several geoscientific problems. Acta Petrologica Sinica, 16, 233–244.

Dallos, Z., Arató, R., Obbágy, G., Burhanuddin, B., Burtscher, M., and Melcher, F. (under review). Analytical characterization of graphitic raw ores and natural graphite concentrates: Linking residual mineral phases to source provenance. SSRN 6065626.

Dehaine, Q., Tijsseling, L. T., Glass, H. J., Törmänen, T., and Butcher, A. R. (2021). Geometallurgy of cobalt ores: A review. Minerals Engineering, 160. https://doi.org/10.1016/j.mineng.2020.106656

Dietrich, V. E. (2024). Development of an analytical proof of origin method for natural graphite deposits. PhD thesis, Montanuniversität Leoben, Austria.

Gäbler, H. E., Melcher, F., Graupner, T., Bahr, A., Sitnikova, M. A., Henjes-Kunst, F., Oberthür, T., Brätz, H., and Gerdes, A. (2011). Speeding up the analytical workflow for coltan fingerprinting by an integrated mineral liberation analysis/LA-ICP-MS approach. Geostandards and Geoanalytical Research, 35(4), 431–448.

Ganio, M., Latruwe, K., Brems, D., Muchez, P., Vanhaecke, F., and Degryse, P. (2012). The Sr–Nd isolation procedure for subsequent isotopic analysis using multi-collector ICP-mass spectrometry in the context of provenance studies on archaeological glass. Journal of Analytical Atomic Spectrometry, 27, 1335–1341. https://doi.org/10.1039/C2JA30154G

Ghosh, M., Chavan, T. A., Reddy, G. L. N., Devi, P. S. R., Kumar, S., and Swain, K. K. (2022). Determination of impurities in graphite using proton induced gamma ray emission, total reflection X-ray fluorescence and instrumental neutron activation analysis. Analytical Chemistry Letters, 12(4), 437–450.

Gourcerol, B., Gloaguen, E., Melleton, J., Tuduri, J., and Galiegue, X. (2019). Re-assessing the European lithium resource potential: A review of hard-rock resources and metallogeny. Ore Geology Reviews, 109, 494–519.

IEA. (2025). Global Critical Minerals Outlook 2025. Report.

Kesler, S. E., Gruber, P. W., Medina, P. A., Keoleian, G. A., Everson, M. P., and Wallington, T. J. (2012). Global lithium resources: Relative importance of pegmatite, brine and other deposits. Ore Geology Reviews, 48, 55–69.

Funded by the European Union

Konnunaho, J., Eilu, P., Törmänen, T., Karinen, T., Ranta, J.-P., Rasilainen, K., Nykänen, V., Pokki, J., and Dehaine, Q. (2023). A mining industry overview of cobalt in Finland: Exploration, deposits and utilization. Geoenergy, 1. https://doi.org/10.1144/geoenergy2023-016

Kwiecińska, B., and Petersen, H. (2004). Graphite, semi-graphite, natural coke, and natural char classification—ICCP system. International Journal of Coal Geology, 57, 99–116.

Laznicka, P. (2006). Giant metallic deposits: Future sources of industrial metals. Springer.

Linnen, R. L., and Cuney, M. (2005). Granite-related rare-element deposits and experimental constraints on Ta–Nb–W–Sn–Zr–Hf mineralization. In R. L. Linnen and I. M. Samson (Eds.), Rare-element geochemistry and mineral deposits (Geological Association of Canada Short Course Notes 17, pp. 45–68). Geological Association of Canada.

Lu, Y., Lesher, C. M., and Deng, J. (2019). Geochemistry and genesis of magmatic Ni–Cu–(PGE) and PGE–(Cu)–(Ni) deposits in China. Ore Geology Reviews, 107, 863–887. https://doi.org/10.1016/j.oregeorev.2019.03.024

Lünsdorf, N. K., Dunkl, I., Schmidt, B. C., Rantitsch, G., and von Eynatten, H. (2017). Towards a higher comparability of geothermometric data obtained by Raman spectroscopy of carbonaceous material. Part 2: A revised geothermometer. Geostandards and Geoanalytical Research, 41, 593–612.

Manard, B. T., Hintz, C. J., Quarles, C. D., Jr., Burns, W., Zirakparvar, N. A., Dunlap, D. R., Beiswenger, T., Cruz-Uribe, A. M., Petrus, J. A., and Hexel, C. R. (2022). Determination of fluorine distribution in shark teeth by laser-induced breakdown spectroscopy. Metallomics, 14(7), mfac050.

Meisel, T. C., Webb, P. C., and Rachetti, A. (2022). Highlights from 25 years of the GeoPT programme: What can be learnt for the advancement of geoanalysis. Geostandards and Geoanalytical Research, 46(2), 223–243.

Moldoveanu, G. A., and Papangelakis, V. G. (2016). An overview of rare-earth recovery by ion-exchange leaching from ion-adsorption clays of various origins. Mineralogical Magazine, 80(1), 63–76. https://doi.org/10.1180/minmag.2016.080.051

Moradell Casellas, A., Lohier, T., Laperche, V., Aupart, C., and Desaulty, A. M. (in prep.). Better, faster, stronger: Using handheld, mobile XRF instruments and statistical treatment to track on-site the origin of lithium mineral concentrates.

Müller, A., Simmons W., Beurlen, H., Thomas, R., Ihle, P. M., Wise, M., Roda-Robles, E., Neiva, Ana M.R., Zagorsky, V. (2022) A proposed new mineralogical classification system for granitic pegmatites – Part I: History and the need for a new classification. https://doi.org/10.3749/canmin.1700088

Natarajan, V., Porwal, N. K., Babu, Y., Rajeswari, B., Dhawale, B. A., Kumar, M., Godbole, S. V., and Manchanda, V. K. (2010). Direct determination of metallic impurities in graphite by EDXRF. Applied Radiation and Isotopes, 68(6), 1128–1131.

Paton, C., Hellstrom, J., Paul, B., Woodhead, J., and Hergt, J. (2011). Iolite: Freeware for the visualisation and processing of mass spectrometric data. Journal of Analytical Atomic Spectrometry, 26, 2508. https://doi.org/10.1039/C1JA30154B

Funded by the European Union

Rantitsch, G. (2023). Graphite thermometry by interactive fitting of Raman spectra. International Journal of Coal Geology, 271, 104232.

Schatz, C. R. M. (2025). World Mining Data 2025, p. 266.

Scherrer, P. (1912). Bestimmung der inneren Struktur und der Größe von Kolloidteilchen mittels Röntgenstrahlen. In Kolloidchemie: Ein Lehrbuch (pp. 387–409). Berlin, Heidelberg: Springer Berlin Heidelberg.

Shang, Y., Dehaine, Q., Liu, X., Myllyperkiö, M., Bertelli, M., Kinnunen, P., Christine, F., and Lahaye, Y. (in prep.). Sulphur isotope forensics: Bridging the traceability gap from magmatic sulphide ore to battery product.

Shaw, R. A. (2021). Global lithium (Li) mines, deposits and occurrences. Keyworth, Nottingham: British Geological Survey.

Suárez-Criado, L., Rado, C., Losno, D., & Vanhaecke, F. (2026). Determination of REEs in permanent magnets and their production chain using ICP-MS. Journal of Analytical Atomic Spectrometry.

Thiéblemont, D., Guerrot, C., Négrel, Ph., Braucher, R., Bourlès D.L., Thiéblemont, R. (2014) Nd-isotope evidence for the distal provenance of the historical (c. <3000 BP) lateritic surface cover underlying the Equatorial forest in Gabon (Western Africa). Aeolian Research.

Van Achterbergh, E., Ryan, C. G., Jackson, S. E., and Griffin, W. L. (2001). Data reduction software for LA-ICP-MS. In P. J. Sylvester (Ed.), Laser-Ablation-ICPMS in the Earth Sciences – Principles and applications (Mineralogical Association of Canada Short Course Series, Vol. 29, pp. 239–243). Mineralogical Association of Canada.

Wang, S. Q. (1989). Characteristics of ore-bearing formation and genesis of the Xinghe graphite deposit in Inner Mongolia. Mineral Deposits, 8, 85–96.

Yang, Q. Y., Santosh, M., and Wada, H. (2014). Graphite mineralization in Paleoproterozoic khondalites of the North China Craton: A carbon isotope study. Precambrian Research, 255, 641–652.

YLE News. (2026, February 12). Finland opens Europe's first lithium mine. https://yle.fi/a/74-20209826